University of Sussex

Temporal Structure of Neural Oscillations Underlying Sensorimotor Coordination

a theoretical approach with evolutionary robotics

Bruno Andre Santos

Submitted for the degree of Doctor of Philosophy

University of Sussex

September 2012

Declaration

I hereby declare that this thesis has not been and will not be submitted in whole or in part to another University for the award of any other degree.

Signature:

Bruno Andre Santos

UNIVERSITY OF SUSSEX

Bruno Andre Santos, Doctor of Philosophy

temporal structure of neural oscillations underlying sensorimotor coordination: a theoretical approach with evolutionary robotics

Summary

The temporal structure of neural oscillations has become a widespread hypothetical "mechanism" to explain how neurodynamics give rise to neural functions. Despite the great number of empirical experiments in neuroscience and mathematical and computational modelling investigating the temporal structure of the oscillations, there are still few systematic studies proposing dynamical explanations of how it operates within closed sensorimotor loops of agents performing minimally cognitive behaviours. In this thesis we explore this problem by developing and analysing theoretical models of evolutionary robotics controlled by oscillatory networks. The results obtained suggest that: i) the informational content in an oscillatory network about the sensorimotor dynamics is equally distributed throughout the entire range of phase relations; neither synchronous nor desynchronous oscillations carries a privileged status in terms of informational content in relation to an agent's sensorimotor activity; ii) although the phase relations of oscillations with a narrow frequency difference carry a relatively higher causal relevance than the rest of the phase relations to sensorimotor coordinations, overall there is no privileged functional causal contribution to either synchronous or desynchronous oscillations; and iii) oscillatory regimes underlying functional behaviours (e.g. phototaxis, categorical perception) are generated and sustained by the agent's sensorimotor loop dynamics, they depend not only on the dynamic structure of a sensory input but also on the coordinated coupling of the agent's motor-sensory dynamics. This thesis also contributes to the Coordination Dynamics framework (Kelso, 1995) by analysing the dynamics of the HKB (Haken-Kelso-Bunz) equation within a closed sensorimotor loop and by discussing the theoretical implications of such an analysis. Besides, it contributes to the ongoing philosophical debate about whether actions are either *causally relevant* or a *constituent* of cognitive functionalities by bringing this debate to the context of oscillatory neurodynamics and by illustrating the constitutive notion of actions to cognition.

Acknowledgements

I would like express my sincere gratitude to my supervisors Prof. Phil Husbands and Xabier Barandiaran for their continuous support, motivation and precise comments. I was very lucky to have them guiding me through the hard times of my PhD. I also would like to thank my thesis committee: Prof. Takashi Ikegami and Chris Thornton for insightful comments. Thanks to my fellow labmates in CCNR: Jose Fernandez Leon, Renan Moioli, Matthew Egbert, Lucas Wilkins, James Thorniley, Tom Froese and Nicholas Tomko for helpful discussions. A special thanks to Renan Moioli who has inspired me to work with oscillatory networks. Thanks to Ezequiel Di Paolo for the discussions during the first year of my PhD. I am very thankful to my family, girlfriend and friends for their support.

Thanks to the Brazilian National Council of Research (CNPq) for the financial support and to the Computer Engineering Department of the Federal Centre for Technological Education (Cefet-MG) that granted me a working leave to carry out this research.

Preface

Some of the content presented in this thesis have been published in peer-reviewed conference proceedings and international journals as follows.

Chapter 3

- Santos, B. A., Barandiaran, X. E., and Husbands, P. (2011). Metastable dynamical regimes in an oscillatory network modulated by an agents sensorimotor loop. In 2011 IEEE Symposium on Artificial Life (ALIFE), pages 124-131. IEEE.

- Santos, B. A., Barandiaran, X. E., and Husbands, P. (2011). Neurodynamic regimes of phase relation and behavior in robotic models. BMC Neuroscience, 12 (Suppl 1): 155.

- Santos, B. A., Barandiaran, X. E., and Husbands, P. (2012). Synchrony and phase relation dynamics underlying sensorimotor coordination. Adaptive Behavior, 20(5):321-336.

Chapter 5

- Santos B. A., Barandiaran X. E., Husbands P., Aguilera M., Bedia M. (2012). Sensorimotor Coordination and Metastability in a Situated HKB Model. Connection Science. 24(4):143-161.

Chapter 6

- Santos, B. A., Husbands, P., and Froese, T. (2010). Accommodating homeostatically stable dynamical regimes to cope with different environmental conditions. In Proceeding of the 12th International Conference on Artificial Life. pages 395-402

Contents

List of Figures

Chapter 1

Introduction

1.1 Overview

The so-called artificial-life-route-to-AI (Steels and Brooks, 1995), originally emphasized the situated, emergent, self-organized, often non-representational, and dynamic nature of cognition. Design principles were also claimed to be biologically inspired. Such biological inspiration was mostly limited to state that cognitive systems had to be built from the bottom-up (from the simplest to the more complex, like evolution proceeded for natural cognition) and to favour insect-like behavioural patterns. In some cases "biological inspiration" meant also the use of artificial neural networks as control systems but rarely did such networks bear much relevance to neuroscience. The scientific context has radically changed since those early years of Artificial Life (AL). Neuroscience has made considerable progress developing empirical and theoretical frameworks where self-organization, emergent patterns, phase-synchrony, and oscillatory rhythms are now common issues in studies of brain dynamics (Haken, 1978; Buzsaki, 2006; Traub and Whittington, 2010; Fell and Axmacher, 2011; Aviyente et al., 2011; Dubovik et al., 2012; Kaliukhovich and Vogels, 2012). Whereas the AL approach to cognitive science still has much to explore within this framework, large-scale neuroscience has yet to be integrated with insights into the situated and embodied nature of cognitive dynamics. The current work aims to help fill this gap, merging situated and evolutionary robotics with some current trends in large-scale neuroscience.

The last two decades have witnessed an increasing focus on oscillatory brain dynamics as essential for a variety of cognitive phenomena. In neuroscience, oscillatory phenomena are present in different levels of the nervous system's activity. At the individual neural level, neurons undergo cyclic alterations on its membrane potential following different

dynamical regimes depending on the cell properties (Izhikevich, 2007). At higher levels, global oscillations is a collective phenomenon generated by groups of neural cells that fire synchronously – entrained by pacemaker cells or as a result of recurrent network activity with inhibitory-excitatory connections (Buzsaki, 2006). Different recording techniques have provided experimental results that are consistent with the oscillatory nature of neural activity, among them: intracellular recording; extracellular single unit recording; multiunit recording; and intracortical and scalp electroencephalography (Vertes and Stackman, 2011). While intracellular and extracellular single unit recordings capture the membrane potential and neural action potentials (spikes) of individual neurons, respectively; the other upper level recordings mainly capture action potentials and the local field potential of neuronal groups. By investigating these oscillatory signals, coherent dynamical properties can be found and systematically related to sensory and motor coordination (Buzsaki, 2006; Singer, 2011; Hipp et al., 2011; Perfetti et al., 2011; Cohen and van Gaal, 2012; Parameshwaran et al., 2012).

The *temporal structure* of the oscillations is a property that has been consistently revealing the dynamic mechanisms underlying sensory and motor coordination. It can be investigated by the following different approaches, such as the inter spike intervals from individual neurons or neuronal populations (Mainen and Sejnowski, 1995; Bair and Koch, 1996; Reich et al., 1997; Reinagel and Reid, 2002), the timing of the first spike related to a stimulus onset (Heil, 2004; VanRullen et al., 2005; Gollisch and Meister, 2008), the spike of a neuron related to the local field potential on its background (Sinclair et al., 1982; Fries et al., 2007; Denker et al., 2007; Montemurro et al., 2008; Kayser et al., 2009), the time-locked spiking activity of locally or spatially distributed neurons (Izhikevich, 2006; Izhikevich and Hoppensteadt, 2009), and the synchronisation of spikes from local and distant neurons (Hipp et al., 2011; Perfetti et al., 2011; Cohen and van Gaal, 2012).

Generally speaking, this thesis explores the temporal structure of neural oscillations underlying sensorimotor coordination and is based on two central issues: i) informational content and causal relevance of the temporal structure of neural oscillations in relation to the sensorimotor dynamics, and ii) dynamical analysis of oscillatory dynamics within sensorimotor loops. These issues are explained in details in sections 1.1.1 and 1.1.2, respectively.

1.1.1 Informational content and causal relevance of oscillatory dynamics in relation to the sensorimotor loop

A relevant property of the temporal structure of neural oscillations that has been receiving a lot of attention from the cognitive science community is the synchronisation between oscillatory signals. Synchrony has become the hypothetical "mechanism" that is repeatedly invoked to explain how spatially segregated neural oscillators get integrated into functional transient clusters giving rise to cognitive functions such as coherent sensorimotor coordination, perception and conscious experience (von der Malsburg, 1981; Gray and Singer, 1989; Engel et al., 1990; Tononi and Edelman, 1998; Varela et al., 2001; Fries, 2005; Uhlhaas et al., 2009; Pockett et al., 2009; Singer, 2011; Hipp et al., 2011). Synchrony refers only to one aspect of the temporal relation among oscillatory signals: *i.e.* that in which the phase relation between oscillatory signals remains (relatively) constant. A dynamical description of an oscillatory network in terms of its synchronous transient clusters is a reduced description from its entire phase relation dynamics; that is, it does not take into consideration how the phase relations between desynchronised oscillators are changing over time. Such a reduction in the dynamical description might be leaving out of the equation moments of oscillatory dynamics that are relevant for neural functions.

In this thesis, rather than studying synchrony we focus on desynchronous oscillations and investigate their relevance in the context of an embodied oscillatory network generating functional sensorimotor coordinations. Particularly, the first question we tackle regarding the role of desynchronous oscillations is the following: *how does the informational content of the sensorimotor coordination present in a complete dynamical description of phase relations change as such a description is reduced to the phase relations of synchronous oscillations?* That is, we study how the amount of information available about the sensorimotor coordination changes as the phase relations of desynchronous oscillations are left out of the dynamical description of the oscillatory network. Although it is expected that the amount of information in a reduced description is smaller or equal than the information in a more complete one, it is relevant to analyse *how* this amount of information changes. By doing this analysis it is possible to identify whether there are ranges of phase relations – during synchronised activity, for instance – that carry more information than others about the sensorimotor dynamics.

The second question regarding the role of desynchronous oscillations is the following: *to what extent are desynchronous oscillations as causally relevant as synchronous oscillations for the generation of functional sensorimotor coordination?* The causal relevance is quan-

tified by the effects on the sensorimotor coordination after applying perturbations to the underlying oscillatory network during moments of synchronisation or desynchronisation. This study identifies whether there are ranges of phase relations - during synchronous oscillations, for instance – that carry a higher functional causal contribution to the generation of coherent sensorimotor coordination.

The analyses of informational content (first question) and causal relevance (second question) of the phase relations during synchronous and desynchronous oscillations contribute to the understanding of oscillatory dynamics underlying sensorimotor coordination; it might as well provide insights for the assessment of research programs that attribute a privileged explanatory status to synchronous oscillations over desynchronous ones. Both problems are addressed with models of agents behaving in simulated environments and controlled by networks of phase-coupled oscillators.

The second central issued approached in this thesis is presented in the next section.

1.1.2 Dynamical analysis of oscillatory dynamics within sensorimotor loops

Despite the great amount of empirical experiments in neuroscience and mathematical and computational modelling investigating the temporal structure of the oscillations (Izhikevich et al., 2004; Zhang et al., 2008; Aviyente et al., 2010; Ceguerra et al., 2011; Skardal and Restrepo, 2012), there is still little systematic exploration of how the temporal structure of oscillatory signals is modulated by and depends on the dynamics of closed sensorimotor loops. The empirical, theoretical and mathematical approaches for analysing oscillatory signals have mostly worked under the assumption that the temporal structure of neural oscillations can be understood without incorporating the sensorimotor loop into the picture (that is, the continuous and recurrent interaction with the environment, the online coupling of brain and environment through sensory and motor activities). Most approaches have focused on how oscillations can carry information within the brain (Sauseng et al., 2002; Rubino et al., 2006; Neymotin et al., 2010). Models are generally built leaving out the body and the environment and often assuming a representational theory of brain functioning (that is, assuming that the main job of the brain is to create a representation or model of the environment and focusing on neuronal mechanisms capable of supporting the processing of such a model, independently from its environment). Despite the significant progress achieved under this assumption, we believe it might be limiting future development while the role of sensorimotor loops still remains underexplored. In this way, in

this thesis we develop computational models of embodied oscillatory network controlling agents behaving in simulated environments and analyse the dynamics of co-modulation between the agents' internal oscillations and their sensorimotor loops. Particularly, this problem is investigated from three different perspectives, which are described below.

From spontaneous oscillations to functional oscillatory regimes

A neural system is an active system that constantly regenerates its internal oscillatory activity which is modulated by the interaction with the environemnt. In its resting-state (i.e. when it is not engaged in a cognitive task), a neural system does not operate in a silent mode waiting for stimuli from the environment, rather it constantly oscillates and regenerates its own internal activity (Buzsaki, 2006; Sporns, 2010). Functional oscillatory regimes (or the neural dynamics underlying a cognitive task) are then generated as the result of a network's spontaneous oscillations combined with the modulation from the sensorimotor dynamics.

Contrary to this view of an active neural system, the majority of modelling in theoretical neuroscience has focused on stimulus-driven neural models where neurons are typically silent in the absence of input (Vogels et al., 2005). Although this approach has achieved significant progress in understanding brain operations – specifically in the sensory areas – it does not account for the majority of neural dynamics where the sensory activity works as perturbations to the ongoing internally generated oscillations (Vogels et al., 2005). In this way, this thesis develops a model where an agent performs a minimally cognitive task (the discrimination of two objects in an environment) controlled by a network of Kuramoto phase-coupled oscillators (Kuramoto, 1984) and study *how the sensorimotor loop interacts with the network's spontaneous oscillations so that functional oscillatory regimes emerge and the agent correctly performs the task.* We will provide a dynamical explanation of how functional dynamics in the embodied oscillatory network are generated from the network's spontaneous oscillations (decoupled from the sensorimotor loop) by analysing the modifications on attractor landscape of phase relations.

The dependency of functional oscillatory regimes on an agent's motor-sensory dynamics: a case study with the HKB equation

The temporal structure of oscillatory components has been carefully investigated within the empirically grounded theoretical framework of Coordination Dynamics (Kelso, 1995); a prominent work in cognitive science that has motivated many empirical studies of neu-

ral oscillatory dynamics underlying sensory and motor activities (Meyer-Lindenberg, 2002; Swinnen, 2002; Jantzen, 2004; Aramaki, 2005; Lagarde and Kelso, 2006) and has opened up discussions in different areas such as philosophy of cognitive science (Chemero, 2009; Bechtel and Abrahamsen, 2010; Kaplan and Bechtel, 2011; Stepp et al., 2011) and theoretical neuroscience (Kelso and Tognoli, 2009). The main illustrative model for the Coordination Dynamics framework is that described by the HKB (Haken-Kelso-Bunz) equation which captures the temporal structure between the activity of coupled oscillatory elements. This equation has been studied by manipulating a control parameter that modifies the oscillators' natural frequencies or their coupling factor (Kelso, 1995). One of its main dynamical properties is the metastable regime in which the variable representing the temporal relation between two oscillators (i.e. their phase relation) engages when the control parameter crosses a certain threshold.

The metastable regimes have been hypothesized to be the dynamical signature of the nervous system underlying sensorimotor coordination (Kelso and Tognoli, 2009; Tognoli and Kelso, 2009; Bressler and Kelso, 2001). Empirical evidence favouring this hypothesis comes, for instance, from studies showing correlations between sensory stimulation and transiently synchronised networks in the brain of animals performing perceptual and motor coordination tasks (Rodriguez et al., 1999; Varela et al., 2001; Buzsaki, 2006; Pockett et al., 2009; Singer, 2011; Hipp et al., 2011). And yet, despite the evidence supporting the existence of metastable oscillations in the nervous system of behaving animals, to our knowledge there are still very few models (if any) where the HKB equation generates the motor behaviour of an agent interacting in an environment and, at the same time, has its control parameter modulated, through sensory feedback, by the motor behaviour it generates.

In order to fill this gap we analyse the HKB equation within the sensorimotor loop by implementing it as the controller of an agent performing a functional behaviour (gradient climbing) in a simulated two-dimensional environment. The "output" of the HKB equation (the phase relation variable) generates the agent's motor behaviour and, at the same time, its control parameter (in our particular case, the variable representing the oscillators' frequency difference) is modulated by the agent's behaviour through its sensory activity. The analysis of the HKB equation within a closed sensorimotor loop not only contributes to the Coordination Dynamics framework but also gives theoretical insights to understand the interplay between the temporal structure of neural oscillations and sensorimotor dynamics. Particularly, this model allows us to show (in a theoretical level of abstraction) how the

temporal structure of functional oscillatory regimes is tightly dependent on a fine grained coordinated coupling of the agent's motor-sensory dynamics (the term "motor-sensory" is being used to emphasize the modulation of the sensors by the motors through the environment).

Accommodating oscillatory dynamical regimes within homeostatic boundaries

Another related area that deserves more detailed understanding is the analysis of how oscillations are affected by a mechanism of adaptation that changes the network connectivity on a ontogenetic timescale. A problem that arises when connections are modified is that if the network is completely integrated (without functional modules), the modifications can interfere in the network dynamics under conditions to which it had previously adapted – i.e. a problem known as "the neural interference" (Di Ferdinando et al., 2001).

In this thesis we study the problem of neural interference in the context of an oscillatory network within a sensorimotor loop, particularly we *i) analyse how a completely integrated, embodied network acquires a new functional oscillatory regime without affecting the functionality of pre-existing regimes and ii) show how these regimes tightly depend on the closed sensorimotor loop dynamics.* We develop a model where a simulated agent is performing phototaxis maintaining its homeostatically stability (i.e. its oscillations are maintained within homeostatic boundaries). When the agent's visual field is inverted, it becomes homeostatically unstable and does not perform phototaxis. The instability activates synaptic plasticity changing the connectivity of oscillatory network towards a configuration that accommodates functional, stable oscillations under normal and inverted visions. The implementation of this task was motivated by an experiment carried out by Taylor (1962); Kohler (1963) where a subject adapts his/her sensorimotor behaviour to distorted visual field (by intermittently wearing a pair of spectacles). The mechanism of adaptation is implemented following Ashby's work on homeostatic adaptation (Ashby, 1947, 1960; Di Paolo, 2000). We will investigate how functional oscillatory regimes are generated and sustained within the sensorimotor loop; how the mechanism of adaptation changes the attractor landscape without affecting the functionality of the network under previously adapted conditions; and also whether homeostatic stability is necessary for the transition between the dynamical regimes underlying normal and inverted visions.

A summary of the thesis organisation is presented in the next section.

1.2 Thesis organisation

Chapter 2 contains the theoretical background of this thesis, it presents some properties of the temporal structure of neural activity that have been consistently revealing the dynamical mechanisms underlying sensory and motor activities; chapters 3, 4, 5 and 6 contain the computational models and their dynamical analyses; and chapter 7 presents the conclusions and discussions. The content of the experimental chapters are described in more details in the following paragraphs.

Chapter 3 contains a computational model where we analyse in details: a) how the informational content about an agent's sensorimotor behaviour that is present in the temporal structure of its internal oscillations changes when the temporal structure is gradually reduced to the dynamics of synchronous oscillations by removing the information present in desynchronous oscillations; and b) whether either synchronous or desynchronous oscillations carries a privileged functional causal contribution to the generation of coherent sensorimotor behaviour. These problems are addressed by implementing an agent performing phototaxis controlled by a network of phase-coupled Kuramoto oscillators Kuramoto (1984). The analysis of informational content is done by using the standard measures of *entropy* and *mutual information* from information theory (Shannon, 1948; Cover and Thomas, 2005). For the analysis of causal relevance we perform experiments with controlled perturbations applied to synchronous and desynchronous oscillations while the agent is interacting with its environment.

Chapter 4 provides a computational model where we explore: a) how functional oscillatory patterns (patterns underlying the agent's correct behaviours) are generated from the combination of the network's spontaneous oscillations and the agent's sensorimotor loop dynamics; particularly, we focus on the analysis of how the agent's sensory activity dynamically shapes the attractor landscape of phase relations as the agent behaves in the environment; and b) how the informational content present in the temporal structure of the agent's internal oscillations changes as the desynchronous oscillations are removed from the dynamical description of phase relations – which is similar to the problem investigated in chapter 3, but with the agent performing a different task and controlled by a different network (in terms of number of oscillators, connectivity and natural frequencies). The agent's controller is implemented with phase-coupled Kuramoto oscillators and the analyses are carried out by using dynamical system tools and information-theoretic measures. This chapter is the only one where we explore both central issues of the thesis, namely i) the information and causal relevance of oscillatory dynamics in relation to sensorimotor

loops, and ii) the dynamical analyses of oscillatory dynamics within sensorimotor loops.

Chapter 5 contains a computational model where we study the dependency of functional oscillatory regimes on an agent's motor-sensory dynamics. This study is carried out by implementing an agent's performing phototaxis controlled by the HKB equation and by analysing the coordinated coupling between the inward and outward arms of the sensorimotor loop (i.e. the coupling between "sensor → controller → motor" and "motor → environment → sensor"). The implementation of the agent's controller with the HKB equation makes the dynamical analysis relatively simple and yet explanatorily powerful to approach the problem investigated in this chapter. Besides, the analysis of this equation within the sensorimotor is a contribution to the theoretical framework of Coordination Dynamics proposed by Kelso.

Chapter 6 contains a computational model where we study the problem of "'neural interference" by analysing how a completely integrated network acquires a new functional oscillatory regime without affecting the functionality of pre-existing ones, and also how these functional oscillatory regimes depend on the dynamics of a closed sensorimotor loop. Specifically, we analyse how the attractor landscape and the dynamics of a network controlling a phototatic agent under normal vision changes after it adapts to perform phototaxis under inverted vision. The agent's controller is implemented using a continuous-time recurrent neural network (CTRNN) (Beer, 1995), a well-known equation in field of evolutionary robotics which, to our knowledge, has never been studied in terms of its phase dynamics[1]. The phase relations are obtained from the CTRNN dynamics by using Empirical Mode Decomposition and Hilbert Transform (Huang et al., 1998), which will be explained in details chapter 6.

In sum, chapters 3, 4, 5 and 6 contain the computational models we have developed and analysed in this thesis. The analyses of informational content and causal relevance of the phase relations (one of the central issues of the thesis) are approached in chapter 3 and 4 (with more details in the former). The dynamical analyses of oscillatory dynamics within sensorimotor loops (the second central issue of this thesis) is approached in chapters 4, 5 and 6. Chapter 4 focuses on the generation of functional oscillatory regimes from modulation of the network's spontaneous oscillations by the sensorimotor loop; chapter 5 focuses on the dependency of functional oscillatory regimes on the motor-sensory dynamics; and chapter 6 focuses on how a completely integrated network that is constantly modulated by an agent's sensorimotor loop accommodates a new functional oscillatory regime without

[1]The CTRNN does not necessarily oscillate. The analysis of phase dynamics was only possible as the network presented a rhythmic dynamics when coupled to the agent's body.

affecting the functionality and stability of pre-existing regimes.

1.3 Summary of original contributions

This work contributes to the understanding of oscillatory dynamics underlying sensorimotor activity. Most contributions were drawn from the analyses of computational, theoretical models of brain-body-environemnt systems at a high level of abstraction and, as such, they should be taken as proofs of concept that show how neural oscillatory activity could modulate and be affected by sensorimotor coordination dynamics. As the informational content and causal relevance of desynchronous oscillations in relation to the sensorimotor dynamics are concerned, this thesis helps answer the questions:

- *How does the informational content of the sensorimotor activity present in a complete dynamical description of phase relations change as such a description is reduced to the dynamics of synchronous oscillations?* In the context of the model developed, we showed that the informational content about the sensorimotor activity is equally distributed throughout the entire range of phase relations; the more the dynamical description is reduced the less information it carries about the sensorimotor coordination. Neither synchronised nor desynchronised oscillations was found to carry a privileged status in terms of informational content in relation to the agent's sensorimotor activity.

- *To what extent are desynchronous oscillations as causally relevant as synchronous ones for the generation of functional sensorimotor coordination?* In the context of the model developed, we have shown that although the phase relations of oscillations with a narrow frequency difference carry a relatively higher causal relevance than the rest of the phase relations to sensorimotor coordinations, overall there is no privileged functional causal contribution to either synchronous or desynchronous oscillations.

In essence, the analyses of the models suggest that the high level of synchronisation found by empirical experiments might only represent part of the explanatory picture that involves the entire phase relations; the reduction of phase relations to synchrony might be hindering relevant information about the neural oscillatory activity underlying functional sensorimotor coordination.

As the dynamical analyses between the temporal structure of the oscillations and the dynamics of closed sensorimotor loops are concerned, the contributions of this thesis are the following.

- We have provided a dynamical explanation of how an agent's sensory dynamics shape the spontaneous oscillations of a network generating oscillatory patterns that underlie an agent's functional behaviours. This dynamical explanation helps understand how the dynamics of a neural system in a resting state differ from its dynamics when it is engaged in a sensorimotor task.

- The analyses of the models suggested that the emergence of functional oscillatory patterns (e.g. patterns that generate gradient climbing behaviour) depends not only on the structure of the agent's sensory input but also on the coordinated coupling of the agent's motor-sensory dynamics. The modulation of an agent's sensory dynamics by its motor activity assures that the agent's controller converges to functional oscillatory regimes that underlie coherent sensorimotor behaviours; in the absence of this modulation, the oscillations and the motor-sensory activity might become uncoordinated and consequently generate a non-functional interaction between the agent and its environment. More generally, the results suggest that functional oscillatory regimes are tightly dependent on the agent's sensorimotor contingencies, as when what the agent is doing is not coordinated to what it is sensing, then the internal oscillations might converge to non-functional regimes.

- We have implemented and analysed the HKB equation within an agent's sensorimotor loop. This equation is well-known in embodied cognitive science; however, it had never been implemented and analysed in the context where it generates an agent's behaviour and, at the same time, is modulated by the behaviour it generates (through sensory feedback). In this way, such implementation not only helps to understand the interplay of neural oscillations and sensorimotor activity, but also contributes to the theoretical framework proposed by Kelso.

- We have provided a dynamical explanation of how a completely integrated network can accommodate a new oscillatory regime without affecting the functionality of pre-existing ones. This explanation gives some insights on how the brain might solve the problem of neural interference and also has practical implications to the development of artificial neural networks that should learn a multiplicity of behaviours without the implementation of a functionally modular architecture.

- The analyses of the models contribute to the philosophical debate about whether action (and consequently the sensory stimuli resultant from an action) is either a cause or a constituent of a cognitive functionality (e.g. perception). This contribution is

done by bringing this discussion to the context of embodied oscillatory dynamics and illustrating that a functionality is not a standalone entity in a neural system that depends on external stimuli to be activated, rather it is a process that emerges from the coordinated coupling between the brain-body-environemnt system where the actions and the sensory stimuli are *constituents* of the functionality itself.

Chapter 2

Background on neural oscillations

Neural oscillations are present in different spatial and temporal scale in nervous system, from the membrane potential of a single neuron to cortical oscillations (Buzsaki, 2006; Izhikevich, 2007; Traub and Whittington, 2010); however it is still unknown which properties of these oscillations (if any) consistently reveal the dynamical mechanisms underlying an agent's sensory and motor activities. The rate of a spike train within a time window is one of the first properties that has been investigated (this property is briefly reviewed in section 2.1). More recently, the temporal structure of the oscillations (e.g. temporal pattern within a spike train) is another property that has been carefully investigated by carrying out empirical experiments (which are reviewed in section 2.2) and developing computational models (which are reviewed in section 2.3).

2.1 Spiking rate

One of the earliest works that proposes *spiking rate* as a relevant property to understand neural oscillations underlying sensory and motor activity was developed by Adrian (1926). Adrian measured the activity of the nerve in a frog's knee by stretching its leg holding different weights attached to a thread. He found that the number of action potentials, which he called "oscillations", was correlated to the weight used to stretch the leg. Particularly, he observed that the heavier the weight the more frequent were the oscillations.

This correlation of spiking rates to environmental stimuli has also been observed in cold and mechanical receptors in the skin (Darian-Smith et al., 1973; Mountcastle et al., 1966) and in the olfactory system (Getchell, 1986). Two important observations regarding the relation between a stimulus and a neural firing rate are the following: a) the spiking rate remains unchangeable for values of stimulus above or below a threshold which defines

a window of neural sensitivity; b) the lower and the upper boundaries of such a sensitivity window are context dependent and can change through an habituation process (Kandel et al., 2000).

A more sophisticated interpretation for the neural spiking rates was proposed by Hebb (1949). Hebb extends the role of spiking rates from sensory and motor areas to higher order functional areas across the nervous system. He stated that elevated firing rates of neurons located throughout the nervous system constitute a functional neural assembly which gives to the subject the perception of a particular object in the environment. His proposal is criticized for not dealing with the situation where there are multiple objects in the environment. As an assembly is constituted by neurons with elevated firing rates and, at each moment, there is only one whole indistinct assembly activated, how could the perception of multiple objects (multiple assemblies) co-exist in the nervous system? This problem is referred to as "the superposition catastrophe" (von der Malsburg, 1987).

Two possible methods to measure spiking rates are *averaging over time* and *averaging over different trials* (Gerstner, 1999). In the first one, the number of spikes in a time interval T is counted and divided by T. Although the length of T may vary depending on the stimulus and on the type of neuron being recorded, typical values for T are within $[100, 500]$ ms (Gerstner, 1999). The second method consists of performing the same experiment many times and averaging the spikes across the trials aligned with the stimulus onset. The main critics of the spiking rate approach is that by averaging spikes within a time window the timing of the spikes is lost (for a further discussion about spiking rates see Shadlen and Newsome (1994) and Rieke (1999)).

In the next section we review some approaches that investigate the temporal structure of the neural oscillations at different spatial and temporal scales.

2.2 The temporal structure of neural oscillations

The temporal structure of neural activity can be investigated by following different approaches, namely: i) the timing of the first spike related to a stimulus onset (reviewed in section 2.2.1); ii) the interspike interval within a neuron spike train (section 2.2.2); iii) the spike of a neuron related to the local field potential on its background (section 2.2.3); and iv) the locally and spatially distributed synchrony of neural oscillations (section 2.2.4);

2.2.1 Time-to-first-spike

In this approach the time of the first spike related to a reference signal (e.g. the onset of visual stimulus) is hypothesized to carry more information about the external world than the subsequent spikes (Thorpe, 1990; VanRullen et al., 2005). One motivation to take the time-to-first-spike as a relevant variable of the neural dynamics comes from the observation that the recognition of a stimulus (e.g. a familiar object in the visual field) takes place in a relatively short time – less than 150 ms for visual images (Thorpe et al., 1996) – which is not enough time for the flow of many spikes to travel throughout the nervous system. The information contained in the first spikes have been studied in the auditory (Heil, 2004), somatosensory (Johansson and Birznieks, 2004) and visual (Vanrullen, 2003; Gollisch and Meister, 2008) systems.

Gollisch and Meister (2008), for instance, presented a uniform square-wave grating in the salamander visual field and recorded the neural activity near its retina surface (ganglion cells). Typically, the neural activity presented bursts of spikes after the stimulus onset. In certain types of cells (fast and biphasic OFF cells) the number of spikes within a burst was similar during the presentation of different gratings, indicating a limitation of the spiking rate. On the other hand, the spike latency of the same cells varied across different stimuli and was very reproducible for repeated presentation of the same stimulus. They also found that the amount of information conveyed by the number of spikes about a visual stimulus is considerably smaller than the amount of information conveyed by the spike latency.

2.2.2 Interspike interval

The general idea of the interspike interval approach is that different environmental conditions produce different spike trains in a neuron or neuronal group (Mainen and Sejnowski, 1995; Bair and Koch, 1996; Reich et al., 1997). One way to visualize patterns of spike trains for a given stimulus is by plotting the distribution of interspike intervals grouped in bins of fixed width. de Ruyter van Steveninck et al. (1997) measured the activity of a motion-sensitive neuron in a fly's visual system during the presentation of random bars moving across its visual field and reported that the motion-sensitive neuron efficiently transmits information about the bar movements by establishing precise temporal relation between individual spikes. In another experiment, Reinagel and Reid (2002) found that neurons in the thalamus of a cat's brain also engage in temporal patterns of spike intervals during visual stimulation.

2.2.3 Phase between spikes and the LFP

Another property of the oscillations that has been studied is the temporal relation between local spiking activity and oscillatory cycles generated by neuronal populations (Sinclair et al., 1982; Fries et al., 2007; Denker et al., 2007; Kayser et al., 2009), see illustration in Fig. 2.1. O'Keefe and Recce (1993) found that the phase relation between the spiking bursts of place cells and theta oscillations in the hippocampus changes systematically as a rat runs through a place field. In another experiment, Montemurro et al. (2008) recorded the spiking activity and the local field potential (LFP) from neuronal populations in the visual area V1 of anaesthetized macaque monkeys watching film and reported that the phase of a spike in relation to the phase of the LFP on its background carried an additional information about the visual scenes that was not present in the spiking rate alone. This additional information was found only in oscillatory frequencies smaller than 24 Hz. For higher frequencies the phase relation between the spikes and the LFP did not provide extra information about the visual scene.

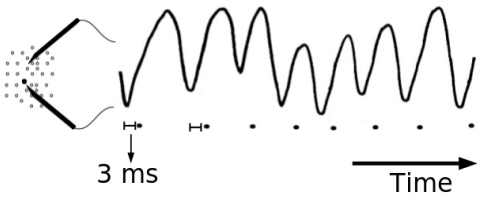

Figure 2.1: Phase lags between spikes and the local field potential on its background. A neuronal group is represented by a set of grey dots on the left. The activity of this neuronal group is represented by the oscillatory signal. A trace of black dots below the oscillatory signals represents the spike train of a single neuron within the neuronal group. The spikes of this neuron are 3 ms delayed in relation to the trough of the oscillatory signal. The phase of this neuron in relation to the oscillatory cycle has been proposed to carry relevant information about sensory signals.

2.2.4 Neural synchrony

In the context of this thesis, neural synchrony is a very important property as one of the main contributions of the current work is the analysis of informational content and causal relevance of synchronous and desynchronous oscillations in relation to sensorimotor dynamics (which were explained in the previous chapter and will be studied in chapters 3 and 4).

Synchronization has become a widespread hypothetical "mechanism" that is repeatedly invoked to explain cognitive phenomena such as perception, functional behavior and conscious experience (von der Malsburg, 1981; Gray and Singer, 1989; Engel et al., 1990; Tononi and Edelman, 1998; Rodriguez et al., 1999; Varela et al., 2001; Lutz, 2002; Buzsaki, 2006; Pockett et al., 2009; Singer, 2011; Hipp et al., 2011). The core idea of this approach is that neurons form dynamical transient functional neural assemblies by synchronising their activities; such assemblies last for long enough, usually fraction of seconds, to accomplish an elementary cognitive act. The synchronisation takes place in several spatial scales, ranging from individual neuronal groups to a set of neuronal groups located across different brain hemispheres.

The root of the approach that privileges synchrony as being functionally relevant to neural functions dates back to von der Malsburg (1981) who pointed out a deficiency in existing brain theory – how integration occurs among functionally distinct brain areas – and discussed at a conceptual level how to fill this gap. He proposed that fast synaptic modulation is the mechanism through which functionally different active cells become integrated and express the whole set of different features of an external object; the integrated cells are defined by their synchrony activity in a temporal fine structure of [2,5] msec. resolution. Since then, von der Malsburg's hypothesis has been extended and empirically tested; some experiments and variations of his idea are presented bellow.

Synchronization in the visual cortex: the visual binding problem

The first evidence supporting von der Malsburg's hypothesis came from empirical studies of integration in the visual cortex, a research field denoted as *the visual binding problem* (Eckhorn et al., 1988; Gray and Singer, 1989; Engel et al., 1990; Roskies, 1999). This problem can be stated as follows: "how are the different attributes of an object brought together in a unified representation given that its various features (edges, color, motion, texture, depth and so on) are treated separately in specific visual areas?" (Varela et al., 2001, p.231). By carrying out multiunit recordings on the primary visual cortex Gray et al. Gray and Singer (1989) found the presence of gamma oscillations in the local field potential (LFP) and the synchronised activity of adjacent neurons. These findings suggested that oscillations, defined as recurrent synchronous spiking bursts of neuronal groups[1], could be the building blocks for cortical representations, and synchronisation could be the mechanism for binding spatially separated neuronal groups Engel et al. (1992).

[1]See Burns et al. (2010) for a study comparing oscillations in local field potential and spiking activity measured by multiunit recordings.

Following up the discovery of oscillations in individual neuronal groups using multiunit recordings, researchers found stimulus-evoked synchronised oscillations among different neuronal groups in the primary visual cortex of anaesthetized and awake cats by recording neural activity using multiple electrodes (Gray and Singer, 1989; Engel et al., 1990). Besides that, at a higher spatial resolution, synchronised oscillations were also observed among primary, secondary and associative areas of the visual cortex (Eckhorn et al., 1988) and also among visual cortex areas in both cerebral hemispheres (Engel et al., 1991a).

Coexistent assemblies of synchronised activity were also observed among neuronal groups in the primary visual cortex when two independent stimuli were presented at the same time to anaesthetized cats. This result indicates that scene segmentation and integration of the features of an individual object might be accomplished by the formation of transiently synchronised assemblies (Engel et al., 1991b; Gray, 1999).

Synchronization across the brain

At a larger scale neural synchrony has also been found and hypothesized as the binding mechanism of neuronal groups spatially distributed in the cortex – not only the visual ones – of animals (Bressler et al., 1993; Roelfsema et al., 1997) and humans (Rodriguez et al., 1999) performing a motor behaviour according to the perception of sensory stimuli. Roelfsema et al. (1997), for instance, trained a cat to either press or release a lever according to the rotation of a grating presented on his visual field. They found that synchronised activity was higher when the animal was engaged in the task (paying attention to the grating, pressing and releasing the lever) than when it was being rewarded or at rest. They also observed that the pattern of synchronised activity among visual areas changed when the stimulus switched from stationary to moving grating. These results indicate that synchronisation patterns are correlated to perception of visual stimuli and functional behaviour.

In another early experiment, Bressler et al. (1993) trained a macaque monkey to coordinate its motor response (either releasing or keeping depressed a lever with its hand) according to visual stimuli (lines and diamonds) and recorded the local field potential at 15 sites in one cortical hemisphere. Regarding the synchronisation activity, they observed that a) during the perception of the visual stimulus, which was $\approx$[100,250] ms after the stimulus onset, there was a high level of frequency correlation between the striate and parietal cortex; and b) during the motor response the correlation was higher when the monkey released the lever than when keeping it depressed. These results also indicate that visual

stimuli and motor coordination are correlated with synchronised neural activity.

In humans, Rodriguez et al. (1999) analyze how gamma oscillations relate to synchronisation by recording scalp EEG signals of a subject performing a cognitive task. In the task a subject coordinates his/her motor movements by pressing one of two buttons with different fingers in order to indicate either 'perception' or 'no-perception' of a face in an image presented to him/her (upright and upside-down Mooney face). On average, each trial took ∼1 sec. from the stimulus onset and with the subjects pressing either buttons at ∼800 ms. For both 'perception' and 'no-perception' trials, oscillations in gamma frequency were spatially homogeneous and presented two peaks at ∼200 and ∼800 ms with a small difference in amplitude. Despite similarities in gamma frequency, the synchronisation dynamics were different. While during 'perception' trials the signals presented two synchronisation patterns at ∼200 and ∼800 ms, respectively; during 'no-perception' trials a synchronisation pattern emerged only during motor commands at ∼800 ms. According to the authors these findings show that: a) the presence of gamma oscillations do not indicates synchronised activity; and b) only face perception, as opposed to meaningless images, correlates to a synchronised pattern.

The aforementioned works represent a small sample of early research favouring synchrony as a fundamental property of neural oscillations underlying cognitive phenomena. Since then, different methods of analysing synchrony have been proposed and empirical evidence has been found (Rilk et al., 2011; Perfetti et al., 2011). Hipp et al. (2011), for instance, provide further evidence supporting the existence of dynamic functional large-scale synchronised networks in human beings underlying cross-modal perception. They developed an unbiased methodological framework to identify such networks and applied it to analyse EEG signals recorded from a subject performing a cognitive task. The task consists of a subject who is presented to an identical ambiguous audiovisual stimulus of two vertical bars approaching each other, overlapping and then moving apart with a click sound played at the overlapping moment. The subjects indicated whether after the click sound they perceived bars crossing one another or bouncing off each other. They showed the presence of transiently synchronised oscillatory network at beta and gamma frequencies across distributed brain areas and also found that the magnitude of synchronisation in the beta and gamma networks could predict the subject's perception (bounce or pass trials); particularly, the bounce trials presented more cross-modal integration than pass trials.

This section has presented some empirical experiments that focus on the analyses of

neural oscillations in relation to sensory and motor activities. The next section presents a theoretical framework and some computational tools to study oscillatory systems.

2.3 Computational models to study oscillatory dynamics

Oscillatory dynamics at different spatial and temporal scales in neural systems is a complex dynamic phenomenon. Computational models can help deal with this complexity by providing theoretical insights to explain the generative mechanisms underlying oscillations, by allowing the modeller to more easily test the behaviour of the system under different parameter configurations and by allowing hypotheses and predictions about the behaviour of the real system to be raised. This section presents some computational models that have been developed to investigate oscillatory dynamics. Specifically, section 2.3.1 presents the HKB equation which is a computational model developed within the Coordination Dynamics framework. This model has been developed to investigate the coordination of oscillatory components at undetermined level of abstraction and has provided many theoretical insights about neural functioning. Section 2.3.2 presents the Kuramoto model of phase-coupled oscillators, a mathematical model that has been extensively used to study the behaviour of oscillatory systems.

2.3.1 The Coordination Dynamics framework

Coordination dynamics is a consistent framework which can be used to investigate the neural oscillatory temporal structure underlying sensorimotor behaviour. It was proposed and developed by Kelso (1995) based on Haken's work on synergetics (Haken, 1978) and combines experiments and theoretical models formulated mathematically to study how oscillatory components of a system interact and produce coherent coordination patterns. This framework is aimed at studying the coordination of living systems acting in their environments and can be applied to describe the interaction of oscillatory components at different levels of observation. For instance, it offers a means to relate the coordination dynamic of parts of the brain to the stimuli and responses given by a living system interacting with its environment (Kelso, 1995; Jirsa and Kelso, 2004). As Kelso and Jirsa put it:

> Coordination dynamics - the science of coordination - describes, explains and predicts how patterns of coordination form, adapt, persist and change in natural systems. [...] [It] seeks to identify laws, principles and mechanisms

> underlying coordinated behavior in different kinds of system at different level of description. [...] [It] aims to characterize the nature of the coupling within a part of a system (e.g. the firing of cells in the heart or neurons in a part of the brain), between different parts of a system (e.g. parts of the brain, parts of the body, members of an audience) and between different kinds of systems (e.g. stimuli and responses, organisms and environments, perception and action, etc.). Ultimately Coordination dynamics is concerned with how things come together in space and time, and how they split apart (Jirsa and Kelso, 2004, p.VIII).

The main illustrative model for the Coordination Dynamics framework is that described by the HKB equation (Haken-Kelso-Bunz) which captures the temporal relation between the activity of coupled oscillatory elements (Haken et al., 1985). This model was originally designed to replicate the type of phase relation dynamics observed in an empirical experiment involving rhythmic behaviour of human fingers. In this experiment a subject rhythmically moves his right and left index fingers in a horizontal plane at the same frequency of a pacing metronome. The HKB model replicates how the angle between the left and right fingers changes over time (the phase relation dynamics) given different initial conditions – fingers in-phase or anti-phase – and at an increasing metronome frequency (Kelso, 1995, p.46). This model was mainly used to explore the in-phase and anti-phase stable synchronisations, the transition between them, and their basins of attraction.

Later on, Kelso extended the HKB model by adding a parameter of symmetry-breaking in order to replicate a type of phase relation dynamic between non identical oscillatory components, *i.e.* components with different natural frequencies, which is a more realistic phenomenon in nature . As Kelso and Engstrm (2008) put it:

> After over 20 years of detailed study, it is probably time to put the more idealized HKB model of coordination to bed. It has served its purpose well. By explicitly showing that crucial observations about the stability and change of human behaviour could be understood in terms of self-organizing dynamical systems, the HKB model stimulated a great deal of empirical research and theoretical development. But biological coordination seldom deals with identical components and pure symmetry. The newer, still quite elementary version of the coordination law presented here [based on the extended model] not only is able to handle all the previously observed phenomena treated by the HKB model, it also embraces both symmetry and broken symmetry (symmetry

creating symmetry breaking) and leads to altogether novel effects and totally unexpected consequences, both of a scientific and epistemological nature.

One of the main properties of this model is the existence of *metastable dynamics* where the variable representing the temporal relation (*i.e.* phase relation) constantly moves in a transient dynamics through regions of the phase space with low potential energy (representing moments of transient synchronisation) followed by regions with high potential energy (representing moments of desynchronisation) and without settling down in point attractors (representing moments of stable synchronisation). The equation governing the dynamic of the relative phase is presented in Eq. (2.1).

$$\dot{\phi} = \delta\omega - a\ sin\ \phi - 2\ b\ sin(2\phi) \tag{2.1}$$

where ϕ is the phase relation between two interacting oscillatory components; $\delta\omega$ is the intrinsic difference between oscillators (parameter of symmetry-breaking); a and b are the coupling strength. The graphic in Fig. 2.2 depicts the stable and unstable points of the phase relation and its derivative for different values of $\delta\omega$ and constant coupling (a=1; b=1). Observe that, for small values of the intrinsic difference between the components ($\delta\omega$), the system is multistable with stable points ($\dot{\phi} = 0$) near the in-phase ($\phi = 0$) and anti-phase ($\phi = \pi$). These points define regions where the oscillators are stable synchronised. As the intrinsic difference increases the fixed points move and eventually disappear. As the parameter of symmetry breaking increases and crosses a threshold ($\delta\omega > 3$), the phase relation no longer presents fixed points and the relative phase engages in a metastable dynamical regimes with moments of metastable synchronisation in the regions where the stable points ($\dot{\phi} = 0$) used to be. A numerical analysis of this equation for a specific set of parameters will be presented in Chapter 5.

Bressler and Kelso (2001) describe the presence of metastable dynamical regimes of phase relations in oscillatory brain signals by recording the LFP from up to 15 sites in one cortical hemisphere of a macaque monkey performing a visual discrimination task. They analyzed the density distribution function of phase relations between pairs of LFP signals and detected that two cortical sites transiently synchronised with phase relation near -54 degrees during the interval $[105, 155]ms$ after the stimulus onset. Apart from that time window, during the whole task ($[-70, 400]ms$) the same cortical sites did not present any other significant peaks on the distribution phase relations, which according to them indicates the functional involvement of these sites at a specific stage of the visual discrimination task. Other cortical sites presented different temporal patterns of coordination

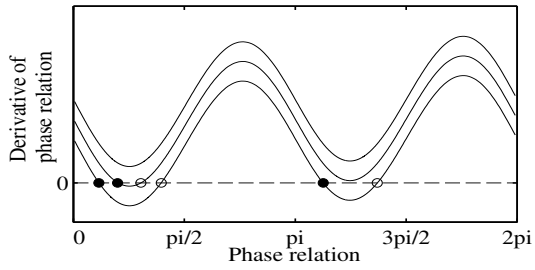

Figure 2.2: Schematic representation of the HKB equation attractor landscape. Each curve depicts the derivative of phase relation (y axis) throughout its state space (x axis) given 3 different values for the symmetry breaking parameter (lower, middle, and upper curves). Stable points are represented by filled circle and unstable ones by open circles. The phase relation dynamics changes from multistable (lower curve) to monostable (middle curve) and eventually metastable (upper curve).

presumably reflecting different functional involvement during the task.

Besides the metastable dynamic depicted by this model, *coordination variable* and *control parameter* are also important concepts in the coordination dynamics framework. A *coordination variable* is an "upper level" variable which captures the collective dynamics of "lower level" interacting components; in Eq. (2.1) it is represented by the relative phase ϕ. In Haken's framework this variable is denoted as *order parameter*. A *control parameter* is a variable which qualitatively changes the collective dynamics of the system when a threshold is crossed. In Eq. (2.1) the *control parameter* can be either the coupling strengths (a, b) or the parameter of symmetry breaking $\delta\omega$. Two variables are *coordination variable* and *control parameter* when varying the latter leads to collective dynamic transitions which are captured by the former (Kelso, 2002, p.118)

Despite its simplicity, the extended-HKB has been capable of capturing the dynamics of different behavioural, neural and social coordination dynamics (Jirsa et al., 1998; Bressler and Kelso, 2001; Kelso et al., 2009) and still remains a paradigmatic example of dynamical and embodied cognitive science (Chemero, 2009). The region in the model where the system is metastable is of particular interest as in it the system achieves a compromise between the intrinsic dynamics of its individual oscillators and the global dynamics of the network, allowing for a flexible trade-off between segregation and integration (the hallmark of brain complexity (Tononi and Edelman, 1998)) and for the emergency of transiently synchronised networks.

2.3.2 The Kuramoto model of phase-coupled oscillators

Kuramoto phase-coupled oscillators (Kuramoto, 1984) have been used to study biological phenomena of collective synchronisation such as pacemaker cells in the heart, circadian pacemaker cell in the brain and flashing fireflies (Strogatz, 2000a). They are based on a previous model of coupled oscillators proposed by Winfree (1967, 1980) that describes the dynamics of oscillators with different natural frequencies interacting by a function representing their sensitivity to the phase of each other. The dynamics of each Kuramoto's oscillator is governed by the equation defined in (2.2) (Kuramoto, 1984):

$$\dot{\theta}_i = \omega_i + \sum_{j=1}^{N} k_{ji} sin(\theta_j - \theta_i) \tag{2.2}$$

where θ_i is the phase of the i^{th} oscillator, ω_i is the oscillator's natural frequency, N is the number of oscillators in the network, and k_{ji} is the coupling factor from the j^{th} to the i^{th} oscillator. Notice that this equation does not describe the oscillatory signal itself, but its phase dynamics. Networks of Kuramto's oscillators have been studied under different configuration, such as a scale-free topology (Moreno and Pacheco, 2004), with time delays (Yeung and Strogatz, 1999), with discrete time and delays (Triplett et al., 2006). They have been used to explore mechanisms underlying oscillations in the human cortex (Breakspear et al., 2010) and different aspect of brain dynamics such as self-organized criticality (Kitzbichler et al., 2009).

Kuramoto oscillators have also been used with evolutionary robotics to study the role of neural synchronisation for embodied cognitive behaviours (Moioli et al., 2010, 2012). Moioli and colleagues have studied the effects of different degrees of coupling in the agents oscillatory neural network, which encourages more or less synchrony in the network dynamics, on the performance of the agent's behaviour, and the circumstances in which more (or less) synchrony is better suited to the generation of adaptive behaviour. Kuramoto oscillator based models will be studied in Chapters 3 and 4.

2.4 Summary

The temporal structure of neural oscillations at different temporal and spatial scales (e.g. synchrony, interspike interval) has been providing dynamical explanations of brain functioning underlying sensory and motor activities. Such explanations have been proposed based on the basis of empirical experiments – as explained in section 2.2 – and computational models – as explained in section 2.3. In this thesis we develop minimal models

of oscillatory networks controlling an agent performing minimal cognitive tasks (e.g. a gradient climbing behaviour) and explore i) the information and causal relevance of the oscillations in relation to the agent's sensorimotor loop (chapters 3 and 4) and ii) how the temporal structure of the oscillations interact (in terms of dynamics) with the agent's sensorimotor loop (chapters 4, 5 and 6). The models do not target any specific level of abstraction; i.e. the oscillators do not describe the dynamics of a single neuron nor of a neuronal group; our purpose is to develop theoretical models that allow us to raise theoretical issues about neural oscillations in the context of situated, embodied cognitive behaviour.

Chapter 3

Synchrony and phase relation dynamics underlying sensorimotor coordination

3.1 Introduction

Synchronous oscillations have been hypothesized to be a mechanism of large-scale integration and communication that allows the brain areas to coordinate their activity giving rise to coherent behaviour and cognition (von der Malsburg, 1981; Gray and Singer, 1989; Engel et al., 1990; Tononi and Edelman, 1998; Fries, 2005; Uhlhaas et al., 2009; Pockett et al., 2009; Singer, 2011; Hipp et al., 2011), as stated by Varela et al. (2001):

> "The experimental evidence consistently shows that synchronous networks emerge and disappear in waves that last 100−300 ms; these transients represent a meaningful temporal scale of brain operation." (p.237)

> "There is some evidence that phase synchronisation is accompanied by phase scattering in other bands or between different neuron pairs. We suggest that this novel observation is crucial for the understanding of large-scale integration, which must implicate not only the establishment of dynamic links, but also their active uncoupling to give way to the next cognitive moment." (p.237)

Desynchronisation is then left with the role of undoing the preceding "meaningful" synchronised cluster for the emergence of the next one. Such a role is also mentioned

by Rodriguez et al. (1999): "transition between two distinct cognitive acts (such as face perception and motor response) should be punctuated by a transient stage of undoing the preceding synchrony [by active desynchronisation] and allowing for the emergence of a new ensemble" (p.432).

It is undeniable that research in oscillatory neurodynamics has made significant progress in understanding brain operation by focusing on synchrony. In this work, however, we focus on desynchronous oscillations comparing its relevance to synchronous ones. In particular, we address the questions: a) how does the informational content of the sensorimotor activity present in a complete dynamical description of phase relations change as such a description is reduced to the dynamics of synchronous oscillations? and b) to what extent are desynchronous oscillations as causally relevant as synchronous ones to the generation of functional sensorimotor coordination? These questions are addressed with a model of a simulated agent performing a functional sensorimotor coordination task controlled by an oscillatory network.

The results suggest that: i) desynchronised phase relations carry as much information about sensorimotor activity as synchronised ones; and ii) phase relations between oscillators with near-zero frequency difference carry a relatively higher causal relevance than the rest of the phase relations to the sensorimotor coordination; however, overall a privileged functional causal contribution can not be attributed to either synchronous or desynchronous oscillations. The analyses of these questions contribute to the understanding of oscillatory dynamics underlying sensory and motor activities and provide theoretical insights to works that attribute a privileged explanatory status to synchronous oscillations over desynchronous ones.

The next section formalises the concepts of *complete* and *reduced* dynamical descriptions of an oscillatory network. This formalization will make clearer the problem and methods approached in this chapter. The following up sections present the computational model, analyses, results and conclusions.

3.2 Complete and reduced dynamical descriptions

Consider a network of N phase-coupled oscillators where the periodic phase θ_i of an oscillator i is given by $\theta_i(t) = f_i(\theta_1, \theta_2, ..., \theta_N)$. The phase relation dynamics between two oscillators i and j can be analysed by the absolute value of their phase difference, as shown in Eq. (3.1):

$$\phi_{i,j}(t) = |\theta_i(t) - \theta_j(t)|\,, \tag{3.1}$$

where $\phi_{i,j}(t) \in R : [0, 2\pi)$ radians and represents how the phase relation between i and j is changing over time. A complete dynamical description of an oscillatory network is given by the phase relations between all oscillatory components, as shown in (3.2), where P is a vector function containing all the dynamics of phase relations between all pairs of oscillators i and j.

$$P(t) = \langle \phi_{1,2}(t), \phi_{1,3}(t), ..., \phi_{i,j}(t) \rangle \,, \tag{3.2}$$

Before presenting the reduced dynamical description of P, we discuss two approaches to study synchronisation, namely *zero-lag synchronisation* and *phase synchronisation*. While in the former oscillators are said to be synchronised only when they are phase-locked at zero (or near zero) radian, in the latter synchronisation takes place when oscillators are phase-locked at any phase. Formally, we can say that i and j are *zero-lag synchronised* if $\dot{\phi}_{i,j} = 0$ and $\phi_{i,j} = 0$; and *phase synchronised* if $\dot{\phi}_{i,j} = 0$ and $\phi_{i,j} = c_p$, where c_p is a constant $\in [0, 2\pi)$ radians. Note that zero-lag synchrony is only a particular case of phase-synchronisation. An important difference between these approaches is that π-phase-locked oscillators (*i.e.* $\dot{\phi}_{i,j} = 0$ and $\phi_{i,j} = \pi$) are considered completely desynchronised in the zero-lag synchronisation approach and completely synchronised in the phase synchronisation one. Oscillators could also be considered synchronised when their frequency ratio is constant (e.g. $\Omega_i = 10Hz$ and $\Omega_j = 20Hz$ with frequency ratio 1:2); which, in this case, $\phi_{i,j}$ linearly changes over time. In our work we consider that a pair of oscillators is synchronised when their frequency ratio is 1:1 and when they are phase locked at any phase $\phi_{i,j} = c_p$, which is the most studied case of synchrony in the brain (Varela et al., 2001). For more details about synchrony see (Pikovsky et al., 2003; Strogatz, 2000b, p.96).

Given this definition of synchrony, a simple dynamical description that represents how clusters of synchronised oscillators change over time can be defined as in (3.3).

$$S_a(t) = \langle x_{1,2}(t), ..., x_{i,j}(t) \rangle; \; x_{i,j}(t) = \begin{cases} 1 & if \; \dot{\phi}_{i,j}(t) \leq t_s \\ 0 & otherwise, \end{cases} \tag{3.3}$$

where S_a represents how the synchronised state between each pair of oscillators is changing over time; $x_{i,j}(t)$ is a step function which gives 1 when i and j are phase synchronised and 0 otherwise. Notice that the synchronised condition has been changed from $\dot{\phi}_{i,j}(t) = 0$ to $\dot{\phi}_{i,j}(t) \leq t_s$. The parameter t_s is a threshold for $\dot{\phi}_{i,j}(t)$ up to which two oscillators are considered synchronised. This relaxation of the strict $\dot{\phi}_{i,j}(t) = 0$ condition for synchrony better represents what is generally considered synchronisation between neural oscillators.

The vector function S_a is a reduced dynamical description of P that only informs whether a pair of oscillators is either synchronised or not. A richer description of the synchronised oscillations would contain the phase relation dynamics during moments of synchronisation; *i.e.* it would contain the actual phase relation ϕ when $\dot{\phi}_{i,j} \leq t_s$, as shown in Eq. (3.4).

$$S_b(t) = \langle y_{1,2}(t), ..., y_{i,j}(t) \rangle;\ y_{i,j}(t) = \begin{cases} \phi_{i,j}(t) & if\ \dot{\phi}_{i,j}(t) \leq t_s \\ shuffle & otherwise, \end{cases} \tag{3.4}$$

where S_b is the vector function containing the phase relation dynamics between all synchronised oscillators. If the oscillators i and j are synchronised then the vector function contains their phase relations – *i.e.* if $\dot{\phi}_{i,j}(t) \leq t_s$, then $y_{i,j}(t) = \phi_{i,j}(t)$. On the other hand, when the oscillators i and j are desynchronised during a time window T – *i.e.* $\dot{\phi}_{i,j}(t) > t_s \forall\ t \in T$ –, their actual values of phase relations $\phi_{i,j}$ during T – *i.e.* $\phi_{i,j}(T)$ – will be shuffled. The shuffling algorithm picks each value of phase relation in T and swaps it with another one from a random position in T. The lack of information about the phase relation dynamics – or the reduced descriptions of phase relations – is then modelled by shuffling the actual values of phase relation $\phi_{i,j}$. By doing that, potential correlations between the $\phi_{i,j}$ and any other time series are removed; this will be important for measuring how the informational content of a reduced dynamical description changes in relation to a more complete one.

Both vector functions S_a and S_b are particular ways to represent how the core of synchronised oscillators are changing over time. While S_a is a sharp reduction, S_b can be continuously reduced by decreasing the parameter t_s. Notice that if t_s is greater or equal than the maximum value of $\dot{\phi}_{i,j}$ in a time window T then the content of S_b is equal to P.

3.3 Theoretical model and methods

We present an evolutionary robotic model that performs phototaxis controlled by a network of 5 phase-coupled Kuramoto oscillators.

Phototaxis requires the agent to approach a light source from different starting positions and can be taken as a paradigmatic example of a minimal (yet not completely trivial) "goal-directed" sensorimotor coordination task. It was chosen for simplicity as a minimal coordination task where the problems considered in the previous section could be addressed.

3.3.1 The agent and its network of coupled oscillators

The model consists of a two-dimensional simulated environment, an agent and a light source. The agent's movement is controlled by a network of phase-coupled oscillators which receives signals from two sensors and controls the activation of two motors. The agent has a circular body of 5 units diameter; two sensors s_1 and s_2 separated by $120\,^\circ \pm 10\,^\circ$ and whose output signal is given by $s_q = e^{-0.04 d_q}$, where q represents each sensor, and d is the distance from sensor q to the light source. The agent has two diametrically opposed motors m_1 and m_2 whose activation is given by (3.5) and (3.6), respectively.

$$m_1 = (sin(\theta_4 - \theta_3) + 1)/2 \tag{3.5}$$

$$m_2 = (sin(\theta_5 - \theta_3) + 1)/2 \tag{3.6}$$

where θ_n is the phase of the oscillator n. The agent's behaviour is controlled by a network of five phase-coupled oscillators (Kuramoto, 1984), defined in Eq. (3.7):

$$\dot{\theta}_i = (\omega_i + s_q w_{qi}) + \sum_{j=1}^{N} k_{ji} sin(\theta_j - \theta_i), \tag{3.7}$$

where θ_i is the phase of the i^{th} oscillator which is integrated with time-step 15 ms. using the Euler method, ω_i is the oscillator's natural frequency (range for the genetic algorithm [9, 18] hertz), s_q is the q^{th} sensory signal (out of 2), w_{qi} is the sensory input strength from the sensor q^{th} to the oscillator i^{th} (range [1,20]), N is the number of oscillators (here 5), and k_{ji} is the coupling factor from the j^{th} to the i^{th} oscillator with $k_{j,i} = 0 \; \forall \; i = j$ (range [0,20]). The sensors s_1 and s_2 are connected to the oscillators θ_1 and θ_2, respectively; the other oscillators do not receive sensory signals.

3.3.2 Optimization with a genetic algorithm

A total of 27 network parameters encoded in a genotype as a vector of real numbers in the range [0,1] (linearly scaled, at each trial, to their corresponding range) were evolved using the *microbial genetic algorithm* (Harvey, 2001). There is no specific reason why this algorithm was chosen; the system is relatively simple and could have been optimized with other genetic algorithms. The genetic algorithm setup is: population size (80); mutation rate (0.05); recombination (0.60); reflexive mutation; normal distribution for mutation $\left(\mu = 0, \sigma^2 = 0.1\right)$; trial length (180 s); and trials for each agent (30). At the end of the

30^{th} trial the worst fitness (out of 30) is used as the selective fitness of the agent. The fitness function is defined by (3.8):

$$F = \begin{cases} 1 - \frac{d_f}{d_i}; & if\ d_f < d_i; \\ 0; & otherwise; \end{cases} \tag{3.8}$$

where F is the fitness; d_i and d_f are the initial and final distances to the light source, respectively. The analysis of the model is done using the fittest agent found by the genetic algorithm.

It was possible to optimized the parameters of the system in order to obtain an agent doing phototaxis using 3 and 4 oscillators. However, the dynamics obtained using less oscillators were not adequate to analyse the relevance of desynchronised oscillations as most of the time the oscillatory network was completely synchronised. Specifically, while the agent was approaching the light the oscillators were totally synchronised and while it was moving around the light there were some short time windows of desynchronised oscillations.

3.3.3 Methods of analysis

Our first problem is to analyse how the information about the sensorimotor dynamics in the oscillatory network changes as the description of phase relations is reduced. The agent's sensorimotor dynamics is given by a vector function shown in (3.9).

$$SM(t) = \langle s_1(t), s_2(t), m_1(t), m_2(t) \rangle\,, \tag{3.9}$$

where SM is the sensorimotor activity, s_1, s_2, m_1 and m_2 are the agent's sensors and motors. We are interested in analysing how the mutual information between SM and S_b changes as the threshold t_s decreases; *i.e.* $I(SM, S_b)$ for different values of t_s. As both time series are multidimensional, the mutual information will be measured between pairs of components from each time series – *e.g.* $I(SM(s_1), P(\phi_{1,2}))$ and $I(SM(m_2), P(\phi_{3,4}))$.

The analysis is done by using the standard measures of *entropy* and *mutual information* from information theory, as described in (5.5) and (5.6), respectively (Shannon, 1948; Cover and Thomas, 2005).

$$H(X) = -\sum_{i=1}^{N} p(x_i) log_b(x_i), \tag{3.10}$$

where X is a set of discrete random variables and $p(x_i)$ is the probability mass function

of the outcome x_i.

$$I(X;Y) = H(X) + H(Y) - H(X,Y), \tag{3.11}$$

where $H(X)$, $H(Y)$ are the entropies of the sets X and Y, respectively, and $H(X,Y)$ is the joint entropy of both sets. The entropies are measured based on a time window T of 6 seconds length. In order to obtain more robust measures of the probability distributions all time series are linearly interpolated from a time-step of 15 ms (Euler step integration of the simulation) to 1 ms. In this way, a time window of 6 seconds length contains 6000 points. In order to define the length of T the probability distributions of all individuals and pairs of components – *e.g.* $H(s_1)$ and $H(m_1, \phi_{3,4})$ – were measured using different lengths from 100 ms to 7.0 s. Due to the stationarity of the time series the distributions do not change for time windows greater than 5.0 seconds. By shifting the time window T we capture how the entropies change as the agent interacts with the environment. As the values of phase relations $\phi_{i,j}$ are continuous in the interval $[0, 2\pi)$ they are discretized into 50 equally spaced bins. The sensors and motors are also discretized into 50 equally spaced bins according to their minimum and maximum value within each time window T.

The second problem we are interested in studying is the causal relevance of the information transferred during desynchronised $\dot{\phi}_{i,j} > t_s$ and synchronised $\dot{\phi}_{i,j} \leq t_s$ oscillations for the generation of functional sensorimotor dynamics SM. The causal relevance is analysed by perturbing the information transferred in either of the conditions $\dot{\phi}_{i,j} > t_s$ or $\dot{\phi}_{i,j} \leq t_s$ and measuring the functionality SM using the fitness function in (3.8). More details about this problem will be presented during the presentation of the results.

3.4 Results

The results are divided into three main parts. In the first one, the dynamical analyses of SM, P, S_a, and S_b are presented. In the second one, the analysis of mutual information between SM and the reduced descriptions of phase relations S_b is shown. In the third one, the causal relevance of synchronisation and desynchronisation for the generation of functional SM is analysed.

3.4.1 Dynamical analyses

Sensorimotor dynamics (SM)

Fig. 3.1 shows the agent's trajectory during a single trial of phototaxis. During $T_1 = [50, 55]$ s the agent's trajectory is characterized by a movement towards the region of highest light intensity at an average linear speed of 0.76 units/s and slowly turning to the right at an average angular speed of 5.2 deg/s (not shown in the graphic). In $T_2 = [90, 95]$ s the agent is returning to the region of highest light intensity at an average linear speed of 0.62 units/s and turning to the left at an average angular speed of 12.7 deg/s. The sensorimotor dynamics SM for the time windows T_1 and T_2 are presented in Fig. 3.2 and will be referred to as SM_{T1} and SM_{T2}, respectively.

In the next subsections the oscillatory dynamics underlying SM_{T1} and SM_{T2} are analysed. These time windows were chosen to represent two reasonably well separated periods in the overall behaviour and to reflect the two main 'phases' of the behaviour (approaching the light from a distance and then moving around it). There is nothing particularly special about these two periods, the main purpose is only to present the dynamical descriptions on P, S_b S_a manifolds underlying two moments of the agent's sensorimotor coordination during a trial of phototaxis.

Phase relation dynamics (P)

We shall start by presenting the complete phase relations of a single pair of oscillators (see Fig. 3.3). The transient synchronisation between θ_1 and θ_5 takes places at different phases during different periods, namely: $T_{1a} = [-48, -33]$, $T_{1c} = [33, 40]$ and $T_{2a} = [-26, 11]$ degrees, as shown in the graphics **A** and **C** or **B** and **D** (Fig. 3.3).

In dynamical system terms, we can say that the attractor landscape of $\phi_{1,5}$ during SM_{T1} has low potential energy at [-48, -33] and [33, 40] degrees and during SM_{T2} these regions of low potential energy collapse into a single one around [-26, 11] degrees. The difference in the attractor landscape is represented in graphic E (Fig. 3.3); where: a) positive values represent regions that have had their potential energy decreased ($[-26, 26]$) and became more attracting; b) negative values represent regions that have had their potential energy increased ($[-70, -26]$ and $[26, 70]$) and lost their attraction; and c) values near zero represent regions that did not have a significant change on their potential energy.

As P has ten dimensions, we use density distributions, as shown in Fig. 3.3-B and D, to show statistical properties of the components in P (see Fig. 3.4). The lower the entropy (shown on the top of the graphic) the longer the oscillators i and j (x-axis) keep

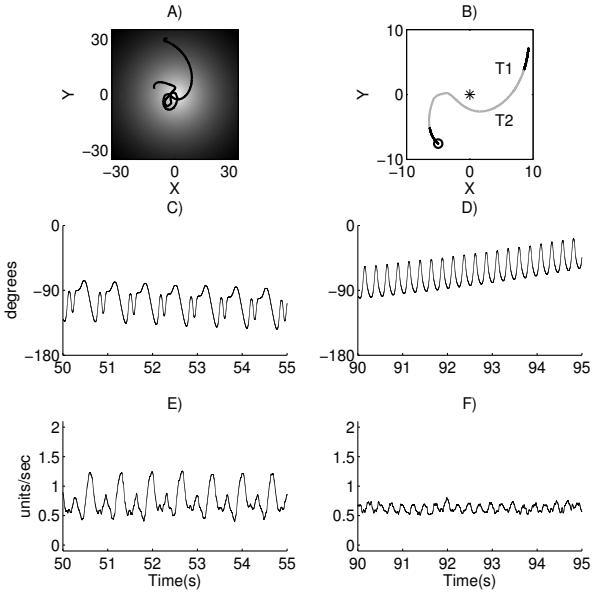

Figure 3.1: **Graphic A** shows an agent's trajectory in the environment during its lifetime (180 seconds). The light intensity throughout the environment is represented by the grey scale, where the whiter the area the higher the light intensity. The agent moves towards the region of highest light intensity (position X=0, Y=0) and then starts moving around it. **Graphic B** zooms into the agent's trajectory during t=[50,95] s;. The star at X=0 and Y=0 indicates the position of highest light intensity. The highlighted black trajectories indicate the agent's trajectory during two short time windows of 5 seconds: T_1=[50,55] s and T_2=[90,95] s. **Graphics C and D** show the angle of the agent's body in T_1 and T_2, respectively. The agent's body continuously oscillates to the right and left following different patterns at each time window. **Graphics E and F** show the agent's average linear speed for a moving time window of 200 ms in T_1 and T_2, respectively. The agent's average linear speed is 0.76 units/s in T_1 and 0.62 units/s in T_2.

synchronised at a particular phase indicated by peaks in the density distribution (the whiter areas of the graphics). In other words, the lower the entropy the smaller the potential energy at the phase relations represented by whiter areas.

Some differences between the phase relation dynamics underlying SM_{T1} and SM_{T2} are: a) while in SM_{T1}, $\phi_{1,2}$ is relatively spread ($H_{(\phi_{1,2})} = 0.81$) across $\approx [0, 90]$, in SM_{T2} it has a higher phase coherence ($H_{(\phi_{1,2})} = 0.34$) within $\approx [30, 60]$; b) while in SM_{T1}, $\phi_{2,3}$ is relatively spread ($H_{(\phi_{2,3})} = 0.82$) across $\approx [50, 140]$, in SM_{T2} it is concentrated ($H_{(\phi_{1,2})} = 0.34$) within $\approx [85, 115]$. Note that though both pairs of oscillators (θ_3,θ_4) and (θ_3,θ_5) that send signals to the motors have low phase coherence (indicating low level of

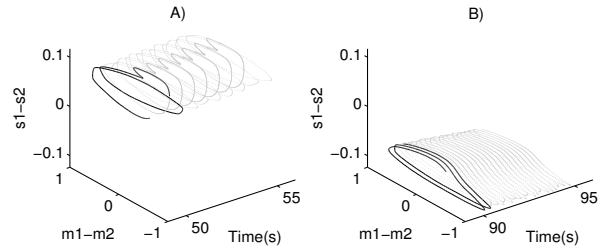

Figure 3.2: **Graphics A and B** show the sensorimotor dynamics $SM(t) = (s_1(t), s_2(t), m_1(t), m_2(t))$ during T_1 and T_2. The x-axis shows the time in seconds, the y-axis shows the difference in activation of the right and left motors $(m_1 - m_2)$ and z shows the difference in activation of the right and left sensors $(s_1 - s_2)$. The black trajectories in both graphics highlight the first 600 ms of each time window.

synchrony) – as shown by high entropies $H_{(\phi_{3,4})} = 0.97$ and $H_{(\phi_{3,5})} = 0.94$ in SM_{T1} and $H_{(\phi_{3,4})} = 0.93$ and $H_{(\phi_{3,5})} = 0.90$ in SM_{T2} – the agent's behaviour is still completely functional.

Synchronization dynamics (S_b)

The multidimensional synchronisation dynamics S_b is also shown for the single pair of oscillators θ_1 and θ_5, see Fig. 3.5. The synchronisation dynamics were generated for a threshold $t_s = 15$ rad/s (see Eq. 3.3), meaning that two oscillators are considered synchronised when their frequency difference is within $[-15, +15]$ rad/s or $[-2.39, +2.39]Hz$. During moments of desynchronisation – which can be interpreter as $\dot{\phi}_{1,5} > 15$ rad/s for this specific case – there is no information about how the phase relation is changing, shown by the shuffled phase relations in T_{1b} and T_{2b}. The oscillators get synchronised during T_{1a}, T_{1c} and T_{2a} with phase difference in between $[-48, -33]$, $[33, 40]$, $[-26, 11]$ degrees, respectively.

Notice that the density distributions are the same as those of the complete phase relations $P(\phi_{1,5})$ shown in graphics 3.4-B and D. This is important for the measure of mutual information as the shuffled data maintains the entropy of the time series and increases its joint entropy in relation to others. This guarantees that any variation in the mutual information between components of SM and S_b – *e.g.* $I(SM(s_1), S_b(\phi_{2,3}))$ – is caused by changes in their statistical correlations measured by the joint entropy (see Eq. 5.6).

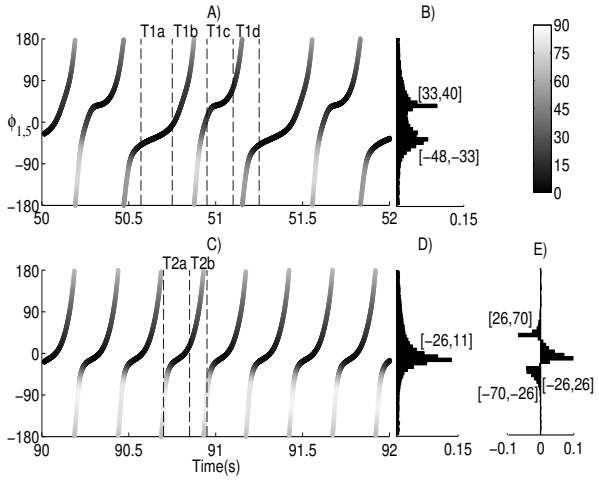

Figure 3.3: Phase relations between θ_1 and θ_5 ($P(\phi_{1,5})$) underlying sensorimotor regimes SM_{T1} (**graphic A**) and SM_{T2} (**graphic C**). The relation $\phi_{1,5}$ is shown in the y-axis and time in the x-axis. The color bar shows $\dot{\phi}_{1,5}$ in rad/s, where the darker the color the lower the derivative. For ease of description we highlight four small time windows during T_1: T_{1a}, T_{1b}, T_{1c} and T_{1d} of 180, 200, 150 and 150 ms, respectively (see dashed lines in graphic A) and other two time windows during T_2: T_{2a} and T_{2b} of 150, 100 ms, respectively (see dashed lines in graphic C). Note that the x-axis depicts only 2 s ([50,52]) rather than 5 s ([50,55]). While underlying SM_{T1} the phase relation $\phi_{1,5}$ has two regions where it slows down (see T_{1a} and T_{1c}); underlying SM_{T2} it has only one around 0 degree (see T_{2a}). This difference can be seen by the peaks of density distributions of $\phi_{1,5}$ shown in graphics **B** and **D**. These distributions were generated for the two-seconds time window [50,52] s and [90,92] s, respectively. **Graphic E** shows the difference between the density distributions shown in B and D.

Synchronization dynamics (S_a)

The synchronisation dynamics $S_a(t) = \langle x_{1,2}(t), ..., x_{4,5}(t) \rangle$ underlying SM_{T1} and SM_{T2} are shown in Fig. 3.6-A and 3.7-A. In T_{1a}, all five oscillators form a single synchronised cluster. At the end of T_{1a}, θ_4 and θ_5 start decreasing their real frequencies towards their natural ones ($w_4 = 10.9Hz$, and $w_5 = 10.6Hz$, not shown in the graphic). In T_{1b}, θ_4 and θ_5 no longer participate in the synchronised cluster, which now consists of θ_1, θ_2 and θ_3. At the end of T_{1b}, the frequency of θ_5 is increasing and, at the beginning of T_{1c}, θ_5 joins the synchronised cluster, which now consists of θ_1, θ_2, θ_3 and θ_5. The frequency of θ_4 starts increasing at the beginning of T_{1c} and during the second half of this time window it is $\approx 15Hz$, which is near the frequency of the others oscillators. In T_{1d} two synchronised

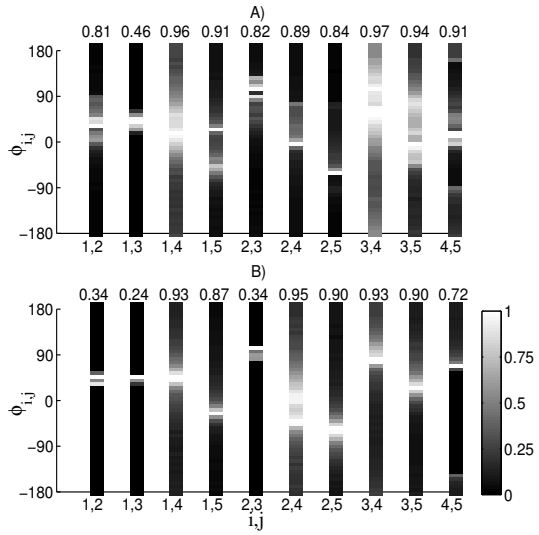

Figure 3.4: Density distribution $\phi_{i,j}$ for all pairs of oscillators (x-axis) during SM_{T1} (**graphic A**) and SM_{T2} (**graphic B**). Y axis shows the phase relation from -180 to 180 degrees. The grey scale (see color bar) represents the density of a particular phase relation (y-axis) between a pair of oscillators (x-axis). Data are normalized so that the densest phase for each $\phi_{i,j}$ is equal to 1. The space from -180 to 180 is divided into 50 equally spaced bins. The number on the top of the graphics represent the Shannon entropy of each distribution of phase relations normalized to 1 (see Eq. 5.5).

clusters emerge; the first one consisting of θ_1 and θ_3 at $[16, 20]Hz$ and the second one consisting of θ_4 and θ_5 (see their frequency regimes in graphic B). The oscillator θ_2 also joins the second synchronised cluster delayed by a small time lag (see the real frequency of θ_2 in graphic B). In this time window θ_2 leaves the area near its natural frequency ($w_2 = [14.5, 15.2]Hz$, not shown in the graphic) and joins the second cluster at a lower frequency ($\approx 10Hz$). At the end of T_{1d}, all oscillators synchronize again and a similar regime of transiently synchronised clusters (as in T_{1a}, T_{1b}, T_{1c} and T_{1d}) repeats over and over until the end of T_1.

The synchronisation dynamics underlying SM_{T2} is simpler than the one underlying SM_{T1} (see Fig. 3.7). In T_{2a}, all five oscillators form a single synchronised cluster with θ_4, θ_5 joining the assembly slightly delayed. In T_{2b}, θ_4 and θ_5 fall apart leaving the synchronised cluster with θ_1, θ_2 and θ_3. Similar regime of synchronisation (as in T_{2a}, T_{2b}) repeats over and over until the end of T_2.

In this section we have analysed the dynamics of the embodied oscillatory network underlying short intervals of the agent's sensorimotor coordination. It was presented three

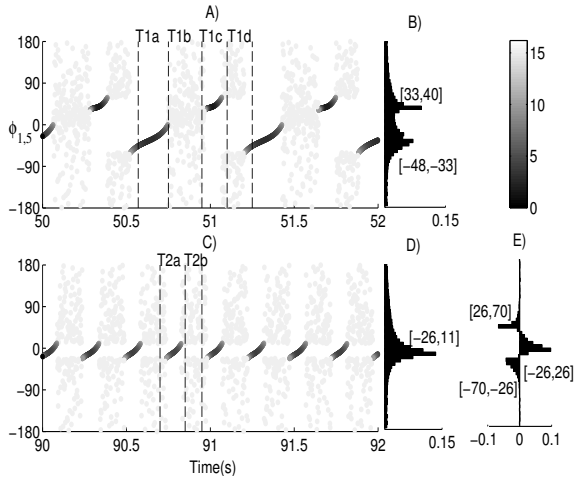

Figure 3.5: Synchronization dynamics for θ_1 and θ_5 ($S_b(\phi_{1,5})$) underlying sensorimotor regimes SM_{T1} (**graphic A**) and SM_{T2} (**graphic C**). The relation $\phi_{1,5}$ is shown in the y-axis and time in the x-axis. The color bar shows $\dot{\phi}_{1,5}$, where the darker the color the lower the derivative. Dashed lines highlight the small time windows T_{1a}, T_{1b}, T_{1c} and T_{1d} (graphic A) and T_{2a} and T_{2b} (graphic C). These graphics were generated for $t_s = 15$ rad/s. Disperse grey dots represent phase relations that were shuffled. The derivative $\dot{\phi}_{1,5}$ is greater than 15 rad/s during the entire time windows T_{1b} and T_{2b}. Graphics **B** and **D** show the density distribution of each regime of phase relation. Graphic E shows the difference on the density distributions.

dynamical descriptions of the oscillatory dynamics: P, S_a and S_b. The phase relation dynamics P provided a complete description of the oscillations, we have studied particularly $P(\phi_{1,5})$. The synchronisation dynamics S_b provided the dynamics during moments of synchrony and left out the information about the phase relations during moments of desynchronisation. The binary synchronisation dynamics S_a provided only the information of whether a pair of oscillators was either synchronised or not and left out the phase of synchrony. In the next section we analyse how the information present in S_b about SM varies as the value of t_s decreases.

3.4.2 Informational content in reduced descriptions of P

Fig. 3.8-A presents the individual entropies of the sensorimotor components s_1, s_2, m_1 and m_2. During the whole trial the entropies maintain around 5 and 5.5 bits with higher variations from 80 seconds, which corresponds to moment where the agent starts moving around the light. The mean entropies for each component over the whole trial are $\overline{H(s_1)} =$

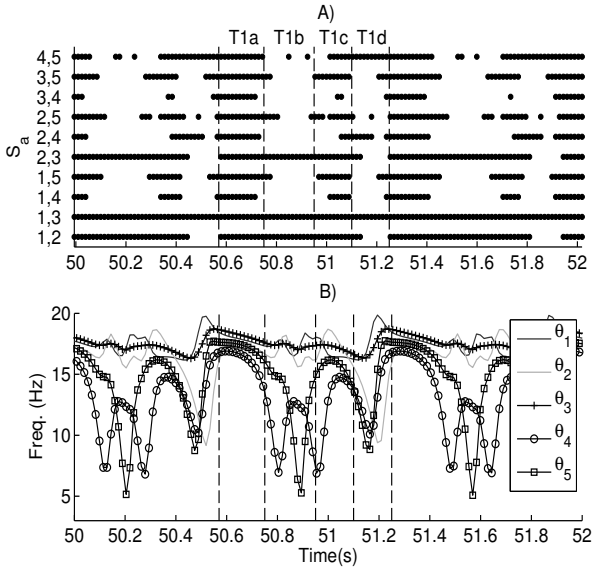

Figure 3.6: **Graphic A** shows the synchronisation dynamics for the multivariate time series S_a underlying SM_{T1}. The y-axis contains all pairs of oscillators and each black point in the graphic corresponds to a moment of synchrony. **Graphic B** shows the frequency dynamics of all 5 oscillators (see legend).

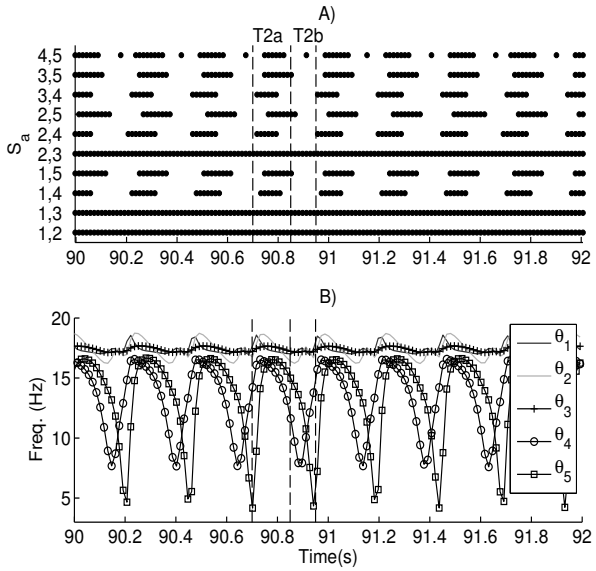

Figure 3.7: **Graphic A** shows the synchronisation dynamics S_a underlying SM_{T2}. Each black point corresponds to a moment of synchrony between the pair of oscillators depicted in the y-axis. **Graphic B** shows the frequency dynamics of all 5 oscillators (see legend).

5.34, $\overline{H(s_2)} = 5.38$, $\overline{H(m_1)} = 5.03$ and $\overline{H(m_2)} = 5.21$ bits (values not shown in the graphic).

The mutual information between a component from SM and another from the complete description P are presented in Fig. 3.8-B. Although the sensor s_1 has a mean entropy $\overline{H(s_1)} = 5.34$ bits, the highest mutual information between s_1 and the network phase relations is given by $I(SM(s_1); P(\phi_{5,4}))$ which has a peak of 1.74 bits at the beginning of the agent's lifetime – see the dark black line in graphic 3.8-B – and a mean $\overline{I(SM(s_1); P(\phi_{5,4}))} = 1.17$ bits over the trial. The highest mutual information between s_2 and the phase relations is given by $I(SM(s_2); P(\phi_{5,1}))$ with a peak of 2.05 bits at 90 seconds – see the grey line in graphic 3.8-B – and a mean $\overline{I(SM(s_2); P(\phi_{5,1}))} = 2.05$ bits over the trial. The high values of $H(s_1)$ and $H(s_2)$ (around 5 bits) and the low values $I(SM(s_1); P(\phi_{i,j}))$ and $I(SM(s_2); P(\phi_{i,j}))$ suggest that the information about the sensory dynamics is distributed over the network.

The mutual information between motors and phase relations is high in the relation $\phi_{4,3}$, as shown by $I(SM(m_1); P(\phi_{4,3}))$ in graphic 3.8-B. This high value is expected as m_1 is controlled by $\phi_{4,3}$, as in Eq. (3.5). The value of $I(SM(m_2); P(\phi_{5,3}))$ (not shown in the graphic) is also high as m_2 is controlled by the relation $\phi_{5,3}$. Despite the predominance of information about m_1 and m_2 in $\phi_{4,3}$ and $\phi_{5,3}$, respectively; the others phase relations also contain information about the motor dynamics. $I(SM(m_2); P(\phi_{3,2}))$, for instance, maintains near 2.5 bits during the first $\sim$75 seconds and then it decays to $[0.5, 1.5]$ bits with a peak around 145 s, see dashed line in graphic 3.8-B.

We have shown the mutual information between 4 different pairs of components, but in total there are 40 possible combinations considering 4 elements in SM and 10 in P (or S_b). In order to capture how the mutual information in the phase relations decreases as P is reduced to S_b, we take the mean of all 40 possible combinations of mutual informations, which will be referred to as $I(SM, P)$ and $I(SM, S_b)$ for the complete and reduced dynamical descriptions, respectively. Fig. 3.9 presents $I(SM, P)$ and $I(SM, S_b)$ for three different values of t_s. The highest mean mutual information over the trial is given by the complete description $\overline{I(SM, P)} = 1.50$ bits. As P is reduced by decreasing the threshold t_s, the mutual information also decreases. For the values of t_s analysed $t_s = 18$, $t_s = 9$ and $t_s = 3$, the mutual information reduced to $\overline{I(SM, S_{b1})} = 1.05$, $\overline{I(SM, S_{b2})} = 0.74$, and $\overline{I(SM, S_{b3})} = 0.40$ bits, respectively.

In order to analyse the relation between mutual information and different values of threshold, the mean $\overline{I(SM, S_b)}$ is used. The maximum value of $\overline{I(SM, S_b)}$ is 1.50 bits, which is obtained with a high value of t_s that makes $S_b = P$ (in our model, $S_b = P$ when $t_s = 90$). In order to get a better visualization of the decay in mutual information as the

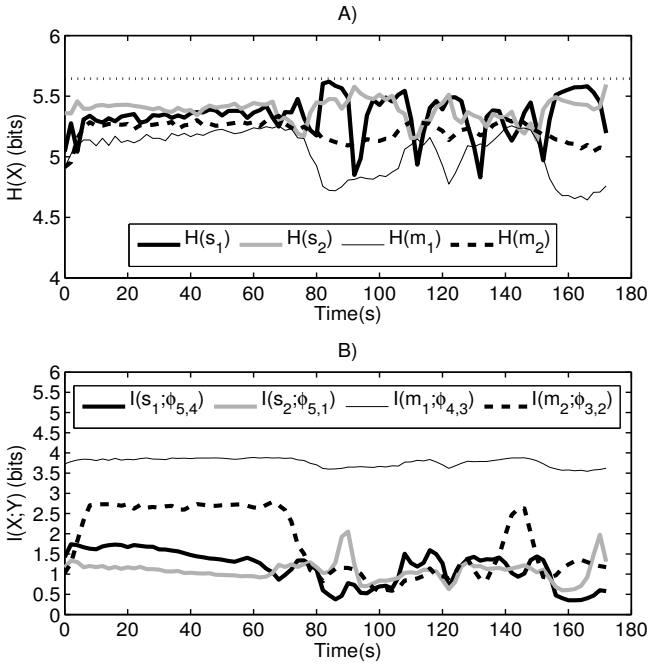

Figure 3.8: **Graphic A** shows the entropy (y-axis) of each sensorimotor component (see legend) during the agent's lifetime (x-axis). Straight dotted line at the top (y=5.64 bits) represents the maximum possible value for the entropies. **Graphic B** shows the mutual information between four combinations of components from SM and P, namely $I(SM(s_1); P(\phi_{5,4}))$, $I(SM(s_2); P(\phi_{5,1}))$, $I(SM(m_1); P(\phi_{4,3}))$ and $I(SM(m_2); P(\phi_{3,2}))$, see legend.

value of t_s decreases, the maximum mutual information $\overline{I(SM, S_b)} = 1.50$ bits for $t_s = 90$ was rescaled to 1 (see Fig. 3.10-A).

As the threshold decreases from 90 to 40, the phase relations lose only 10% of its information about the sensorimotor dynamics, as shown by $\overline{I(SM, S_b)} = 1$ for $t_s = 90$, and $\overline{I(SM, S_b)} = 0.9$ for $t_s = 40$ rad/s. As t_s decreases, the rate of decay for $\overline{I(SM, S_b)}$ increases. For $t_s = 20$ rad/s the phase relations still carry 0.73 of the total information and from $t_s = 20$ to $t_s = 1$ the information drops to 0.21. The rapid decay of information for low values of t_s initially suggests that the more synchronised the phase relations the more information they carry about sensorimotor dynamics.

This result, however, should be analysed together with the amount of (de)synchronised phase relations for each threshold. If the values of $\dot{\phi}_{i,j}$ were uniformly distributed in the range [0,90], then just by moving the threshold we would know the amount of synchronised and desynchronised phase relations. As in our model this distribution is not uniform, as

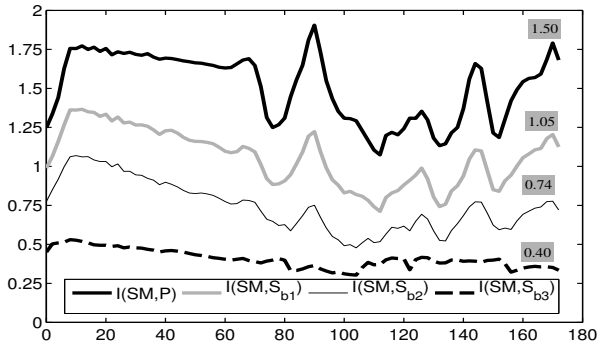

Figure 3.9: Mean mutual information between all 40 pairs of sensorimotor and phase relation components. $I(SM, P)$ shows the maximum mutual information in the phase relations throughout the trial (see time in the x-axis). $I(SM, S_{b1})$, $I(SM, S_{b2})$ and $I(SM, S_{b3})$ represent the mutual information from 3 reduced descriptions with thresholds $t_s = 18$, $t_s = 9$ and $t_s = 3$ rad/s respectively. The lower the t_s the less information present in the reduced descriptions. The numbers highlighted with grey background at the end of each line represent the mean mutual information over the whole trial, namely $\overline{I(SM, P)} = 1.50$, $\overline{I(SM, S_{b1})} = 1.05$, $\overline{I(SM, S_{b2})} = 0.74$, and $\overline{I(SM, S_{b3})} = 0.40$ bits.

represented by the grey line in Fig. 3.10-A, it is important to analyse how the mutual information $\overline{I(SM, S_b)}$ changes in relation to the amount of data in the reduced description (i.e. the amount of phase relations considered to be synchronised), as presented in 3.10-B. As the amount of data in the dynamical description increases – by increasing the threshold – the mutual information $\overline{I(SM, S_b)}$ also increases. When 0.5 of the most synchronised oscillations are included in the dynamical description then $\overline{I(SM, S_b)} = 0.51$, meaning that half of the phase relation dynamics carry half of the information about the sensorimotor dynamics.

The reason why $\overline{I(SM, S_b)}$ is not zero when all phase relations are shuffled (see in graphic 3.10-B that $\overline{I(SM, S_b)} = 0.17$ when the amount of data in the dynamical description is zero) is that the joint entropy between a sensorimotor component and a phase relation dynamics is slightly smaller than the sum of their individual entropies due to the number of data points in the time series. In one of the time windows of 6 seconds (with 6000 data points), for instance, $I(SM(m_2); S_b(\phi_{3,2})) = 0.296$ bits for $t_s = 0$ with $H(SM(m_2)) = 5.043$, $H(S_b(\phi_{3,2})) = 5.111$ and $H(SM(m_2), S_b(\phi_{3,2})) = 9.858$. The value of the joint entropy $H(SM(m_2), S_b(\phi_{3,2}))$ should be equal to the sum of the individual entropies (i.e. $5.043 + 5.111 = 10.154$); however, by using 6000 data points this value is slightly smaller (i.e. 9.858), which gives a residual mutual information of 0.296 (i.e.

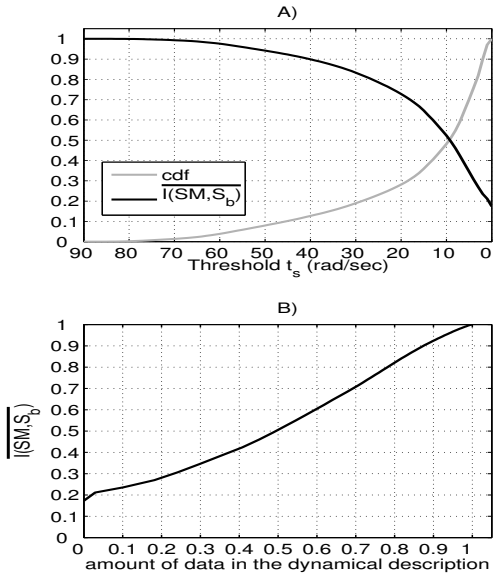

Figure 3.10: Mutual information between the phase relations and the sensorimotor dynamics different values of t_s. The black line in **graphic A** shows how $\overline{I(SM, S_b)}$ changes as the threshold t_s decreases (notice inverted x-axis). The values of $\overline{I(SM, S_b)}$ are normalized in [0,1] with 1 representing the maximum $\overline{I(SM, S_b)} = 1.50$ bits. The grey line shows the cumulative function distribution (cdf) of $\dot{\phi}_{i,j}$. It represents the amount of $\dot{\phi}_{i,j}$ greater than a t_s; for instance, 20% of $\dot{\phi}_{i,j}$ are greater than 30 rad/s **Graphic B** shows how $\overline{I(SM, S_b)}$ (y-axis) changes in relation to the amount of data in the dynamical descriptions (i.e. the amount of phase relations considered to be synchronized), where 1 (x-axis) represents the complete description and smaller values represent reduced descriptions obtained by decreasing the threshold. For instance, when S_b contains 0.3 of the dynamics of phase relations (the other 0.7 are desynchronised oscillations) then $\overline{I(SM, S_b)} = 0.34$; i.e. 30% of the most synchronised oscillations carry 34% of the total amount of information about sensorimotor dynamics; the other 70% of oscillations, which are desynchronised, carry the rest of 66% of the total information.

$10.154 - 9.858$). We have done the same analyses of mutual information, but subtracting the residual mutual information obtained when $t_s = 0$ from the mutual information when $t_s > 0$. The results were qualitatively the same; particularly, the mutual information in graphic 3.9 decreased and the slope of the line in graphic 3.10-B increased. We have also used more data points (up to 10000) and also divided the intervals $[0, 2\pi)$ (for the phase relations) and $[0, 1]$ (for the sensors and motors) in less bins (40, rather than 50). The results were qualitatively the same and, more importantly, the take-home message (that we explain in the following paragraph) has hold under these different parameters of analysis.

The relationship between the mutual information and the amount of data in the dynamical description suggests that *neither synchronised nor desynchronised oscillations carry a privileged status in terms of informational content about sensorimotor dynamics.* The informational content is equally distributed throughout the entire range of phase relations. The more a dynamical description leaves phase relations in the oscillatory network out of the equation, the less information it carries about the sensorimotor coordination, independently whether the left out phase relations represent either synchronous or desynchronous oscillations.

3.4.3 Causal relevance of synchronous and desynchronous oscillations

In this section we present the experiment we carried out to investigate the causal relevance of desynchronous and synchronous oscillations in the generation of functional sensorimotor dynamics. In the experiment we compare the agent's behavioural performance using the fitness function in (3.8) after applying perturbations to its oscillatory network in either of the situations: a) during moments of synchronisation ($\dot{\phi}_{i,j}(t) \leq t_s$), or b) during moments of desynchronisation ($\dot{\phi}_{i,j}(t) > t_s$). The perturbation is applied to the connections between the oscillators i and j ($k_{i,j}$ and $k_{j,i}$) by adding a random number from a gaussian distribution ($\mu = 0, \sigma^2 = \alpha\ k_{i,j}$), where α is a perturbation level parameter. If the agent's performance equally drops under the same perturbation level α applied to synchronous and desynchronous oscillations then it indicates that both oscillatory dynamics have the same relevance to the generation of functional sensorimotor coordinations. On the other hand, if the performance does not decay equally then the oscillatory dynamics that causes a greater decay is the more relevant.

A critical point of this experiment is the *threshold* from which an oscillation is considered to be either synchronised or desynchronised. If we consider, for instance, that synchronous oscillations are below 2 rad/s then perturbations applied to desynchronous oscillations will probably cause a greater decay in the agent's performance as the range of perturbations is wider ($\dot{\phi}_{i,j} > 2$ rad/s). Fig. 3.11 presents the agent's fitness for three different values of thresholds t_s and perturbation levels α. Each fitness represents an average over 200 trials.

For $t_s = 1$, desynchronised oscillations are more relevant than synchronised ones to the agent's performance, which can be seen by the fitness difference (grey line) and by $\overline{F_s - F_d} = 0.24$. Notice that for $t_s = 1$ and $\alpha < 0.1$ (see graphic A) the agent's performance is not affected when perturbations are applied to synchronous oscillations. As α increases

from 0.1 to 0.2 both fitnesses decay, and for $\alpha > 2$ the perturbations to desynchronous oscillations have a greater effect on the agent's fitness, as shown by an increase in the fitness difference. For $t_s = 9$, both types of oscillations are equally important as the fitness difference maintain near zero for all levels of perturbation which gives a mean $\overline{F_s - F_d} = 0$. For $t_s = 80$, all levels of perturbation to desynchronous oscillations do not affect the agent's performance (the dark grey line maintains near 1 for all perturbations). The reason for that is that there are very few occurrence ($\approx 0.04\%$) of $\dot{\phi}_{i,j} > 80$ rad/s.

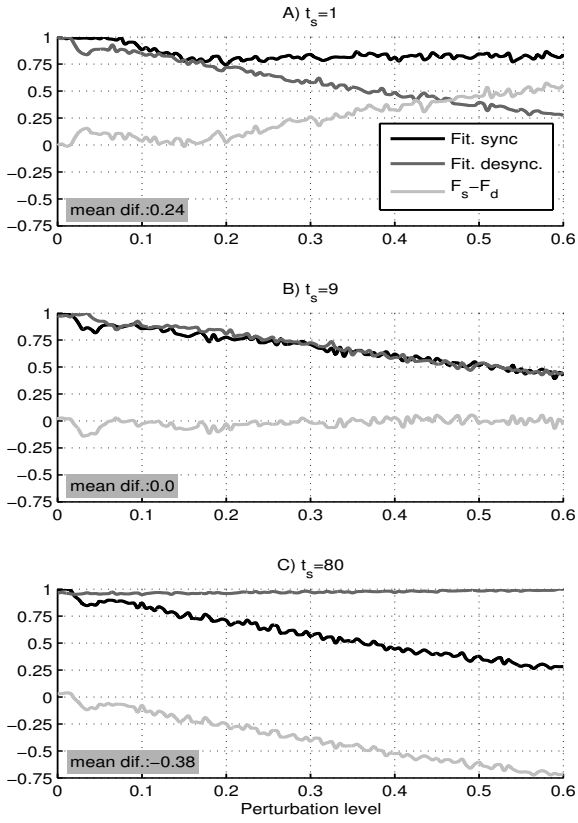

Figure 3.11: Agent's fitness (y-axis) for different levels of perturbations α (x-axis) and thresholds $t_s = 1$ (graphic **A**), $t_s = 9$ (graphic **B**), and $t_s = 80$ (graphic **C**). Black and dark grey lines show the fitnesses of the agent when perturbation is applied to synchronous and desynchronous oscillations, respectively (see legend). Light grey line is the fitness difference $Fitness_{(synchronisation)} - Fitness_{(desynchronisation)}$ (see legend). The numbers highlighted with a grey background show the mean of the fitness difference over all perturbation levels. This mean will be referred to as $\overline{F_s - F_d}$.

In order to analyse how the relevance of desynchronous oscillations changes in relation to the threshold, the mean of the fitness difference ($\overline{F_s - F_d}$) is used (see Fig. 3.12). The values of $\overline{F_s - F_d}$ vary within $\approx [-0.4, 0.4]$, where -0.4 indicates that desynchronisation is

not relevant for sensorimotor behaviour and 0.4 indicates its maximum relevance. This interval is also presented in a scale $[0, 1]$ – right y-axis in graphic 3.12 – and from now on we are going to use this scale to discuss the relevance of desynchronous oscillations. For values of threshold below ≈ 7 rad/s desynchronous oscillations are more relevant than synchronous ones, which can be seen by $\overline{F_s - F_d} > 0.5$. Both types of oscillations are equally relevant when $t_s \approx [7, 11]$ and above this range the relevance of desynchronous oscillations is smaller. For $t_s = 40$, for instance, desynchronisation has ≈ 0.125 of relevance to agent's sensorimotor coordination. The relevance of desynchronous oscillations measured only in terms of the threshold do not take into account the distribution of $\dot{\phi}_{i,j}$ over the range [0,90] rad/s. Similarly to the analysis of mutual information presented in the previous section, a more robust measure of causal relevance should also consider the distribution of $\dot{\phi}_{i,j}$.

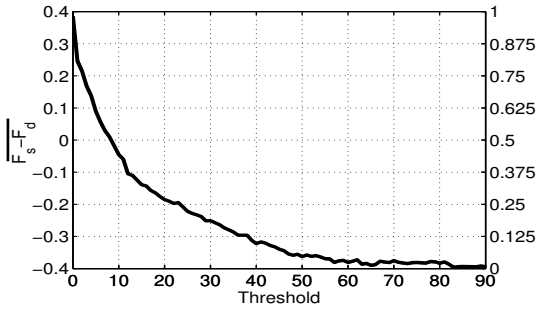

Figure 3.12: Mean of fitness difference $\overline{F_s - F_d}$ (y-axis on the left) for different thresholds t_s (x-axis). Positive values indicate that desynchronisation is more relevant than synchronisation for the generation of functional sensorimotor coordination. The y-axis on the right side represents $\overline{F_s - F_d}$ rescaled to [0,1]. When the rescaled $\overline{F_s - F_d}$ is 0.5, for instance, both types of oscillations are equally relevant. The rescaled $\overline{F_s - F_d}$ works as an index of relevance for desynchronous oscillations, where 0 indicates no relevance and 1 maximum relevance.

As the threshold increases, the quantity of phase relations that are considered desynchronised decreases, this relation is represented by distribution function of $\dot{\phi}_{i,j}$ shown in Fig. 3.13-A. This result is similar to the one presented for the single agent we have analysed in the previous section; here, however, we perturbed the desynchronous oscillations with $\alpha \in [0, 0.6]$ and for each pair (α, t_s) we ran 200 trails. When $t_s = 20$, 0.30 of the total amount of phase relations are desynchronised, and when t_s increases to $t_s = 40$, for instance, the amount of desynchronised phase relations decreases to 0.13 of the total phase relations.

Graphic 3.13-B shows the relevance of desynchronised oscillations – *i.e.* $\overline{F_s - F_d}$ – in relation to the quantity of phase relations considered desynchronised – *i.e.* $\dot{\phi}_{i,j} > ts$. When 0.5 of the total number of phase relations – which includes all $\dot{\phi}_{i,j} > 10$ – are considered desynchronised then these oscillations will have 0.48 of relevance for the agent's fitness; and when 0.95 of the total amount of phase relations – which includes all $\dot{\phi}_{i,j} > 1$ – are considered desynchronised then these oscillations will have 0.82 of relevance. Notice that the synchronised phase relations below 1 rad/s actually carries an important role in the generation of the agent's behaviour. While 0.95 of phase relations – which includes all $\dot{\phi}_{i,j} > 1$ – has 0.82 of relevance, the rest 0.05 of phase relations – which includes all $\dot{\phi}_{i,j} \leq 1$ – has 0.18 of relevance.

This result indicates that oscillations synchronised with a narrow window of frequency difference – in our model this window was of 1 rad/s in a range of frequency differences from 0 to 90 rad/s – are relatively more causal relevant for the generation of functional sensorimotor coordination than the rest of oscillations with higher frequency differences. That is not to say that the "rest" of oscillations are not relevant, as they still carry 0.82 of relevance. Apart from the range of $\dot{\phi}_{i,j} \leq 1$, the causal relevance of the phase relations are distributed over the range of possibles $\dot{\phi}_{i,j}$ without any privileged status of causal relevance to either synchronous or desynchronous oscillations

3.5 Discussion

As far as methodological aspects are concerned, we have combined evolutionary robotics with Kuramoto oscillators to study the roles played by synchronous and desynchronous oscillations in the context of a sensorimotor coordination task. We have used information-theoretic measures and dynamical system concepts to analyse the system. The model was not meant to target any specific level of abstraction from individual neurons and very small circuits (Izhikevich, 2007) to the whole cortex and brain activity (Varela et al., 2001; Buzsaki, 2006). Our goal was rather to reproduce at a merely conceptual level of generality the *type* of data from which the significance of synchronisation is generally privileged and to show how a system does in fact functionally exploit the whole phase dynamic to achieve a coherent sensorimotor coordination. Such a proof of concept should not be taken as an empirical model – see Barandiaran and Moreno (2006), for a distinction between conceptual and empirical models.

The results obtained from the analysis of the model give some insights to help answer the question: *how does the informational content of the sensorimotor activity present in a*

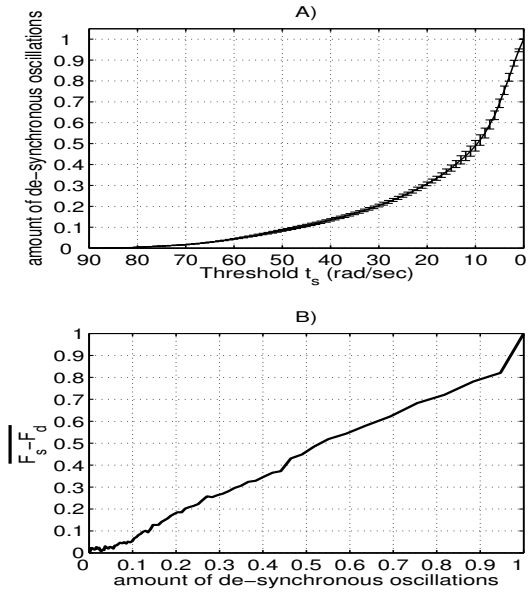

Figure 3.13: **Graphic A** shows how the amount of desynchronous phase relations changes (y-axis) for different thresholds (x-axis). Bars represent the standard deviations. Near 50% of the phase relations have their derivative $\dot{\phi}_{i,j} < 10$ rad/s. **Graphic B** shows how the relevance of desynchronised oscillations – *i.e.* $\overline{F_s - F_d}$ rescaled to [0,1] – changes in relation to the amount of phase relations considered desynchronised (x-axis).

complete dynamical description of phase relations change as such a description is reduced to the dynamics of synchronous oscillations? In our particular model, the informational content was equally distributed throughout the entire range of phase relations; the more the dynamical description was reduced the less information it carried about the sensorimotor coordination. Neither synchronised nor desynchronised oscillations was found to carry a privileged status in terms of informational content in relation to the agent's sensorimotor activity. It is important to notice that the analysis we have presented not only suggests that the phase relations of desynchronous oscillations carry relevant information about sensorimotor behaviour but, more importantly, it shows *how* the informational content changes as the dynamical description of the oscillatory network is reduced by gradually removing the phase relation dynamics of desynchronous oscillations.

The results also gave some insights to address the questions: *to what extent are desynchronous oscillations as causally relevant as synchronous ones to the generation of functional sensorimotor coordination?* In our particular model, although the phase relations of oscillations with a narrow frequency difference carried a relatively higher causal relevance than the rest of the phase relations to sensorimotor coordinations, overall there was no

privileged functional causal contribution to either synchronous or desynchronous oscillations. Notice that the analysis we have presented not only suggests that desynchronised neural activity has functional significance to sensorimotor behaviour but, more importantly, it shows the relevance of desynchronous oscillations in relation to synchronous ones considering a gradual reduction of the threshold delimiting both types of oscillations.

It is not a surprise that desynchronous oscillations carry some information about and have causal contribution to sensorimotor coordinations. However, what was not expected in our studies, could not have been predicted in advance, and what our results have suggested is that i) the information and the causal contribution are evenly distributed throughout the whole range of phase relation dynamics (note that we have analysed *how* the information and the causal contribution were distributed in the phase relations).

It is important to notice that the experiment studied here start to shed some light on roles of neural oscillations in sensorimotor behaviour, particularly it provides results that suggest we should rethink the traditional approach that privileges synchronous over desynchronous oscillations. In the future, to help make this contribution more empirically compelling further investigations are required. Firstly, the model developed here is relatively simple (with only 5 oscillators), in a more complex system with thousands of neurons, the oscillatory network could engage in independent oscillatory regimes, each one causally contributing to different neural functions and independently related in terms of informational content. Secondly, the motor behaviour of the agent developed here is controlled by the phase relation of the oscillators (as described in Eq. (3.5) and (3.6)); alternatively, it could be controlled by the frequency of the oscillators – i.e. by the derivative of the phase or by the number of cycles of an oscillator within a moving time-window. By using the frequency to control the motors, the timing between the oscillatory activity would not be directly related to the motor activity. In both cases – in a more complex system and in a model where the motor is controlled by the frequency – the results could come out differently with other distributions of information and causal contribution throughout the phase relation dynamics. Thus, despite the fact that the results found here are a first step towards a wider investigation (with variations of the experiment), the current model has consistently contributed to the understanding of neural oscillatory dynamics by raising the discussion about whether we should carry on privileging synchrony (e.g. searching for synchronous dynamics correlated to sensory and motor activities, as is the norm in many parts of the literature (Fries, 2005; Uhlhaas et al., 2009; Pockett et al., 2009; Singer, 2011; Hipp et al., 2011; Sharafi et al., 2012; Huyck and Passmore, 2013; Sakurai et al., 2013;

Stanley, 2013)) or add desynchronous oscillations into the equation and take the whole regime of phase relation as the explanatory unit of neural oscillatory dynamics as we have attempted to do here.

3.6 Summary

In this chapter we have compared the functional role and the informational content between synchronous and desynchronous oscillations in relation to the agent's sensorimotor behaviour. In the next chapter we develop a model where an agent is performing a different task (discrimination of objects in the environment) and analyse i) the informational content in the oscillations about the sensory dynamics – similar to the analysis we have presented in the current chapter – and ii) how an agent's sensory dynamics modulate its network's spontaneous oscillations generating oscillatory patterns that underlie the agent's coherent behaviours. The results presented in the next chapter support the claims made in the current one and also provide dynamical explanations of how an agent's oscillatory network operates within a sensorimotor loop.

Chapter 4

From spontaneous oscillations to functional oscillatory regimes within a sensorimotor loop

4.1 Introduction

A neural system is not an on- and off-system activated by external stimuli; instead, it is an active system that constantly regenerates its internal oscillatory activity which is modulated by environmental perturbations (Buzsaki, 2006; Sporns, 2010). This view of an active nervous system has its roots in the work of Brown (1914) and contrasts with the view of a nervous system primarily reflexive and driven by stimulus from the environment, which dates back to Sherrington (1906), (Raichle, 2010). The majority of modelling in theoretical neuroscience has focused on stimulus-driven neural models where neurons are typically silent in the absence of sensory input (Vogels et al., 2005). Although the stimulus-driven approach has achieved significant progress in understanding the brain operation mainly in the sensory areas, it does not account for the majority of neural dynamics where the sensory activity works as perturbations to the ongoing internally generated oscillations (Vogels et al., 2005).

In this chapter we implement and study an oscillatory network that spontaneously oscillates in the absence of sensory stimulation and, when it is coupled to an agent's body, generates a coherent sensorimotor activity that enables the agent to perform a minimally cognitive task – namely the discrimination between the shapes of a circle and a triangle. The network will firstly be analysed in its "resting state" – i.e. without receiving sensory stimulation from the environment and without generating motor behaviour – and then

under the continuous modulation of the agent's sensorimotor loop. The results provide a dynamical explanation of how a continuously changing sensory activity shapes the temporal structure of a network's spontaneous oscillations generating oscillatory patterns that underlie the agent's coherent behaviour.

Apart from this dynamical analysis, we further explore the process of modulation by measuring the statistical correlations between the sensory and the network dynamics. Particularly, we will measure i) the mutual information between the phase relations in the network and the sensory activity, and ii) how the amount of information in the phase relations about the sensory activity changes as the phase relation dynamics are reduced to the dynamics of synchronised oscillations (similar to the problem we have analysed in the previous chapter). These measures help to support the claims made in the previous chapter and also to understand the information dynamics between the environment and the network during the process of modulation.

Notice that this chapter contributes to both central issues of this thesis by analysing i) how the temporal structure of a network's spontaneous oscillations changes within an agent's sensorimotor loop, and ii) how the informational content about the sensory activity present in the temporal structure changes as the dynamical description of phase relations is reduced to synchronous oscillations.

The model developed and the dynamical analyses are presented in the following sections.

4.2 Theoretical model and methods

4.2.1 The agent and the task

The model minimally replicates, at a conceptual level of abstraction, a behavioural phenomenon where a subject has to identify the shape of an object by actively scanning it in order to get sensory stimuli which will eventually lead to a coherent sensation of the object's shape. Specifically, the model consists of an agent moving back and forth along a horizontal line in a two-dimensional environment reading the distance from its sensor to an object placed in fixed position in the environment (see Fig. 4.1). In each trial of the experiment, a total of 20 objects (10 triangles and 10 circles) are presented to the agent in a random sequence. Each object is presented during 6 seconds and the whole trial lasts 120 seconds. The agent should actively scan the object and move either to the right if it is interacting with a circle or to left if it is interacting with a triangle. Notice that, the

agent has to keep interacting with the object during the whole trial (without moving far away to the left or to the right) in order to detect the shape transition that might happen at every 6 seconds. The sensor activation is *zero* when the agent is vertically aligned with the centre of the object and increases as the agent moves either to the right or the left; its maximum value is *one* when the agent is not touching the object.

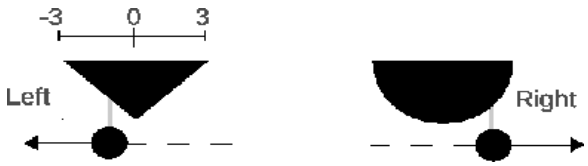

Figure 4.1: Schematic representation of the simulated environment where the agent is performing the discrimination task. The agent is represented by the small black circle. Both the base of the triangle and the diameter of the circle have 6 units. The agent moves along the horizontal line and has a distance sensor (represented by the grey line).

4.2.2 The agent's controller

The agent is controlled by a network of 3 phase-coupled oscillators. Only the oscillator θ_1 (described below) is connected to the distance sensor. The agent has two lateral motors m_R and m_L, where the subscripts R and L stand for right and left. The activation of each motor is defined by $m_R = c_1(cos((\theta_2 - \theta_1) + (2\pi c_2))) + 1)$ and $m_L = c_3(cos((\theta_3 - \theta_1) + (2\pi c_4))) + 1)$, respectively; where θ_n is the phase of the oscillator n, $c_1 = 12.61$, $c_2 = 0.7873$, $c_3 = 18.81$ and $c_4 = 0.8678$ are constant parameters evolved by a genetic algorithm (explained below). The agent's horizontal movement is given by $(m_R - m_L)$. Each node of the agent's oscillatory network is governed by the Kuramoto's equation defined in (4.1) (Kuramoto, 1984):

$$\dot{\theta}_i = (\omega_i + s_i c_5) + \sum_{j=1}^{N} k_{ji} sin(\theta_j - \theta_i) \tag{4.1}$$

where θ_i is the phase of the i^{th} oscillator which is integrated with time step 0.001 seconds using the Euler method, ω_i is the oscillator's natural frequency, s_i is the sensory input from the distance sensor, c_5=*6.83* is a constant representing the sensory input strength (the sensor is connected only to the oscillator θ_1), N is the number of oscillators (here 3), and k_{ji} is the coupling factor from the j^{th} to the i^{th} oscillator.

4.2.3 Methods to obtain an agent for the dynamical analysis

The *microbial genetic algorithm* (Harvey, 2001) was used to adjust the parameters of the model, namely the motor strengths c_1, c_2, c_3 and c_4; the sensory strength c_5; the natural frequencies $\omega_i \in [8, 17.5]Hz$; and the connections $k_{i,j} \in [0, 20]$ (numbers in brackets represent the search space for the genetic algorithm). There is no specific reason why this genetic algorithm was chosen; the system is relatively simple and could have been optimized with other genetic algorithms. The parameters are encoded in a genotype as a vector of real numbers in the range [0,1] and linearly scaled, at each trial, to their corresponding range. The genetic algorithm setup is: population size (30); mutation rate (0.05); recombination (0.60); reflexive mutation; normal distribution for mutation $\left(\mu = 0, \sigma^2 = 0.1\right)$.

Each agent ran for 20 trials starting at a random initial position within a distance of $[-3, 3]$ units from the centre of the object and with random value of θ_i within $[0, 2\pi)$ radians. A total of 10 circles and 10 triangles were presented to the agent at a random sequence during each trial. Each object was presented for 6.0 seconds giving a total 120 seconds for a trial. At the end of each trial, the fitness of the agent was measured by the Eq. (4.2):

$$
\begin{aligned}
F_{trial} = \quad & F_{triangle} F_{circle} \\
F_{triangle} = \quad & \tfrac{1}{10} \textstyle\sum_{p=1}^{10} \begin{cases} 1; & if \;\; d_f < -0.5; \\ 0; & otherwise; \end{cases} \\
F_{circle} = \quad & \tfrac{1}{10} \textstyle\sum_{p=1}^{10} \begin{cases} 1; & if \;\; d_f > 0.5; \\ 0; & otherwise; \end{cases}
\end{aligned}
\tag{4.2}
$$

where F_{trial} is the fitness of the agent at the end of a trial, F_{circle} and $F_{triangle}$ are the mean fitnesses over 10 presentations of circles and triangles, respectively; and d_f is the final distance from the agent to the centre of the object at the end each six-second section. The final fitness of the agent was given by the mean of F_{trial} over 20 trials.

After evolving the parameters we ran each individual of the population for an additional 500 trials (without evolving the parameters) and selected the fittest one. In total, the fittest agent interacted with 10000 objects (500 trials and 20 presentations at each trial). In 6 trials the agent presented an erratic behaviour by moving far away from the object. In 9880 object presentations (494 trials) the agent correctly responded to the object's shape

in 92.2% of cases. The rest 7.8% of object presentations, the agent incorrectly responded to a circle and triangle in 4.2% and 3.6% of the cases, respectively. The fittest agent was selected for the analyses of behaviour and internal dynamics, which are presented in the next sections.

4.3 Agent's behaviour and its internal oscillations

Figure 4.2-A shows the agent's behavioural response during a single trial of the experiment. During the first 24 s, the agent is interacting with a circle (see black line) continuously moving back and forth along the horizontal line within range [0.77, 2.3]. When the object's shape switches to a triangle, at t=24 (see grey line), the agent goes to the left side of the object and keeps moving back and forth in the range [-3.04, -0.26]. From t=48 to t=66 s, the agent correctly responds to a sequence of shape transitions at every 6 s. In the rest of the trial (t=[66,120] s), the agent interacts with a triangle for 12 s, then with a circle for 24 s, and finally with a triangle again during the last 18 s.

The underlying oscillatory dynamics corresponding to the agent's behaviour when it is interacting with a triangle and a circle are presented in Figure 4.2-B and C, respectively. During the interaction with a circle (graphic 4.2-B), the oscillatory network is in a transient dynamics during the first $\approx$ 6 s (grey line) and converges to a stable the limit cycle in $t = [6, 24)$ s. During the interaction with a triangle (graphic 4.2-C), the oscillatory network is all the time in a transient dynamics within the basin of attraction of a stable limit cycle. As we will see, when the agent interacts with a triangle for longer periods of time (no longer than $t = 210$ s) its oscillatory network settles down in the limit cycle attractor.

The graphics 4.2-B and 4.2-C give us a qualitative overview of the functional oscillatory regimes underlying the agent's interaction with circle and triangle, respectively. In the next sections we show in details how these regimes are generated from the modulation of the network spontaneous oscillations (section 4.4), and also show the informational content they carry about the agent's sensory activity (section 4.5).

4.4 Modulation of the network spontaneous oscillations

The analysis of how the ongoing oscillations are modulated by the sensory activity is carried out in three parts. In section 4.4.1 we analyse the coupling strength of the oscillatory network. This analysis helps understand the generative mechanism of the network's oscillations and also the sensitivity of the network to sensory stimuli – e.g. the spontaneous

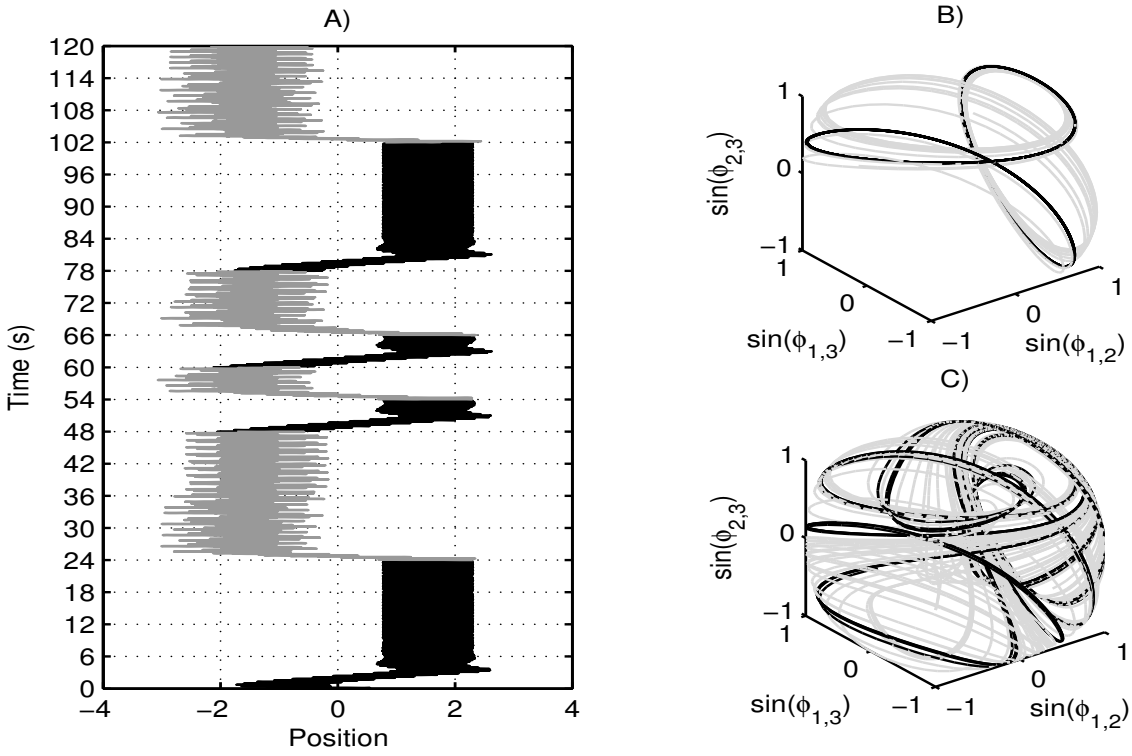

Figure 4.2: Agent's behaviour and its internal dynamics. **Graphic A** shows the agent's position in relation to the centre of the object (x-axis) over a trial (time is shown in the y-axis). The behaviour of the agent during the interaction with a circle is represented by the black line and during the interaction with a triangle by the grey line. **Graphics B and C** show the agent's internal oscillatory dynamics corresponding to t=[0,24) s (graphic B) and t=[24,48) s (graphic C). The axes show the *sin* function of the phase relations between each pair of oscillators. In graphic B, the grey line highlights t=[0,6) s and the black one t=[6,24) s. In graphic C, the grey line highlights t=[24,42) s and the black one t=[42,48)s.

oscillations of a weakly coupled network can be easily perturbed by sensory stimuli. In section 4.4.2 we analyse the network dynamics *decoupled* from the sensorimotor loop. The main point of this analysis is to show the spontaneous dynamics of the network and to understand how a controlled input ("manually" changed) affects the attractor landscape of phase relations. This analysis sets the ground to understand the process of modulation when the network is *coupled* to the sensorimotor loop, which is presented in section 4.4.3.

4.4.1 Coupling strength of the oscillatory network

The strength of the coupling is relative to the difference in the oscillators' natural frequencies; that is, the same value for the coupling factor $k_{i,j}$ might be weak when the difference

between the oscillators' natural frequencies is relatively high, or it might be strong when this difference is relatively low. The values of the coupling factors $k_{i,j}$ are shown in Figure 4.3-A. The connections between θ_1 and θ_2 have the highest value of $k_{i,j}$, namely $k_{1,2} = 0.92$ and $k_{2,1} = 0.44$ ($k_{1,2} + k_{2,1} = 1.36$); and the connections between θ_1 and θ_3 have the lowest $k_{i,j}$, namely $k_{1,3} = 0.06$ and $k_{3,1} = 0.02$ ($k_{1,3} + k_{3,1} = 0.08$).

The natural frequencies of the oscillators are given by $\omega_1 = 8.06$, $\omega_2 = 13.23$ and $\omega_3 = 16.14$ Hz. In the particular case of θ_1, which is the only oscillator connected to the agent's sensor, its frequency is influenced by s according to: $(\omega_1 + sc_5)$, as described in Eq. (4.1). In order to analyse the difference in natural frequencies between the oscillators, the term $(\omega_1 + sc_5)$ is going to be interpreted as the natural frequency of the oscillator θ_1. Figure 4.3-B shows the difference in natural frequency between the oscillators considering different values for the sensor s within $[-3, 20]$. The difference between θ_2 and θ_3 maintains constant at 2.09 Hz as the natural frequencies of these oscillators are not affected by s. The lowest value of the mean frequency difference takes place when $s = [4.8, 7.4]$ (see black dashed line). When $s = [0, 1]$, which is range of sensory activity when the agent is behaving in the environment, the frequency differences are $\Delta_{(\theta_1,\theta_2)} = [5.17, 4.08]$, $\Delta_{(\theta_1,\theta_3)} = [8.07, 6.99]$ and $\Delta_{(\theta_2,\theta_3)} = 2.09$ Hz (see the interval highlighted by the vertical dashed lines in 4.3-B).

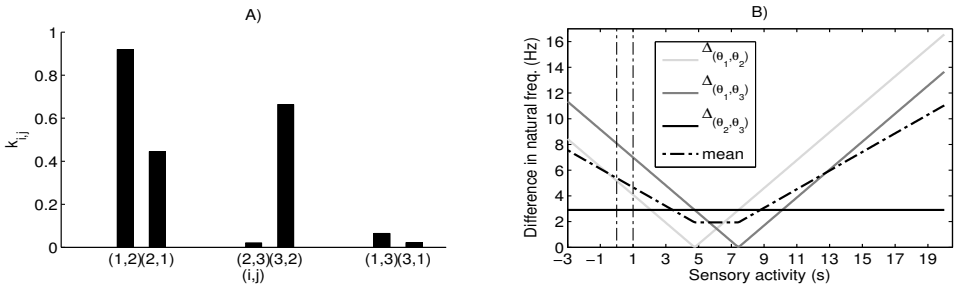

Figure 4.3: Coupling factors and natural frequencies of the oscillatory network. **Graphic A** shows the coupling factor $k_{i,j}$ (y-axis) for each pair of oscillators (i, j) (x-axis) in a scale from 0 to 1. **Graphic B** shows the absolute value of the difference in natural frequencies between each pair of oscillators (see legend) for s within $[-3, 20]$ (x-axis). The black dashed line shows the mean of all frequency differences. Vertical dashed lines highlight the interval where $s = [0, 1]$, which is the range of sensory input when the agent is behaving in the environment.

We are interested in knowing the strength of the coupling factors shown in graphic 4.3-A in relation to the frequency differences shown in graphic 4.3-B when $s = [0, 1]$ –

we are plotting the $s = [-3, 20]$ just to give a bigger picture of parameter space. As the oscillators have different natural frequencies, the coupling strength can be quantified by the Shannon's entropy (Shannon, 1948) of the phase relations $\phi_{i,j}$. When the network is decoupled from the agent's body, two oscillators i and j will get synchronised only if they interact via their coupling. If the coupling strength is null, the oscillators will be all the time desynchronised, generating a uniform distribution of phase relations $\phi_{i,j}$ (maximum entropy). On the other hand, if the coupling strength is strong, the oscillators will be all the time synchronised at a constant phase relation producing a degenerate distribution of $\phi_{i,j}$ with $H(\phi_{i,j}) = 0$ (minimum entropy).

The entropies of the phase relations for the sensor values $s = [-3, 20]$ are shown in Fig. 4.4-A. When $s \approx [1, 7]$, the oscillators θ_1 and θ_2 are more synchronized than the others ($H(\phi_{1,2}) \approx 0.5$). The highest synchronisation level of the network takes place when $s \approx [7, 9]$ with $H(\phi_{i,j}) \approx [0.1, 0.2]$. When $s > 9$, the oscillators θ_1 and θ_2 and the oscillators θ_1 and θ_3 are highly desynchronised (high entropy). Figure 4.4-B zooms into the entropies of the phase relations in the range $s = [0, 1]$. The oscillators θ_1 and θ_3 are highly desynchronised ($H(\phi_{1,3}) = 1$, $\forall\, s \in [0, 1]$), and θ_1 and θ_2 are the ones most synchronised. When $s = 0$, $H(\phi_{1,2}) = 0.86$ and $H(\phi_{2,3}) = 0.91$; as s increases up to 0.3 the entropies $H(\phi_{1,2})$ and $H(\phi_{2,3})$ also increase (i.e. the oscillators become more desynchronised). When s=0.3, $H(\phi_{1,2}) = 0.97$ and $H(\phi_{2,3}) = 0.99$ (i.e. the oscillators are highly desynchronised) and, from s=0.3 to s=1, $H(\phi_{1,2})$ decreases (i.e. θ_1 and θ_2 become more synchronised) and $H(\phi_{2,3})$ maintains high (i.e. θ_2 and θ_3 maintain highly desynchronised). The high values of entropies within the range $s = [0, 1]$ show that *the oscillatory network is weekly coupled for the range of sensory input when the agent is behaving the environment.*

4.4.2 Oscillatory network *decoupled* from the sensorimotor loop

In this section we analyse the oscillatory network outside the agent's sensorimotor loop; particularly, we will "manually" change the variable s, corresponding to the agent's sensor when the network is coupled to the sensorimotor loop, and study its effects on the vector field of phase relations.

Frequency dynamics under constant sensory input

We shall start by showing the frequency dynamics of θ_1, θ_2 and θ_3 for three constant values of s (see Figure 4.5). For $s = 0$ (graphic 4.5-A), the frequency of θ_2 oscillates

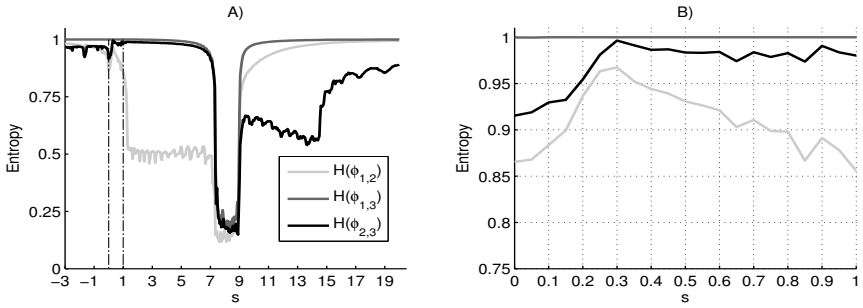

Figure 4.4: **Graphic A** shows the entropy of the phase relations $\phi_{1,2}$, $\phi_{1,3}$ and $\phi_{2,3}$ (see legend) for different constant values of sensory input in the range $[-3, 20]$ (x-axis). The entropy values were rescaled to the range [0,1] representing the minimum and the maximum values of entropy (see y-axis). Vertical dashed lines highlight $s = [0, 1]$. **Graphic B** zooms into the entropies for the range $s = [0, 1]$.

within the range $\approx [8, 18]$ Hz synchronising with θ_1 at $\approx$9 Hz and with θ_3 at $\approx$16 Hz[1]. For $s = 0.3$ (graphic 4.5-B), most of the time the frequency of θ_2 is at around $\approx$12 Hz (see the density distribution) with short moments of synchrony with either θ_1 or θ_3. For $s = 1$ (graphic 4.5-C), θ_1 and θ_2 oscillate in a similar frequency range, namely $\theta_1 \approx [8, 10.5]$ and $\theta_2 \approx [8, 13]$ Hz, and θ_3 at a higher frequency around 16 Hz. Notice that θ_1 or θ_3 do not synchronise at any time for the three values of s shown. Next we present the same dynamics as shown in graphics 4.5-A, B and C, but in the state space of phase relations.

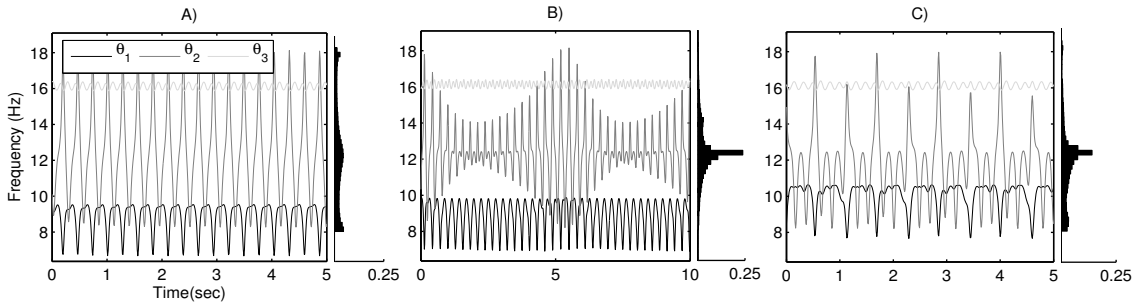

Figure 4.5: Frequency dynamics of the oscillators θ_1, θ_2, and θ_3 (see legend) for s=0 (graphic A), s=0.3 (graphic B) and s=1 (graphic C). Notice different x-axis in graphic B. The vertical histograms represent the distributions of frequency dynamics for the oscillator θ_2.

[1]In the context of this work, two oscillators are considered to be synchronized when they have similar frequencies.

Phase relation dynamics under constant sensory input

The state space of phase relations consists of the three dimensions $\phi_{1,2}$, $\phi_{1,3}$ and $\phi_{2,3}$, but it can be reduced to only two dimensions as one of them can be obtained from the other two. We have chosen to analyse $\phi_{1,2}$ and $\phi_{2,3}$ as their dynamics describe the phase relations of oscillators that get transiently synchronised. The phase relations between θ_1 and θ_3 are less interesting to be studied as they are all the time desynchronised, as we have seen in the previous section that $H(\phi_{1,3}) = 1 \; \forall \; s \in [0, 1]$.

Fig. 4.6 shows the vector fields and the trajectories in the state space of phase relations $\phi_{1,2}$ and $\phi_{2,3}$ for $s = 0$, $s = 0.3$ and $s = 1$. The magnitudes of the vectors are greater than zero for $s = 0$, $s = 0.3$ and $s = 1$, showing that θ_1, θ_2 and θ_3 do not get synchronised altogether at any time. For $s = 0$, synchronisation either takes place between θ_1 and θ_2 or between θ_2 and θ_3; in both cases the oscillators get synchronised with a phase difference at around 1.57 radians (see the peaks on the density distributions). For $s = 0.3$, the oscillators do not get synchronised (see the distributions of phase relations with $H(\phi_{1,2}) = 0.97$ and $H(\phi_{2,3}) = 0.99$). For s=1, θ_1 and θ_2 get transiently synchronised at around 1.57 radians, and θ_2 and θ_3 are most of the time desynchronised ($H(\phi_{1,2}) = 0.98$).

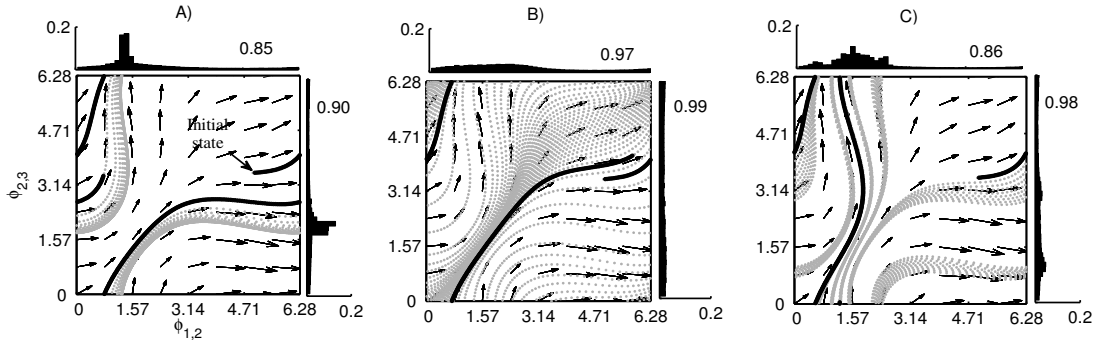

Figure 4.6: Vector fields and trajectories in the state space of phase relations for $s = 0$ (graphic **A**), $s = 0.3$ (graphic **B**) and $s = 1$ (graphic **C**). The state space is defined by $\phi_{1,2}$ (x-axis) and $\phi_{2,3}$ (y-axis). For ease of visualisation, the arrows are three times greater than their original magnitudes. The grey line shows a trajectory in the vector field during a 10 second time-window starting at the initial state $\phi_{1,2} = 5.0$ and $\phi_{2,3} = 3.5$ radians (pointed to by an arrow in graphic A). The black line highlights the first 300 ms of each trajectory. The histograms on the top and on the right of each graphic show the distributions of phase relations for $\phi_{1,2}$ and $\phi_{2,3}$, respectively, for the ten-second trajectory. The number near each distribution represents its entropy.

The black trajectory shown in each graphic depicts the first 300 ms of the phase relation dynamics starting from the same initial state (pointed to by the arrow in graphic A). The main difference between the trajectories can be seen in the range $\phi_{1,2} = [0, 1.57]$ and $\phi_{2,3} = 0$ (bottom left part of the graphics). For $s = 0$ (graphic 4.6-A), the trajectory turns to the right side (≈ 180 degrees in relation to the x-axis) showing that θ_2 and θ_3 are synchronised and θ_1 and θ_3 desynchronised. For $s = 0.3$ (graphic 4.6-B), the trajectory follows a diagonal line as $\dot{\phi}_{1,2} = \dot{\phi}_{2,3} > 0$ and later on it turns to the right showing θ_2 and θ_3 is more synchronized than θ_1 and θ_3. For $s = 1$ (graphic 4.6-C), the trajectory moves upwards (≈ 90 degrees in relation to the x-axis) showing that θ_1 and θ_2 are synchronised. Next we zoom into two specific vectors in the vector field and study how s modifies their angle and magnitude.

Modulation of the vector field by the parameter *s*

Fig. 4.7 shows how s modifies the angle and the magnitude of the vectors $\mathbf{v_1}$ at ($\phi_{1,2} = 1.57, \phi_{2,3} = 0$) and $\mathbf{v_2}$ at ($\phi_{1,2} = 3.14, \phi_{2,3} = 0$). The magnitude and the angle change differently for each vector (see graphics 4.7-A2, A3, B2 and B3). The magnitude of $\mathbf{v_1}$ decreases from 0.0357 when $s = 0$ to 0.0354 when $s = 1$; and the magnitude of $\mathbf{v_2}$ decreases from 0.0325 when $s = 0$ to 0.0257 when $s = 1$. The angle of the $\mathbf{v_1}$ changes from 82.3 degrees when $s = 0$ to 93.4 degrees when $s = 1$ (an increase of 11.1 degrees), and the angle of $\mathbf{v_2}$ changes from 29.3 when $s = 0$ to 35.4 degrees when $s = 1$ (an increase of 6.1 degrees). While $\mathbf{v_1}$ and $\mathbf{v_2}$ change differently, their components $v_{\phi_{1,2}}$ and $v_{\phi_{2,3}}$ undergo the same transformation. The component $v_{\phi_{1,2}}$ linearly decays 0.0068 from $s = 0$ to $s = 1$ for both $\mathbf{v_1}$ and $\mathbf{v_2}$ (see graphics 4.7-A4 and B4), and the component $v_{\phi_{2,3}}$ maintains constant for both $\mathbf{v_1}$ and $\mathbf{v_2}$ (see graphics 4.7-A5 and B5). The components $v_{\phi_{1,2}}$ and $v_{\phi_{2,3}}$ of all vectors in the vector field undergo the same transformation; i.e. $v_{\phi_{1,2}}$ linearly decreases and $v_{\phi_{2,3}}$ maintains constant for all vector in the vector field; despite that, the transformation in the resultant vector (e.g. $\mathbf{v_1}$ and $\mathbf{v_2}$) is different as it depends on the angle and magnitude of the vector (as exemplified by $\mathbf{v_1}$ and $\mathbf{v_2}$ in graphics 4.7-A1 and B1).

So far, the important points of the dynamical analysis can be summarized as follows: i) the oscillatory network is weekly coupled when $s = [0, 1]$ (the range of sensory input when the agent is behaving the environment); ii) as s increases, the component $v_{\phi_{1,2}}$ linearly decreases and $v_{\phi_{2,3}}$ maintains constant; and iii) despite a linear change in $v_{\phi_{1,2}}$ and a constant $v_{\phi_{1,2}}$, the transformation in the vector field vector is not linear as it depends on

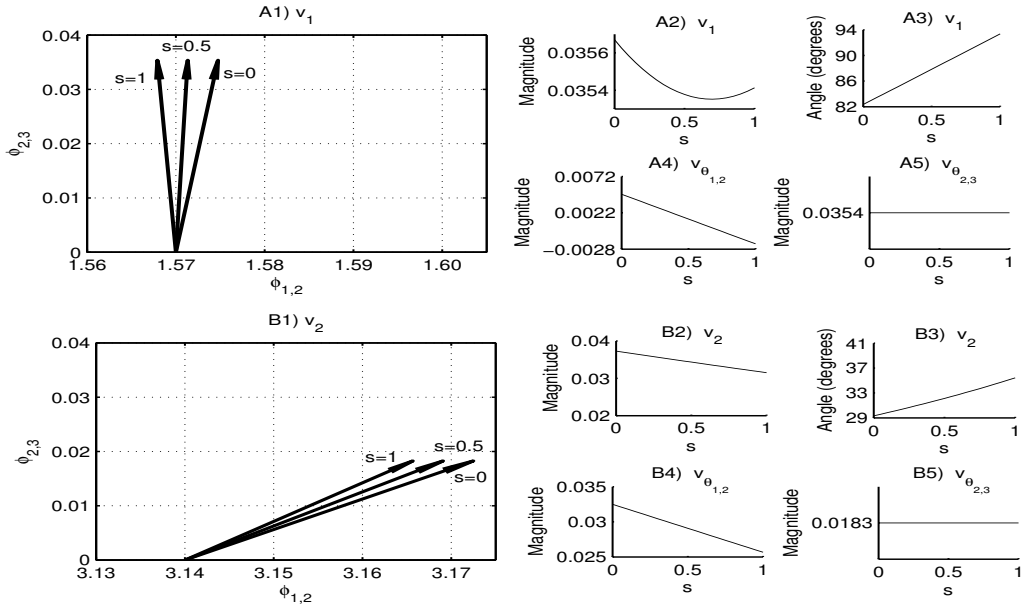

Figure 4.7: Modulation of two vectors by the parameter s. Vectors $\mathbf{v_1}$ at ($\phi_{1,2} = 1.57, \phi_{2,3} = 0$) (graphic A1) and $\mathbf{v_2}$ at ($\phi_{1,2} = 3.14, \phi_{2,3} = 0$) (graphic B1) for s=0, s=0.5 and s=1 (see values near the head of each vector). The small graphics on the right side show how the magnitude and angle of $\mathbf{v_1}$ and $\mathbf{v_2}$ change for $s = [0, 1]$ (see graphics A2, A3, B2, B3). The magnitude of the components of each vector are shown in graphics A4 and A5 (for the vector $\mathbf{v_1}$) and B4 and B5 (for the vector $\mathbf{v_2}$), see the title of the graphics.

the current angle and magnitude of each vector. In the next section we show how a continuously changing s modulates the vector field in a structured way generating functional oscillatory dynamics corresponding the agent's coherent behaviours.

4.4.3 Oscillatory network *coupled* to the sensorimotor loop

The agent's sensory activity continuously modulates the phase relation dynamics in a such a way that coherent oscillatory regimes are generated and the agent performs a correct behaviour. In the following, we analyse the structure of this modulation under the interaction with circle and triangle, respectively.

Figure 4.8-A shows the agent's behaviour under interaction with a circle and within a short time-window of 550 ms (this time-window corresponds to $t = [9, 9.55]$ s of the trial we have presented in Fig. 4.2-A). The agent's behaviour repeats in cycles of 275 ms – note that the agent's movement in the first half of the time-window ($t = [9, 9.275]$ s) and in the second one ($t = [9.275, 9.55]$ s) are similar. The underlying phase relation and

frequency dynamics of the oscillators are presented in Figure 4.8-B and C. The agent's internal oscillations engage in a stable dynamics characterised by a pattern of alternated synchrony between θ_1 and θ_2 or between θ_2 and θ_3. The synchrony between θ_1 and θ_2 takes place in $t = [9, 9.091]$ s, at ≈ 9 Hz, and with a phase difference of ≈ 0.8 radians. The synchrony between θ_2 and θ_3 takes place just after $t = 9.183$ s, at ≈ 16 Hz, and with a phase difference of ≈ 2.8 radians. This regime of phase relations is the signature of the oscillatory dynamics underlying the agent's interaction with a circle. Next we analyse the structure of the modulation that generates the stable oscillatory regime shown in graphic 4.8-B. The point of this analysis is to understand how the sensory activity modulates the ongoing network intrinsic oscillations.

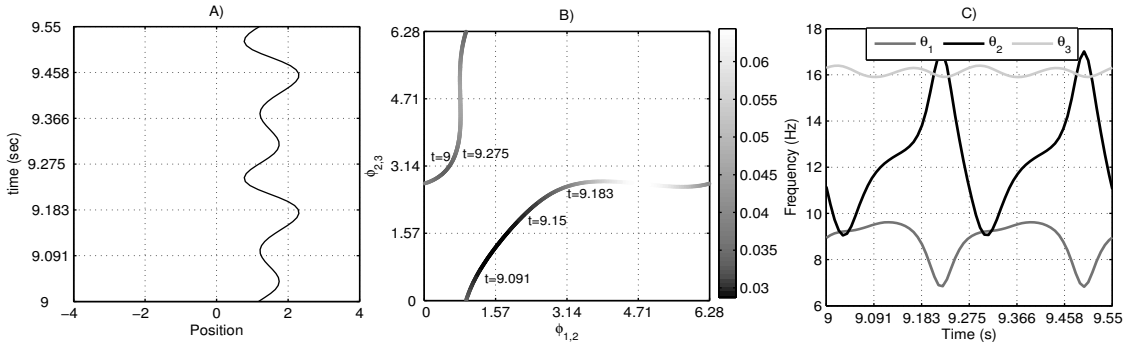

Figure 4.8: Agent's behaviour and its internal dynamics within a short time-window $t = [9, 9.55]$ s. **Graphic A** shows the agent's behavioural response (see position in the x-axis) during 550 ms (y-axis) of interaction with a circle. **Graphic B** shows the trajectory of phase relations corresponding to behaviour presented in graphic A. The grey scale shows the derivative of the phase relation dynamics (see colorbar). Numbers next to the trajectory of phase relations indicate the time in seconds. The phase relation dynamics starts at t=9 s and returns to the same point 275 ms later (at t=9.275 s). **Graphic C** shows the frequency (y-axis) of the oscillators (see legend) over time (x-axis).

In order to present the structure of the modulation, we obtained $\dot{\phi}_{1,2}(t)$ and $\dot{\phi}_{2,3}(t)$ for all phase relations $\phi_{1,2}(t)$ and $\phi_{2,3}(t)$ and the sensory input $s(t)$; where t is a time step of the agent's lifetime (i.e. we obtained the magnitude of each vector component during the agent's behaviour). Then we calculated $\dot{\phi}_{1,2}(t)$ and $\dot{\phi}_{2,3}(t)$ for same states $\phi_{1,2}(t)$ and $\phi_{2,3}(t)$, but for a constant sensory input $s = 0$ (i.e. we obtained the magnitude of each vector component considering that $s = 0$). We then subtracted the magnitudes of the vector components under $s = 0$ from the magnitudes under a continuously changing s (during the agent's behaviour). The result of this operation is a resultant vector repre-

senting the difference in the phase relation dynamics under coupled and decoupled (with $s = 0$) conditions. The magnitude and angle of the resultant vector are shown in Fig. 4.9.

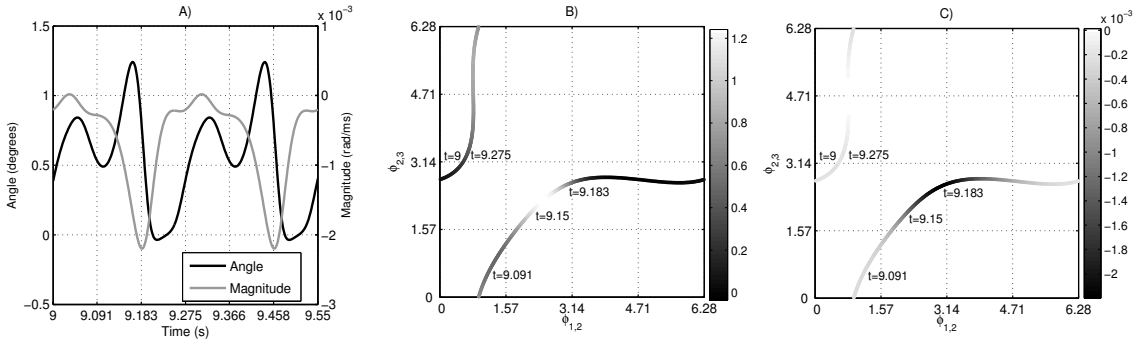

Figure 4.9: Modulation of the oscillatory network when it is coupled to the agent's body and under interaction with a circle. Graphic A shows the difference in angle (left y-axis) and magnitude (right y-axis) between the vectors in the vector field under coupled and decoupled ($s = 0$) conditions (see the main text body for explanation of how these graphics were generated). While graphic A shows the angle and the magnitude over time, graphics B and C show how these variables change in relation to the state of the network – defined by $\phi_{1,2}$ (x-axis) and $\phi_{2,3}$ (y-axis). The colour bars in graphics B and C represent the angle and magnitude, respectively.

At $t = 9$ s, for instance, the state of the oscillatory network is $\phi_{1,2} = 0.64$ and $\phi_{2,3} = 3.30$, and the state of the agent's sensor is $s = 0.076$ (not shown in the graphic). This value of sensory input increases the angle of the vector with origin at $\phi_{1,2} = 0.64$ and $\phi_{2,3} = 3.30$ in 0.039 degrees and decreases its magnitude in 0.0002 in relation to vector in the same position but with s=0. At $t = 9.183$ s, the state of the phase relation is $\phi_{1,2} = 2.92$ and $\phi_{2,3} = 2.57$, and the agent's sensor is $s = 0.356$. For this state, the sensor modulates the tangent vector by increasing its angle in 0.82 degrees and decreasing its magnitude in -0.0022 in relation to the same vector but with $s = 0$. Graphics 4.9-B and C, then, represent the pattern of modulation that generates the stable dynamical regime of phase relations (shown in graphic 4.8-B) under the interaction with a circle.

Under the interaction with a triangle, the oscillatory network takes a longer time to settle down in a stable regime of phase relations; however, the agent is still able to perform the correct behaviour when its network is in a transient dynamics within the basin of attraction of the stable attractor underlying the interaction with a triangle. See the agent's behaviour and its internal dynamics in Fig. 4.10. The periodicity of the network dynamics after approaching the limit cycle attractor is of 2.6 s – more than 9

times greater than the periodicity of the network during the interaction with a circle (0.275 s). The phase relation dynamics cross the state $\phi_{1,2} = 3.14$ eight times at different values of $\phi_{2,3}$ (some states are near to each other in the order of 10^{-3}, as the points 2 and 6 shown in the Poincare map in graphic 4.10-C) before it returns to the same state closing the cycle. The length of time taken for the network to converge to the stable limit cycle will be analysed in section 4.5.

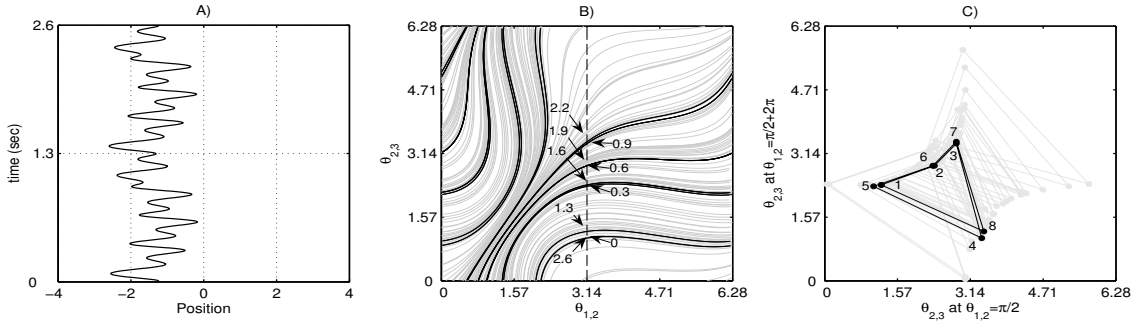

Figure 4.10: Agent's behaviour and its internal dynamics during the interaction with a triangle. **Graphic A** shows the agent's behaviour during a 2.6 s time-window (see y-axis). **Graphic B** shows the phase relation dynamics of the oscillatory network during a 100 s time-window. The grey lines represent the transient dynamics of the oscillations and the black lines the stable attractor to which the network converges. The arrows next to the dashed line at $\phi_{1,2} = 3.14$ point to 8 different values of $\phi_{2,3}$ when $\phi_{1,2} = 3.14$ and after stabilisation in the attractor. Note that the stable trajectory has a period of 2.6 s. **Graphic C** is a Poincare map showing the values of $\phi_{2,3}$ when $\phi_{1,2} = 3.14$. The dark black line with black dots highlights the pattern to which the phase relations converge, and the numbers from 1 to 8 show the sequence of how the state is changing in the map.

In sum, we have seen that the oscillatory network has two limit cycle attractors corresponding to the agent's interaction with a circle and a triangle, respectively. While during the interaction with a circle the oscillatory network quickly converges to the attractor, during the interaction with a triangle the phase relations maintain in a transient dynamics for a longer period of time before settling down in the attractor. We have also shown how the agent's sensory activity modulates the oscillatory network in a structured way – as presented in graphics 4.9-B and C – so that the functional patterns of phase relations are generated and the agent performs a coherent behaviour.

It is important to notice that the functional patterns of phase relations are generated and sustained by a coordinated dynamics of the closed sensorimotor loop. At each time

t during the task, the state of the oscillatory network maps onto a motor behaviour and, depending on the shape of the object and on the position of the agent in relation to the object, the motor behaviour produces a particular sensory input that modulates the vector field in a such way that the network converges to the functional patterns of phase relations. Without a coherent coordination of this closed sensorimotor loop (if the network and the sensory dynamics are not coordinated due to a sensor delay, for instance) the system might converge to non-functional oscillatory regimes. In this analysis we are focusing on how the sensory dynamics shapes the network's intrinsic oscillations, but we should keep in mind that the network is generating the agent's motor behaviour which in turn is changing the agent's sensory activity – in the next chapter (chapter 5) we will add into our analysis the modulation of the sensory dynamics by the motor behaviour.

4.5 Sensory information in the oscillatory network

During the process of modulation, information flows from the agent's sensor to the network and vice-versa. In this section, we analyse i) how much information the phase relations carry about the sensory activity; ii) how the amount of information in the phase relations about the sensory activity changes as the phase relation dynamics are reduced to the dynamics of synchronised oscillations – which will inform us whether the information in the phase relations about the sensory activity is higher during synchronised or desynchronised oscillations. The results presented in this section support the claim made in the previous chapter (chapter 3) about the importance of desynchronous oscillations for the agent's sensorimotor dynamics.

4.5.1 Mutual information between phase relations and sensory activity

Firstly we analyse the information that each phase relation carries about the agent's sensory activity during a single trial of the experiment (see Fig. 4.11). The Shannon's entropy and the mutual information are measured at the end of each time-window of 6 s (when the object's shape can change), which gives a total of 6000 data points for each time series. At the end of the first time-window (at $t = 6$ s), the mutual information in each phase relation is below 1 bit and the entropy of the sensor is ≈ 3.8 bits. From $t = 6$ to $t = 24$ s, the mutual information of the phase relations increases and maintains stable at ≈ 2.7 bits. The mutual information increases because during the first 6 s the oscillatory network spends some time in a transient dynamics, and from $t = 6$ s onwards the oscillatory network settles down in the stable limit cycle underlying the agent's interaction with a

circle. Observe a similar phenomenon from $t = 84$ to $t = 102$ s.

When the agent is interacting with a triangle the entropy of the sensor is ≈ 5.1 bits. At $t = 30$ s, the information in the phase relations about the triangle is around 1 bit. During the next time-windows, the the mutual information slowly increases and, at $t = 48$ s, $I(s, \phi_{i,j}) \approx 1.5$ bits. A similar phenomenon can be seen from $t = 108$ to $t = 120$. The mutual information keeps increasing until the oscillatory network stabilises in the limit cycle underlying the agent's interaction with a triangle.

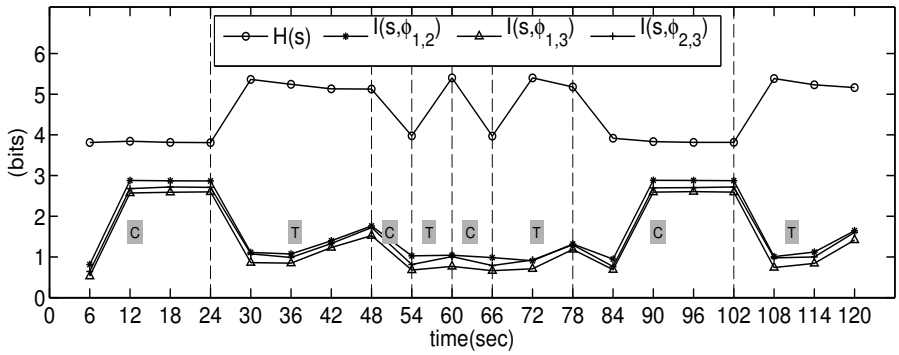

Figure 4.11: Information about the agent's sensory activity present in each phase relation. The information is measured based on a single trial of the experiment (the same trial presented in Fig. 4.2). $H(s)$ represents the entropy of the sensor and $I(s, \phi_{i,j})$ the mutual information between the sensor s and a phase relation $\phi_{i,j}$ (see legend). The letters "C" and "T" in grey background indicate whether the agent is interacting with a circle or a triangle, respectively.

In order to show how the mutual information increases over a long period of interaction with either of the objects we left the agent interacting with the same object for 300 s (50 sections of 6 s each). The average mutual information over 50 trials of interaction with either a circle or a triangle are presented in Fig. 4.12. The mutual information during the interaction with a circle (graphic 4.12-A) stabilise in $I(s, \phi_{1,2}) = 2.87$, $I(s, \phi_{1,3}) = 2.70$ and $I(s, \phi_{2,3}) = 2.59$ bits from the third time-window of 6 s (from 18 s). During the interaction with a triangle (graphic 4.12-B) the mutual information slowly increases over time and stabilises only after the 20^{th} section of 6 s (120 seconds). The stabilisation of the mutual information takes longer during the interaction with a triangle due to the transient dynamics of the phase relations.

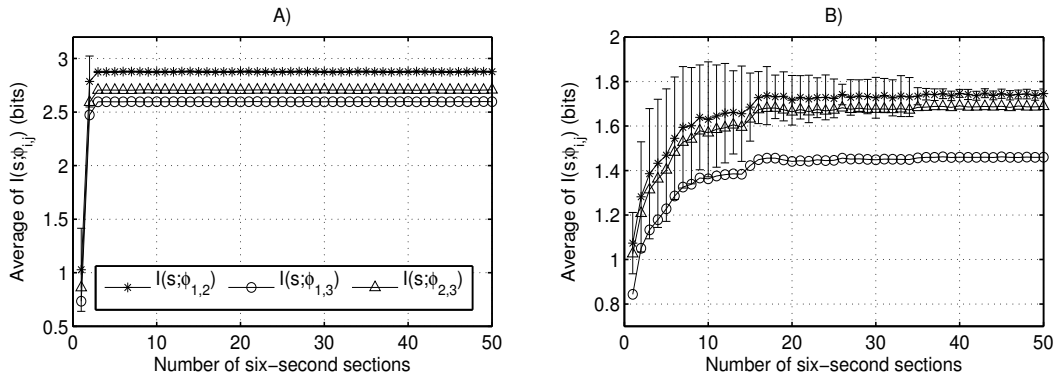

Figure 4.12: Average mutual information during the interaction with either a circle (**graphic A**) or a triangle (**graphic B**). Graphic A and B show the average mutual information between the sensor and the phase relations (see legend) during 50 sections of interaction (300 s). Bars represent the standard deviation of $I(s, \phi_{1,2})$. The other standard deviations are similar to the standard deviation of $I(s, \phi_{1,2})$, for ease of visualisation they are not shown.

4.5.2 Mutual information without desynchronised oscillations

We have seen how much information each phase relation carries about the sensory activity, we now analyse how the amount of information in the phase relations about the sensory activity changes as the phase relation dynamics are reduced to the dynamics of synchronised oscillations. In this work we are considering that i) a phase relation $\phi_{i,j}$ is completely synchronised when $\dot{\phi}_{i,j} = 0$; and ii) the higher the $|\dot{\phi}_{i,j}|$ the more desynchronised is the phase relation $\phi_{i,j}$. In order to remove the information of the desynchronised phase relations, all $\phi_{i,j}$ whose $|\dot{\phi}_{i,j}| > threshold$ are shuffled[2].

The black lines in graphics 4.13-A, B and C show how the mutual information changes as the information present in desynchronous oscillations is removed from the dynamics of phase relations during the interaction with a triangle. The derivative of the phase relations $\phi_{1,2}$ (in graphic 4.13-A), for instance, changes from 0 to 0.068 (see x-axis). The phase relations $\phi_{1,2}$ whose absolute value of derivatives are smaller than 0.04 carry 0.84 of the total amount of information (see grey line in graphic 4.13-A), which means that the desynchronized phase relations ($|\dot{\phi}_{i,j}| > 0.04$) carry 0.16 of the information about the sensory activity. The grey lines in graphics 4.13-A, B and C show how the amount of phase relations changes (in a scale from 0 to 1, see y-axes) in relation to their derivatives (x-axes). For instance, the phase relations $\phi_{1,2}$ whose $|\dot{\phi}_{1,2}| \leq 0.04$ represent 0.85 of the

[2]In this analysis we are using the same methods used in the previous chapter (see Eq. 3.4)

total amount of phase relations, i.e. 0.85 of the most synchronized phase relations carry 0.84 of the information about the sensory activity.

The relation between the mutual information and the amount of phase relations is shown in graphic 4.13-D. Notice that 0.5 of the most synchronised oscillations between θ_1 and θ_2 carry $\sim$ 0.42 of the total information, whereas 0.5 of the most synchronised oscillations between θ_2 and θ_3 carry 0.57 of the total information. The same analyses of mutual information for the interaction with a circle is presented in Fig. 4.14. What the results from both analyses (interaction with triangle and circle) suggest is that there is no privileged status to either synchronous or desynchronous oscillations regarding the amount of information they carry about the sensory activity.

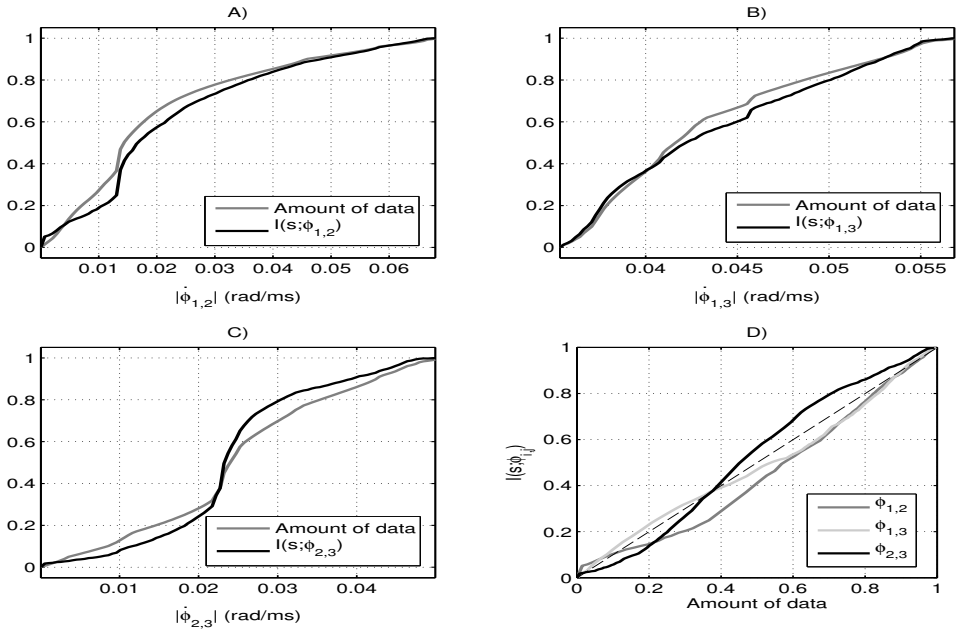

Figure 4.13: Distribution of information throughout the phase relation dynamics during the interaction with a triangle. The black lines in graphics **A**, **B** and **C** show the mutual information $I(s;\phi_{i,j})$ for the phase relations $\phi_{1,2}$, $\phi_{1,3}$, and $\phi_{2,3}$, respectively (see legend). The values of $I(s;\phi_{i,j})$ are in a scale from 0 (minimum) to 1 (maximum), see y-axes. The grey lines in these graphics show the amount of $\phi_{i,j}$ (in a scale from 0 to 1) whose $|\dot{\phi}_{i,j}| \leq threshold$. Graphic **D** shows how $I(s;\phi_{i,j})$ changes with the amount of $\phi_{i,j}$. Each line represent a phase relation (see legend). The dashed line in the diagonal highlights a linear relationship between the amount of phase relations and the mutual information.

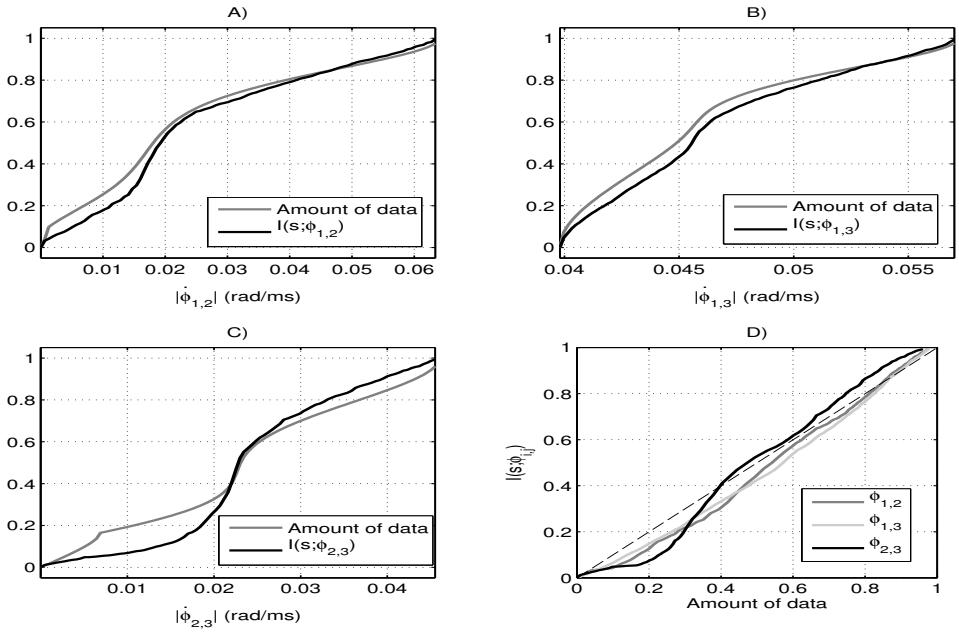

Figure 4.14: Distribution of information throughout the phase relation dynamics during the interaction with a circle. See caption of Fig. 4.13.

4.6 Discussion

We have analysed a model of an oscillatory network that spontaneously oscillates outside a sensorimotor loop and, when it is coupled to an agent's body, generates a functional sensorimotor behaviour. We have firstly shown that the agent's internal oscillations are generated by a weakly coupled network. The strength of the coupling was quantified by the entropy of the phase relations. It is important to notice that it would not be possible to interpret the entropy of the phase relations as the strength of the coupling if the oscillators had similar natural frequencies as the probability distributions of phase relations would be degenerate even in the absence of coupling.

We have analysed how s modulates the vector field of phase relations and shown that as s increases from 0 to 1, the component $v_{\phi_{1,2}}$ linearly decreases and $v_{\phi_{2,3}}$ maintains constant. Despite this linearity, the transformation in the entire vector field is not linear as it depends on the angle and magnitude of each vector. This analysis has contributed to understand how the sensory input can affected the network's spontaneous oscillations.

The analysis of the oscillatory network coupled to the agent's body has shown that the interaction with a circle and a triangle correspond to different limit cycles in the network. The convergence to the limit cycle under the interaction with a circle is quicker than the convergence under the interaction with a triangle. We have seen that it is sufficient for the

network to be in the basin of attraction of a limit cycle – moving in a transient dynamics towards the limit cycle – for the agent to perform a correct behaviour.

Notice that the limit cycle dynamics and the transient dynamics towards the limit cycle depend on a fine grained coordination between the temporal structure of the agent's internal oscillations and the sensory dynamics. If the sensory and the network dynamics are not well coordinated (due to a sensor delay, for instance) the network could converge to a non-functional oscillatory regimes due to a different modulation of the vector field.

It is important to notice as well that although we have been focusing on the modulation of the network's spontaneous oscillations by the agent's sensory dynamics, the network activity also modulates the sensors by moving the agent in the environment (the sensory dynamics depends on the position of the agent in relation to the object, on the object's shape and also on the agent's motor behaviour). That means that the limit cycle dynamics and the transient dynamics do depend not only on a fine grained modulation of the oscillations by the sensory dynamics, but also on the modulation of the sensors by the motors. The dynamics underlying the coherent behaviours (e.g. limit cycle dynamics underlying the agent's interaction with a triangle) are not "standalone" functional entities in the oscillatory network waiting for the correct input to be activated, instead they depend on and exist as part of the entire sensorimotor loop coordinated dynamics.

The information analysis has shown that the information about the sensory activity is evenly distributed in the phase relations without a privileged status to either synchronous or desynchronous oscillations – which supports the results presented in the previous chapter. An interpretation of this result is that the modulation of the network by the sensory dynamics has similar effects on both modes of oscillatory dynamics (synchronous and desynchronous), i.e. none of them is more stimulus-driven than the other, they are equally generated from self-sustained oscillations in the network combined with perturbations from the sensory dynamics.

The results and conclusions presented in this chapter could not have been predicted without a careful analysis of the model. Firstly, it was not possible to predict that the agent would be able to perform the correct behaviour controlled by such a weakly-coupled oscillatory network (the coupling strength was quantified by the entropy of the phase relations, as shown in Fig. 4.4). The agent's left motor, for instance, was controlled by a weakly-coupled and highly desynchronised pair of oscillators ($H(\phi_{1,3}) \approx 1 \ \forall \ s \in [0,1]$). This result has suggested that functional neural activity can be obtained from completely desynchronized oscillations, which differs from the traditional approach where synchro-

nized oscillatory activity is essential for the generation of neural functions as it establishes the communication between functionally distinct and spatially distributed neural areas (Uhlhaas et al., 2009; Singer, 2011; Hipp et al., 2011; Sharafi et al., 2012; Sakurai et al., 2013).

Secondly, it was not possible predict in advance which types of oscillatory dynamics would generate the agent's correct behaviour. While during the interaction with a circle the network quickly converges to a stable limit cycle, during the interaction with a triangle it operates in a transient dynamics in the basin of attraction of a stable limit cycle. In the latter case, the agent performs the correct behaviour even before the dynamics settle down in the limit cycle attractor. These types of dynamics are not the only way the agent could perform the correct behaviour. Alternatively, the dynamics could be given by two different clusters of synchronized oscillators, one for each type of interaction (circle and triangle). The results presented here have contributed to understand how functional sensorimotor behaviours can be generated by different types of sensorimotor dynamics.

Thirdly, it was not possible to predict that the system evolved would present a tight dependence between the agent's sensorimotor loop and its internal oscillations. We have shown that the functional limit cycles underlying the interaction with circle and triangle would not exist without a fine-grained coordination between the oscillatory network and the agent's motor-sensory dynamics. This result has shown a proof of concept that functional neural dynamics are not necessarily standalone entities in a neural system waiting for a stimulus to be activated (as in the stimulus-driven approach discussed in the Introduction (Vogels et al., 2005)). In sum, the model developed in this chapter could have multiple possible outcomes and without a carefully analysis of it, the results and conclusions could not have been predicted in advance.

The results presented in this chapter helps understand how the temporal structure of an oscillatory network changes within an agent's sensorimotor loop and how the informational content present in the temporal structure about the sensorimotor dynamics changes as the temporal relations are reduced to the dynamics of synchronous oscillations.

4.7 Summary

The content of this chapter encompassed both central issues of the thesis, namely i) the informational content of synchronous and desynchronous oscillations, and ii) the dynamical analysis of the oscillatory dynamics within sensorimotor loops. The next chapters focus exclusively on latter; particularly, chapter 5 explores how the sensory dynamics modulates

the temporal structure of an agent's internal oscillations – similar to what we have studied in the current chapter – and additionally it explores how the oscillations modulate the sensory dynamics through the agent's motor behaviour. Chapter 6 explores how functional oscillatory regimes are sustained by an agent's sensorimotor loop under the presence of plastic changes in the structure of the network and also how a network accommodates functional oscillatory regimes (regimes that generate an agent's coherent sensorimotor coordination) by modifying its connectivity without affecting the functionality of pre-existing regimes.

Chapter 5

The dependency of functional oscillatory regimes on an agent's motor-sensory dynamics: a case study with the HKB equation

5.1 Introduction

One of the simplest, yet explanatorily powerful, models of oscillatory coordination dynamics is the extended HKB (Haken-Kelso-Bunz) model which captures the temporal relation between the activity of coupled oscillatory elements (Kelso, 1995; Kelso et al., 1990). This model has been carefully studied by manipulating a control parameter that modifies the oscillators' natural frequencies or their coupling factor. One of its main dynamical properties is the metastable regime in which the phase relation variable engages when the control parameter crosses a certain threshold. Metastable dynamics have been hypothesized to be the dynamical signature of the nervous system underlying sensorimotor coordination (Kelso and Tognoli, 2009; Tognoli and Kelso, 2009; Bressler and Kelso, 2001). Empirical evidence favouring this hypothesis comes, for instance, from studies showing correlation between sensory stimulation and transiently synchronized networks in the brain of animals performing perceptual and motor coordination tasks (Rodriguez et al., 1999; Varela et al., 2001; Buzsaki, 2006; Pockett et al., 2009; Singer, 2011; Hipp et al., 2011). Despite such evidence supporting the existence of metastable regimes in the brain of behaving animals, to our knowledge there are still very few models (if any) where the *HKB equation generates the motor behaviour of an agent interacting in a spatial environment and, at the*

same time, has its control parameter modulated, through sensory feedback, by the motor behaviour it generates. Thus, in this work we investigate the dynamics of the extended HKB equation within a closed sensorimotor loop by implementing it as the controller of an agent performing a functional behaviour (gradient climbing) in a simulated two-dimensional environment. The "output" of the extended HKB equation (the phase relation variable) generates the agent's motor behaviour and, at the same time, its control parameter (in our particular case, the variable representing the oscillators' frequency difference) is modulated by the agent's behaviour through its sensory activity. The extended HKB equation within the agent's sensorimotor loop will be referred to as *the situated HKB model.*

The HKB equation has been used to model cases of sensorimotor coupling such as in Kelso et al. (2009), where a human subject receives sensory feedback from a computer screen and the human's behaviour in turn affects the computer. The novelty of the model we study here is that the coupling is spatial and the HKB is not meant to capture the global feedback dynamics but is used directly as a robotic controller. The resulting dynamics will be shown to have special properties (e.g. multiple metastable regimes).

Briefly, we will show i) how different metastable dynamical patterns in the HKB equation are generated and sustained by the continuous interaction between the agent and its environment; and ii) how the emergence of functional metastable patterns in the HKB equation – i.e. patterns that generate gradient climbing behaviour – depends not only on the structure of the agent's sensory input but also on the coordinated coupling of the agent's motor-sensory dynamics. The analysis of the extended HKB equation within a sensorimotor loop is a contribution to the Coordination Dynamics framework and, as such, it provides theoretical insights to understanding the interplay between neural oscillations and sensorimotor behaviour.

Some theoretical aspects of the HKB model are briefly reviewed in section 5.2 (for more details refer to section 2.3.1). The computational model and its analysis are presented in sections 5.3 and 5.4, respectively.

5.2 Preliminary considerations on the HKB model

The HKB model has been proposed in the context of the Coordination Dynamics framework (Haken et al., 1985; Kelso, 1995). It was originally proposed to account for experimental observations on rhythmical finger and hand coordinations in human beings, and aimed to investigate: i) the formation of ordered states of coordination in human beings, ii) the multistability of these observed states; and iii) the conditions that give rise to

switching among coordinative states (Kelso, 1995, 2008). The model describes the phase relation dynamics of oscillatory components at a high level of abstraction without specific references to underlying mechanisms that generate its dynamics. Such a phenomenological modelling approach of the HKB has been useful for investigating general laws of coordination in oscillatory systems (Haken et al., 1985). The dynamical phenomena described by this model (e.g. metastability and transition between phase and anti-phase coordinative patterns) have been validated with a variety of empirical data from experiments on human rhythmic movement coordination at the behavioural (Forrester and Whitall, 2000; Robertson, 2001; Russell et al., 2010) and neural levels (Bressler and Kelso, 2001; Aramaki et al., 2006; Jantzen et al., 2009). Since its proposal (Haken et al., 1985), the HKB model and the dynamical phenomena it describes have been extensively studied (Jirsa et al., 1998; Fuchs and Jirsa, 2008; Tognoli and Kelso, 2009), and remains an explanatorily powerful model in the field of cognitive science (Kelso, 2012).

Notice that the level of abstraction described by the HKB equation is different from the Kuramto's equation that we have studied in previous chapters. Whereas the HKB depicts the *phase relation dynamics* between oscillatory components, the Kuramoto's equation depicts *phase dynamics*. In the previous models the phase relations were obtained from Kuramoto's equation by subtracting the phase between the network's oscillators (i.e. $\phi_{i,j}(t) = |\theta_i(t) - \theta_j(t)|$, as presented in Eq. (3.1)). The use of the HKB equation, rather than Kuramoto's one, to implement the agent's controller allows us to discuss the dynamical analysis of phase relations within the sensorimotor loop (one of the central issues of this thesis) in the context of the well-established Coordination Dynamics framework developed by Kelso. Besides, the implementation and analysis of this equation within the sensorimotor loop can contribute to Kelso's framework with new theoretical insights to develop the general laws of coordination in oscillatory systems.

5.3 Theoretical model

5.3.1 The agent and its controller

The model consists of a two dimensional simulated environment and a circular agent whose task is to climb a linear gradient towards the centre of the environment where the peak is located. The agent has a body of of 5 units diameter with two diametrically opposed motors and a sensor randomly positioned at $90\,^\circ \pm 5\,^\circ$ relative to the motor axis[1]. The

[1] Although the variation of 5 degrees in the sensor's position increases the likelihood of the optimization algorithm (explained below) to obtain a more robust solution for the gradient climbing behaviour, it is not

agent's sensor is connected to a controller and the latter connected to both motors, as shown in Fig. 5.1. The controller's dynamics are governed by the extended HKB equation where the difference in natural frequencies (ω) is modulated by the agent's sensory input (s), as defined in (5.1).

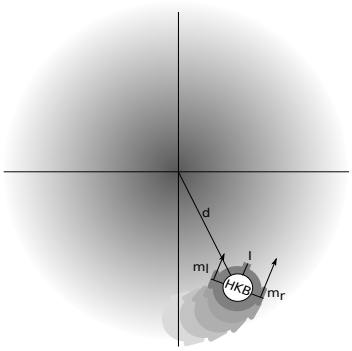

Figure 5.1: Agent and its environment. The agent has a sensory input, two motors m_r and m_l and is controlled by the HKB equation, see Eq. (5.1). The gradient in the environment is represented by the grey scale, where the darker the color the higher the gradient. The highest gradient is positioned at the coordinates $x = 0$ and $y = 0$ in the two-dimensional environment.

$$\dot{\phi} = s\omega - a\ sin\ \phi - 2\ b\ sin(2\phi), \tag{5.1}$$

where ϕ is the phase relation between two oscillators at an undetermined level of abstraction, s is the sensor activation given by $s = c_1\dot{d}$, where c_1 is a constant and $\dot{d}$ is the derivative of the distance from the agent to the centre of the environment; ω is a constant representing the difference in natural frequencies between two oscillators; a and b are constants representing the coupling factor. By sensing the derivative of the distance $\dot{d}$, the agent is able to perceive a linear radial gradient with its peak at the centre of the environment. We have chosen this type of derivative sensing because many organism's behaviour is based on interactions with different types of gradients[3]. Also, for a minimal model, sensing the derivative has the advantage that the agent does not perceive a continuously increasing input, making the dynamics more regular throughout

necessary for evolving the parameters of the model.

[3]Most of small scale adaptive behaviour occurs along chemical gradients. The microscopic world is a world of gradients (like thermal gradients or light gradients but mostly chemical gradients). The adaptive behaviour of small animals (e.g. C. elegans) and individual motile cells (e.g. bacteria but also animal cells migrating during development) is mostly a gradient-related adaptive behaviour. Navigating smell or heat gradients is also a stereotypical adaptive task for higher animals.

the behaviour of the agent.

The equation is integrated with time step 0.001 seconds using the Euler method. The right and left motors of the agent are governed by Eq. (5.2) and (5.3), where c_2, c_3 and c_4 are constants.

$$m_r = c_2(cos(\phi + c_3) + 1) \tag{5.2}$$

$$m_l = c_2(cos(\phi + c_4) + 1) \tag{5.3}$$

5.3.2 Optimization with a genetic algorithm

In order to obtain an agent performing gradient climbing, a total of 7 parameters (c_1, c_2, c_3, c_4, ω, a, b) were optimized with the *microbial genetic algorithm* (Harvey, 2001). These parameters were encoded in a genotype as a vector of real numbers in the range [0,1] linearly scaled, at each trial, to their corresponding range ($a = [0.1, 10]$, $b = [0.1, 10]$, $\omega = [17, 22]$, $c_1 = [0, 3]$, $c_2 = [0, 0.4]$, $c_3 = [0, 2\pi]$, and $c_4 = [0, 2\pi]$). The genetic algorithm (GA) setup was: population size (50); mutation rate (0.05); recombination (0.60); reflexive mutation; normal distribution for mutation $\left(\mu = 0, \sigma^2 = 0.1\right)$; trial length (150 seconds); and trials for each agent (20). At the end of the 20^{th} trial the worst fitness (out of 20) was used as the selective fitness of the agent. The fitness function was defined by (5.4):

$$F = \begin{cases} 1 - \frac{d_f}{d_i}; & if\ d_f < d_i; \\ 0; & otherwise; \end{cases} \tag{5.4}$$

Where F is the fitness; d_i and d_f are the initial and final distances from the agent to the centre of the environment where the peak of the gradient is located. This fitness function selects the agents that perform gradient climbing in an environment with a peak at its centre. The optimized parameters found by the GA were the following: $c_1 = 2.72$, $c_2 = 0.36$, $c_3 = 3.44$, $c_4 = 3.21$, $\omega = 19.67$, $a = 0.99$ and $b = 7.94$. The GA ran for 150 tournaments (equivalent to 6 generations) and the best agent got a fitness of 0.98. Most solutions found by the GA were monostable controllers. In order to obtain metastable dynamics we had to run different instances of GAs, each one with different ranges of ω.

There is no specific reason why the *microbial genetic algorithm* was used, any other optimization method would probably work as the problem is relatively simple. Neither is there a specific reason why c_1 and ω are two different parameters, they could have been optimized as a single variable since their product is what is actually relevant. We have

used two parameters to keep the model coherent in the sense that c_1 represents the sensor strength and the ω the frequency difference.

Notice that the purpose of the model developed here is not to solve the problem of gradient climbing (which could be solved by a simple Braitenberg vehicle), but to raise and discuss theoretical issues about the interplay between oscillatory and sensorimotor dynamics based on the analysis of the HKB equation controlling an agent's behaviour under a metastable regime. In this sense, we are not looking for optimum nor general solutions for the gradient climbing behaviour but for a solution where the controller is metastable while the agent is performing the desired behaviour.

The next sections present the analysis of the fittest agent found the by the GA.

5.4 Results

In **section 5.4.1** we briefly present two distinct sensorimotor behaviours that the agent engages in during its interaction with the environment and their underlying metastable regimes in the situated HKB model. In **section 5.4.2** we analyse how the metastable regimes are generated and how the transition between them takes place. In **section 5.4.3** we perform an experiment to compare the effects of motor-sensory coupling on the dynamical and informational properties of the situated HKB model.

5.4.1 Metastable regimes underlying sensorimotor behaviours

Fig. 5.2-A presents the behaviour of an agent during a single trial of gradient climbing. Fig. 5.2-B shows how the distance from the agent to the region of highest gradient (the centre of the environment) changes for 20 trials of the experiment; the agent's position, orientation and the controller's phase relation (ϕ) have a random value at the beginning of each trial. The agents take from 80 up to 105 seconds to move towards the centre of the environment and then they start moving around it. The patterns of sensorimotor behaviour that the agents engage in when they are approaching the centre and when they are moving around it are shown in Fig. 5.3. These patterns are defined by different (repeatedly observed) closed orbits in the state space of sensory and motor activities and will be referred to as SM_1 and SM_2, respectively (SM_n standing for SensoriMotor pattern n).

Underlying the sensorimotor behavioural patterns SM_1 and SM_2 there are two distinct metastable regimes of the phase relation (ϕ). The regimes are defined as the distinct regions of the agent's dynamics that correspond directly to the empirically observed be-

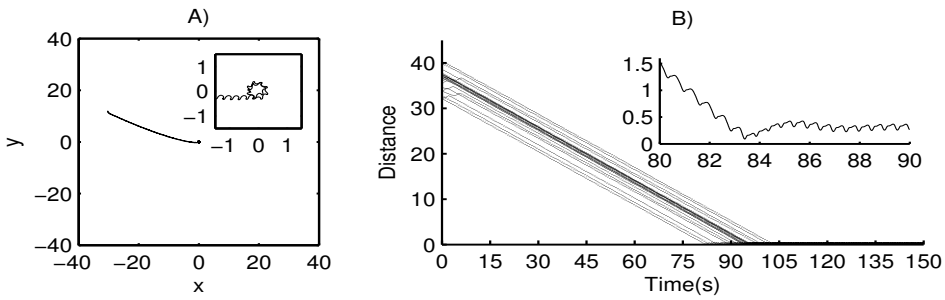

Figure 5.2: **Graphic A.** Single trial of an agent's behaviour in the environment. The agent starts at the position (x=-30,y=12) and moves up the gradient towards the centre (x=0,y=0). When the agent approaches the region of highest gradient it starts moving around it, as shown in the inset that zooms into the agent's behaviour in the interval $t = [80, 90]$ seconds. **Graphic B.** Distance from the agent to the centre of the environment for 20 trials starting at random initial conditions. The inset zooms into the distance from 80 to 90 seconds for the trial shown in graphic A. The agents tested take at least 80 seconds to approach the region of highest gradient.

haviours SM_1 and SM_2. As the following analysis shows, the dynamics in these regions have clear differences. Fig. 5.4-A shows such regimes for 20 successful trials – those presented in Fig. 5.2-B. Notice that these regimes are depicted by showing the state space of the agent's controller ($\phi \in [0, 2\pi)$ in the x-axis) and the derivative of ϕ throughout the state space (in the y-axis). The derivative $\dot{\phi}$ is calculated by Eq. 5.1 at each time step of the simulation. For any initial conditions all controllers converge to the metastable regimes R_1 and R_2 of ϕ for the sensorimotor patterns SM_1 and SM_2, respectively. In both regimes the derivative of the phase relation is always greater than zero showing that the state of the controller never reaches a fixed point. Fig. 5.4-B shows the density distributions of ϕ for R_1 and R_2. These distributions were generated by dividing the state space $[0, 2\pi)$ into 48 equally spaced bins and using the values of ϕ from the time windows $[10, 50]$ s and $[110, 150]$ s (a total of 40000 data points for each time window) considering a single trial of gradient climbing. The regimes R_1 and R_2 have two regions where ϕ slows down, which can be seen by two peaks in the density distribution of each regime (ϕ spends more time in the regions with low derivative, that is why there are peaks in the density distributions). The difference between distributions (represented by the line without marks in the graphic) maintains a level slightly below zero and has a peak in between $[\pi, 3\pi/2]$.

Basically, the purpose of the next section is to understand the coordination between the agent's metastable oscillatory regimes – R_1 and R_2 – and its sensorimotor behaviours –

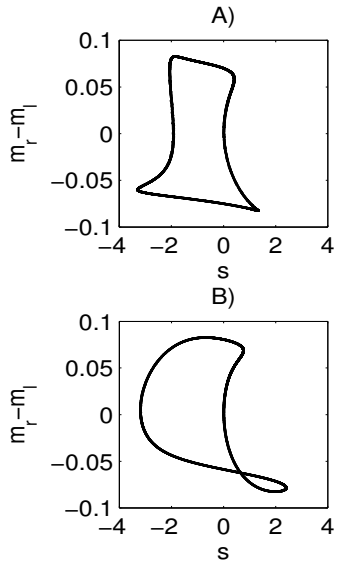

Figure 5.3: Patterns of sensorimotor behaviour in which the agents engage in when they are moving towards the region of highest gradient (**A**) and when they are moving around it (**B**). The agent's sensor is shown in the x axis and the difference in speed between its right and left motors ($m_r - m_l$, defined in Equations 5.2 and 5.3) is shown in the y axis. Black lines highlight the sensorimotor dynamics within the time intervals $[10, 50]$s and $[110, 150]$s in graphic **A** and **B**, respectively. All agents converge to the same pattern of sensorimotor behaviour during those time intervals.

SM_1 and SM_2. We will study how these oscillatory regimes are generated and maintained during the agent's interactions with its environment and also how the transition between them takes place.

5.4.2 Generation and transition between metastable regimes

We shall start by analysing the extended HKB equation *without* the sensorimotor loop. This analysis does not present any new result that has not been previously presented by Kelso et al. (1990) and Kelso (1995). However, it is important in the context of this paper to set the ground to study the situated HKB model. The purpose here is to understand how the control parameter s affects the derivative of ϕ throughout its state space $[0, 2\pi)$. The controller is studied within the parameter range $s = [-3.92, 3.92]$, which is the interval of sensory activation when the agent is behaving in the environment.

Fig. 5.5-A shows $\dot{\phi}$ throughout the state space of ϕ given three constant values of s. When $s = -3.92$ the state space contains an attractor (black-filled circle) and a repeller (white circle). When $s = 0$ and $s = 3.92$ there are no fixed points and the dynamics of ϕ

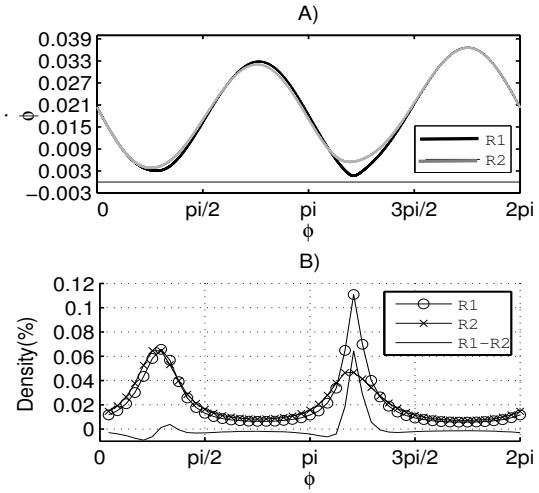

Figure 5.4: Metastable regimes of phase relation (ϕ) that the agent engages in while it is moving towards the centre of the environment and while it is moving around it. **Graphic A** shows the metastable regimes in terms of ϕ (x axis) and $\dot{\phi}$ (y axis) underlying SM_1 (black line) and SM_2 (grey line). These regimes will be referred to as R_1 and R_2, respectively (see legend). **Graphic B** shows the density distributions of R_1 (line with circles), R_2 (line with crosses) and the difference between the distributions (line without markers).

are metastable. By keeping s constant the derivative $\dot{\phi}$ always presents a global minimum at $\phi = 0.796$ and a local minimum at $\phi = 3.916$ radians. From now on these two points will be referred to as ϕ_G and ϕ_L, respectively. Fig. 5.5-B shows how s changes the derivative at minima ϕ_G and ϕ_L; note the linear relationship between these variables. For $s < -3.09$ (see vertical dashed line) the derivative is negative at global minimum ϕ_G and positive at the local minimum ϕ_L, showing that the state space has at least two fixed points. Above $s > -3.09$ the derivative is positive at ϕ_G, showing that the state space does not have fixed points. Fig. 5.5-C shows the bifurcation diagram of ϕ for the independent variable s. As s increases within the range [-3.92, -3.09) both fixed points (attractor and repeller) approach each other; when $s \approx -3.09$ both points merge into a single half-stable point; and when $s > -3.09$ this single point disappears and ϕ's dynamics become metastable. Summing up, s affects the dynamics of the agent's controller by linearly changing the derivative of ϕ throughout the entire state space $[0, 2\pi)$; additionally, a) within a certain range of s the attractor landscape presents two fixed points (an attractor and a repeller) that approach each other as s increases; and b) above this range the fixed points disappear and the phase relation dynamics fall into a metastable regime.

We now move to the analysis of the situated HKB model which has its control param-

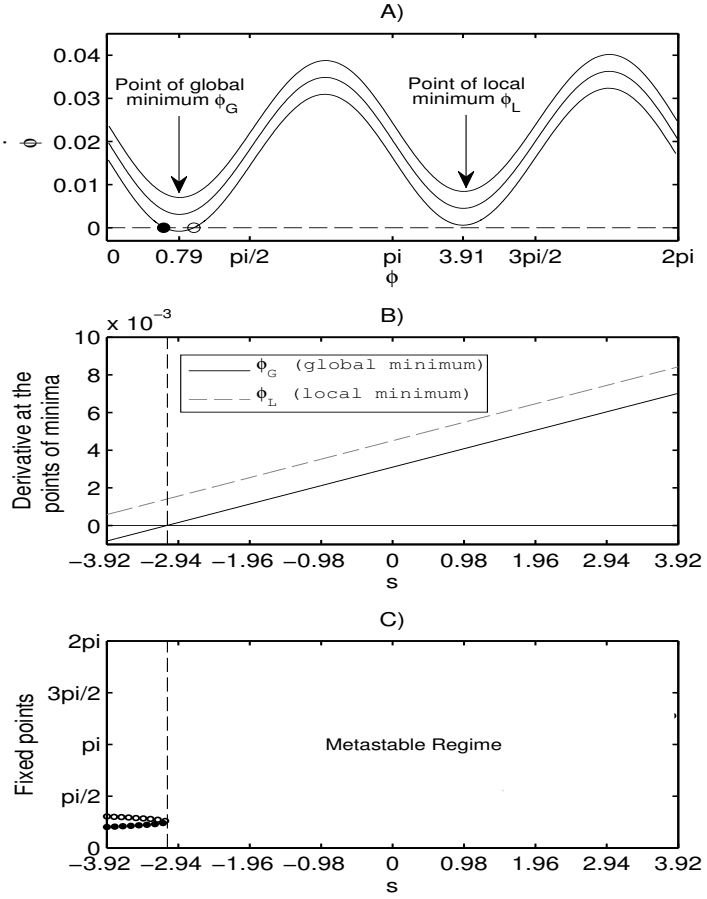

Figure 5.5: **Graphic A.** Phase relation ϕ (x axis) and its derivative $\dot{\phi}$ (y axis) for 3 different values of constant inputs $s = -3.92$ (lower curve), $s = 0$ (middle curve) and $s = 3.92$ (upper curve). When $s = -3.92$ the state space contains an attractor (black-filled circle) and a repeller (white circle). When $s = 0$ and $s = 3.92$ there are two points of minima at $\phi = 0.796$ and $\phi = 3.916$, respectively. **Graphic B.** Relation between s and the derivative at the points of minima $\phi = 0.796$ (black line) and $\phi = 3.916$ (grey dashed line). For $s < -3.09$ (see vertical dashed line) the derivative at $\phi = 0.796$ is negative, and for $s > -3.09$ both points of minima are positive. **Graphic C.** Bifurcation diagram of ϕ (see y axis) for the independent variable s (x axis). Vertical dashed line is at $s = -3.09$. The black-filled circles represent point attractors and the white circles represent the repellers. When $s > -3.09$ the phase relation dynamics are metastable.

eter s and phase relation ϕ co-modulating each other through the sensorimotor loop. We selected a small time window of 1.5 seconds during a single trial of gradient climbing in order to start presenting the dynamics of s and ϕ (see Fig. 5.6). Graphic 5.6-**A** shows how the derivative $\dot{\phi}$ at the points of minima ϕ_G and ϕ_L are changing over time. The sensor dynamics s (in graphic 5.6-**B**) and the derivative at ϕ_G and ϕ_L (in graphic 5.6-**A**) move up and down together due to their linear relationship. Although the fixed points appear in the state space around the minimum ϕ_G during $t_1 = [10.53, 10.60]$ and $t_2 = [11.18, 11.25]$ seconds, the phase relation does not reach the attractor. The reason for that is that during t_1 and t_2 the phase relation ϕ is away from the minimum ϕ_G moving in the region near the local minima $\phi_L = 3.916$ (see horizontal line in graphic 5.6-**C**) and when ϕ reaches the region near ϕ_G the sensor value has increased and the fixed points have disappeared. The main point to understand from this analysis is that the control parameter s linearly changes the derivative throughout the entire state space of ϕ, as a result, although for some values of s the state space shows one or two attractors, the continuous sensorimotor modulation of s in coordination with ϕ never allows the system to settle down on such attractors.

By looking at the values of s shown in Fig. 5.7 we can see how the derivative throughout the state space of ϕ is changing during R_1 and R_2. The greatest difference in the derivative takes place when ϕ is around the local minima ϕ_L; exactly at ϕ_L, for instance, the values of s are ≈ -1.94 and ≈ 1.55 during R_1 and R_2, respectively; showing that when ϕ is at the point of local minima, the derivative throughout the entire state space is lower during R_1 than during R_2. This difference explains why there is a peak in between π and $3\pi/2$ in the graphic of density distribution shown in Fig. 5.4-B. The state space has its lowest derivative and also fixed points around the global minimum ϕ_G in two situations: a) when ϕ is within $[3.69, 3.82]$ during R_1, and b) when ϕ is within $[2.65, 3.12]$ during R_2; both shown in the graphic by the values of s below the horizontal dashed line. Despite the presence of fixed points, ϕ dynamics never reaches a stable or unstable state as the state space changes when ϕ is around the global minimum ϕ_G (see that the values of s are above the horizontal dashed line when ϕ is around the global minimum $\phi_G = 0.796$). The main point to understand from this analysis is how s changes the derivative of the state space of ϕ in different ways during the regimes R_1 and R_2.

We have been describing how s modulates ϕ by changing the derivative of the latter; however, ϕ also modulates the dynamics of s by moving the agent in the environment – i.e. the dynamics of s and ϕ are generated by a process of *co-modulation* between

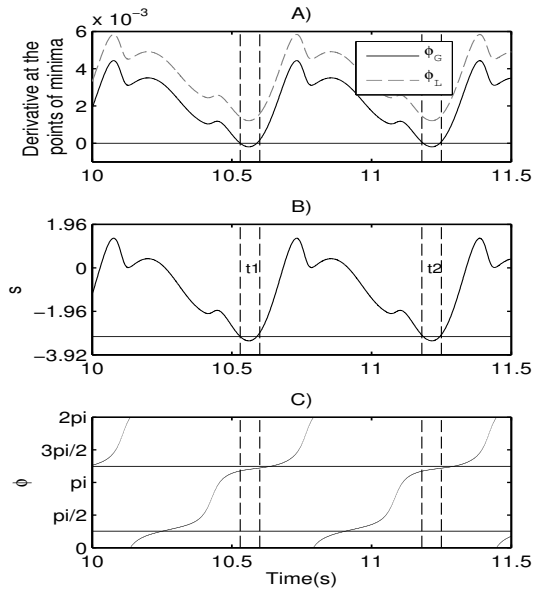

Figure 5.6: **Graphic A** shows how the derivative $\dot{\phi}$ at points of minima ϕ_G (black line) and ϕ_L (grey line) are changing over time. The horizontal line highlights $\dot{\phi} = 0$. **Graphic B** shows how s (y axis) is changing over time. The horizontal line highlights $s = -3.09$, the threshold at above which the fixed points disappear. Note the linear relation between the dynamic of s (in graphic B) and the derivatives at the points of global $\phi_G = 0.796$ and local $\phi_L = 3.916$ minima (in graphic A). **Graphic C** shows how ϕ is changing over time. The horizontal lines highlight the points ϕ_G and ϕ_L. Vertical dashed lines highlight the time intervals $t_1 = [10.53, 10.60]$ and $t_2 = [11.18, 11.25]$ seconds where the fixed points appear in the state space.

these variables. Thus, *the regimes R_1 and R_2 are generated and sustained by continuously modifying the derivative throughout the state space of ϕ in a structured way through s and, at the same time, by continuously modulating s through m_r and m_l*. Notice that as ϕ maps onto m_r and m_l according to Eq. (5.2) and (5.3), respectively, it is possible to analyse the system by considering only s and ϕ; that is, the dynamics of the loop $s \rightarrow \phi \rightarrow (m_r, m_l) \rightarrow s$ can be reduced to the co-modulation dynamics $s \leftrightarrow \phi$. Briefly, the main message of the analysis we have presented so far is that *the regimes R_1 and R_2 are generated and sustained by different dynamics of co-modulation $s \leftrightarrow \phi$*. Having seen how R_1 and R_2 are generated, in the rest of this section we analyse the transition between these regimes in terms of the stability of the co-modulation $s \leftrightarrow \phi$.

The stability of $s \leftrightarrow \phi$ during a single trial of gradient climbing is presented in Fig. 5.8 by using the Poincare map. At $t = 0.2$ and $t = 0.7$ seconds the co-modulation is

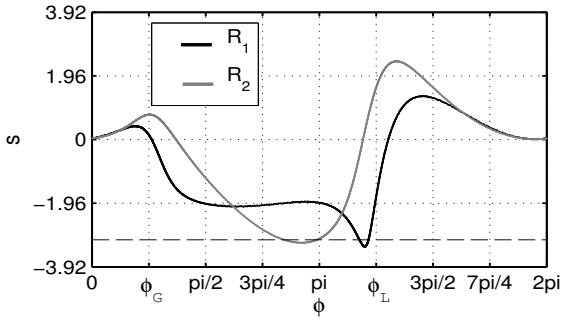

Figure 5.7: Relations between s and ϕ that generate the dynamical regimes R_1 (black line) and R_2 (grey line), respectively. Horizontal dashed line highlight the value of s below which the fixed points appear in the state space of ϕ.

unstable but moving towards the region of stability represented by the diagonal line; at $t = 1.2$ seconds it is near the stable region with $s = -2.3$; at $t = 7.7$ seconds it stabilizes with $s = -1.98$, corresponding to R_1 (some values are not shown in the graphic). The co-modulation dynamics maintains stability while the agent is moving towards the centre of the environment engaged in the sensorimotor behaviour SM_1. As soon as the agent approaches the centre, at $t = 80$ seconds, the co-modulation starts losing its stability, as shown by the sequence of grey points near the region pointed at by the arrow R_1. At $t = 101$ seconds the co-modulation is totally unstable and transiting to another stable region; after $t = 104$ seconds it is near the stable region, and at $t = 107$ seconds it stabilizes with $s = 1.2$. The stabilization completes the transition from R_1 to R_2. In sum, the dynamics of $s \leftrightarrow \phi$ starts unstable, converges to the stable pattern corresponding to R_1, becomes unstable again, and then converges to another stable pattern corresponding to R_2.

The Poincare map can also be interpreted in an alternative way. This map was generated for the phase relation $\phi = \pi/2$ which corresponds to the motor activity $m_r = 1.16$ and $m_l = 0.96$ – according to Eq. (5.2) and (5.3), respectively. We can read the Poincare map as being the representation of the agent's sensory input when its motor states are $m_r = 1.16$ and $m_l = 0.96$. In this case, when the agent is moving towards the centre of the environment these motor states map onto a sensory input $s \sim -1.98$ (point of stabilization in the Poincare map corresponding to the regime R_1); and when it approaches the centre the motor-sensory dynamics become unstable and eventually settle down in a different stable pattern with $s \sim 1.2$ (point of stabilization in the Poincare map corresponding to the regime R_2). For both values of s ($s \sim -1.98$ and $s \sim 1.2$) there is a micro variation in

the order of 10^{-2} as the agent's movement and consequently the derivative of the distance to the centre of the environment, which is measured by the agent's sensor, do not vary smoothly (shown by the small oscillations in the distance depicted in graphic 5.2-B).

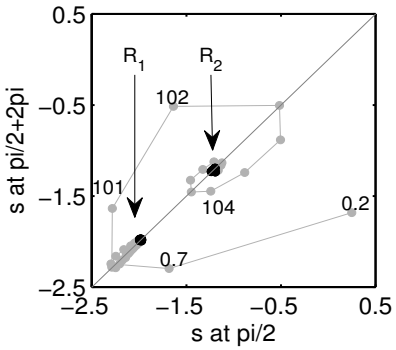

Figure 5.8: Poincare map showing the values of s at every time $\phi = \pi/2$. The diagonal line highlights the region of the map where s remains constant at $\phi = \pi/2$. The numbers near the black points show the approximated time in seconds of the value of s shown on the y axis. The arrows indicate the regions to where the co-modulation dynamics $s \leftrightarrow \phi$ converge during R_1 and R_2. These regions are highlighted by the black points.

Notice that the topology of the state space underlying R_1 is different from the one underlying R_2; more specifically, the transition from R_1 to R_2 is not characterized by a movement of the system to a different region of the state space (e.g. movement to a different basin of attraction), but by a modification on the topology of the state space $[0, 2\pi)$ caused by a different dynamic structure of s.

Also notice that whereas the agent's internal dynamics operates in a metastable regime, the agent as a whole operates in a stable limit cycle dynamics – represented by the trajectories in state space defined by s and ϕ depicted in Fig. 5.7. These regimes are compatible with each other as the fact that the variable ϕ is metastable – characterized by the passage near saddle node bifurcation points (ϕ_G and ϕ_L) – does not exclude the existence of stable limit cycles in the whole system consisting of s, ϕ, m_r and m_l.

Basically, so far we have shown two patterns of sensorimotor behaviours SM_1 and SM_2 and their underlying metastable dynamical regimes R_1 and R_2, we have shown that these dynamical regimes are generated and sustained by the continuous co-modulation between s and ϕ; and have analysed how the transition between regimes takes place in relation to the stability of the co-modulation $s \leftrightarrow \phi$.

5.4.3 Effects of the motor-sensory coordinated coupling on the HKB model

In this section we perform an experiment to analyse how the dynamical and informational properties of the agent's internal oscillatory dynamics change when the modulations $s \to \phi$ and $\phi \to s$ are not coupled with each other. A single trial of the experiment consists of an agent performing gradient climbing starting from a random position and orientation in the environment and with random initial phase relation. We record the sensory dynamics of this agent and then play it back to the same agent starting from the same position and random initial phase relation. By doing that the controller of both agents (normal and recorded) are modulated by the same control parameter dynamics – i.e. $s \to \phi$ is the same for both agents – however only the first agent is able to modulate its own control parameter – i.e. only the first agent has $\phi \to s$ coupled to $s \to \phi$. These agents will be referred to as "coupled" and "decoupled", respectively.

For all initial conditions tested (10000 trials) the dynamics of the internal oscillatory dynamics of the coupled agent always converges to R_1 and then it switches to R_2 (such dynamical pattern transition will be written as $R_1 \rightsquigarrow R_2$). This result is exactly what we have shown in the previous section. On the other hand, the internal dynamics of the decoupled agent might converge either to the same pattern $R_1 \rightsquigarrow R_2$ or to a different one $R_3 \rightsquigarrow R_4$, see the density distributions of phase relations for these patterns in Fig. 5.9. Accordingly, the dynamics between s and ϕ in the coupled and decoupled agents may also differ from each other, as shown in Fig. 5.10.

The probabilities of convergence to either $R_1 \rightsquigarrow R_2$ or $R_3 \rightsquigarrow R_4$ depend on the difference between the initial values of ϕ in the coupled and decoupled agents, as shown in Fig. 5.11. The initial distance from the agent to the centre of the environment and the angle of the agent's body in relation to the centre do not affect the regimes to which the controller converges. The probability of the decoupled agents to converge to $R_1 \rightsquigarrow R_2$ given a initial phase lag within (0,0.17] is 97.6% (see first bar on the left of the graphic); and for a lag within (6.11,6.28] the probability is 99.3% (see last bar on the right of the graphic). The probability of the decoupled agents to converge to $R_3 \rightsquigarrow R_4$ given an initial phase lag within (2.62,2.79] is 98.2% (see the longest grey bar in the region before π radians). When the agent converges to $R_3 \rightsquigarrow R_4$ the agent's behaviour is totally non-functional as it keeps moving in circles around its starting position.

Summing up, the dynamical properties of the agent's controller depends on whether ϕ modulates s; when there is modulation, the controller always converges to $R_1 \rightsquigarrow R_2$. In

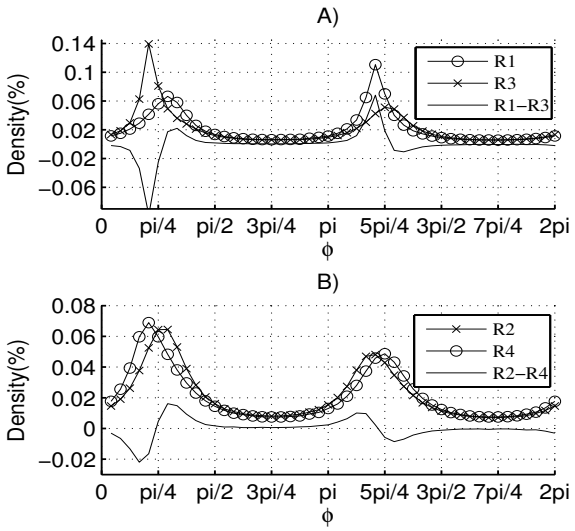

Figure 5.9: Density distributions of the oscillatory regimes that the *decoupled* agents (those that receive the recorded input of an agent with full sensorimotor coupling—see text for details) might converge to. The oscillatory dynamics converges either to $R_1 \rightsquigarrow R_2$ or to $R_3 \rightsquigarrow R_4$ (see legends). Lines without markers show the difference between R_1 and R_3 (graphic A) and R_2 and R_4 (graphic B).

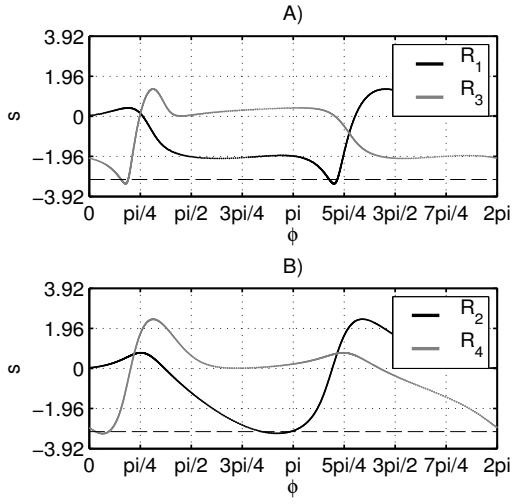

Figure 5.10: Trajectories in the state space of s and ϕ for the decoupled agent. Initially s and ϕ converge to either a pattern that generates R_1 or to another one that generates R_3 (shown in graphic A). Then, they switch either to a pattern that generates R_2 or R_4 (shown in graphic B).

the absence of modulation the controller might converge either to the functional $R_1 \rightsquigarrow R_2$ or to the non-functional $R_3 \rightsquigarrow R_4$. This result suggest that the emergence of functional

metastable patterns in the situated HKB model – i.e. patterns that generate gradient climbing behaviour – depend not only on the structure of the agent's sensory input but also on a coordinated coupling of the agent's motor-sensory dynamics.

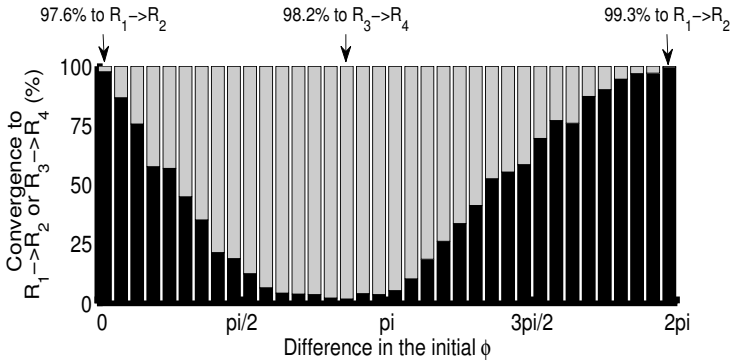

Figure 5.11: Percentage of agents (y axis) that converge to either $R_1 \rightsquigarrow R_2$ (black bars) or $R_3 \rightsquigarrow R_4$ (grey bars) according to the difference between the initial ϕ in coupled and decoupled agents. The state space $[0, 2\pi)$ was divided into 36 equally spaced intervals represented by the bars.

Finally, we study how the informational properties of the system change when the modulations $s \rightarrow \phi$ and $\phi \rightarrow s$ are not coupled to each other. The amount of information that the controller of the decoupled agent carries about sensory stimulation is equal or smaller than the amount of information carried by the controller of the coupled agent. The amount of information is equal when the controller converges to $R_1 \rightsquigarrow R_2$ and smaller when it converges to $R_3 \rightsquigarrow R_4$. This difference is analyzed with information-theoretic measures applied to s and ϕ dynamics considering 20 trials of the experiment in which the coupled agent converges to $R_1 \rightsquigarrow R_2$ and the decoupled one to $R_3 \rightsquigarrow R_4$ (methods are described in the Appendix). Particularly, we measured: a) the Shannon entropy of the sensor – referred to as $H(s)$ – which gives the amount of bits needed to "codify" the sensory dynamics; b) the mutual information between s and ϕ of the decoupled agent – referred to as $I(s; \phi_d)$ – which gives the amount of information the controller has about the sensory dynamics; and c) the conditional mutual information between s and ϕ of the coupled agent given ϕ dynamics of the decoupled agent – referred to as $I(s; \phi_c|\phi_d)$ – which gives the amount of information carried by the controller of the coupled agent that is not already present in the controller of the decoupled agent. In essence these measures will inform us about how the information present in the controller about sensory activity changes with and without the modulation $\phi \rightarrow s$ – see Fig. 5.12.

The agent's sensory dynamics needs ≈ 5 bits to represent all its possible states, as shown by $H(s)$. The controller of the decoupled agent carries ≈ 3.5 bits of information about the sensory dynamics, as shown by $I(s;\phi_d)$; and by adding the modulation $\phi \rightarrow s$ the amount of information increases by ≈ 0.5 bits ($\approx 14\%$), as shown by $I(s;\phi_c|\phi_d)$. This result suggests that the informational content that the agent's controller carries about its control parameter s is greater when ϕ and s modulates each other than when only s modulates ϕ or, in other words, the modulation of sensory activity by motor behaviour increases the amount of information present in the agent's oscillatory network.

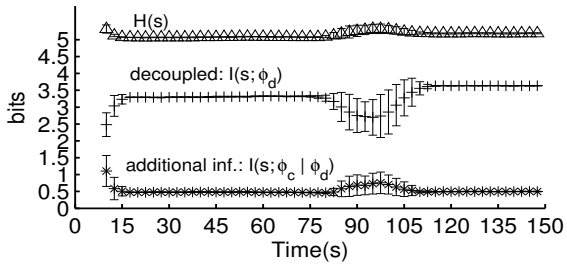

Figure 5.12: Information-theoretic measures for the agent's controller with and without the modulation $\phi \rightarrow s$. All measures represent the mean over 20 trials and error bars their standard deviation. On average the agent's sensor entropy $H(s)$ remains around 5 bits. Under open-loop, the mutual information between the decoupled agent's controller and its sensor $I(s;\phi_d)$ stays at ≈ 3.3 bits while the agent is approaching the centre of the environment (time in seconds is represented on the x axis) and slightly increases to ≈ 3.6 when the agent is moving around the centre of the environment. The controller of the coupled agent carries 0.5 bits of additional information about the sensor that is not present in the controller of the decoupled agent, shown by $I(s;\phi_c|\phi_d)$.

5.5 Discussion

The contribution of this chapter is twofold, it presents a dynamical analysis of the HKB equation within a closed sensorimotor loop and also gives theoretical insights into the interplay of sensorimotor behaviour and neural oscillatory dynamics.

In the experiment carried out by Kelso, the phase relation ϕ (described by Eq. 5.1) models the angle between the right and left fingers, as described in section 5.2. This variable has also been interpreted as the phase relation between neural oscillatory components underlying the fingers' coordination (Kelso and Tognoli, 2009). In the context of

this work, ϕ describes the phase relation of oscillatory components at an undetermined level of abstraction (it can be interpreted, for instance, as the phase relation between individual neurons, or neuronal groups). Our goal here was not to develop a model with empirical accuracy, but to raise theoretical issues about oscillatory dynamics underlying sensorimotor coordination.

We have shown *qualitatively different sensorimotor behaviours – SM_1 and SM_2 – and their underlying metastable regimes of phase relations – R_1 and R_2, respectively.* This result is relevant mainly in the context of the Coordination Dynamics framework as it presents a simple case of the relation between metastability in the HKB model and sensorimotor behaviour. We have also shown that *the regimes R_1 and R_2 are generated and sustained by continuously modifying the derivative throughout the state space of ϕ in a structured way through s and, at the same time, by continuously modulating s through ϕ via m_r and m_l.* In the context of Coordination Dynamics, this result helps to understand how different metastable regimes can be generated and sustained by the HKB model when it is within a sensorimotor loop. More generally, this result suggests that an agent's internal oscillations depend on sensorimotor dynamics to engage in functional metastable regimes; that is, the ongoing interaction involving an agent and its environment generates and sustains the agent's coherent metastable oscillatory regimes.

Another result we have shown is that *the transition from R_1 to R_2 takes place when the co-modulation between s and ϕ becomes unstable.* This result suggests that an agent's internal oscillations switches between functional metastable regimes when the dynamics of interaction involving the agent and its environment becomes unstable. While a pattern of motor activity is mapped onto another pattern on the agent's sensory activity – i.e. the interaction is stable – then the agent's internal dynamics settles down into a metastable pattern (e.g. R_1); but once the same motor activity starts generating a different sensory stimulation – i.e. the interaction becomes unstable – then agent's internal dynamics makes a transition to another metastable pattern (e.g. R_2). This result shows how the transition between dynamical regimes in the situated HKB model depends on the stability of the agent's sensorimotor contingencies.

The experiment with recorded input further investigates the continuous mutual coordination and interdependence between the agent's sensorimotor behaviour and its internal oscillatory dynamics. It shows that *the dynamical properties of the agent's controller depends on whether ϕ modulates s; when there is modulation the controller always converges to $R_1 \rightsquigarrow R_2$ and in the absence of modulation the controller converge to either $R_1 \rightsquigarrow R_2$*

or $R_3 \rightsquigarrow R_4$. In other words, the modulation of the agent's sensory dynamics by its motor activity ($\phi \rightarrow s$) assures that the controller converges to the functional metastable regimes R_1 and R_2 that generate coherent sensorimotor behaviours for the agent to perform gradient climbing. In the absence of this modulation the agent's internal oscillations and its motor-sensory dynamics might become uncoordinated and consequently generate a non-functional interaction between the agent and its environment. More generally, this experiment suggests that functional metastable oscillatory regimes are tightly dependent on the agent's sensorimotor contingencies, as when the agent's sensory activity is not coordinated to what the agent is doing then the internal oscillations might converge to a non-functional regime.

The modulation of the agent's sensor by its motor behaviour through the environment not only influences the dynamical properties of the agent's controller, but might as well increase the mutual information between the agent's controller and its sensory dynamics. Particularly, we have shown that *the mutual information between* ϕ *and* s *is greater when there is co-modulation* $s \leftrightarrow \phi$ *than when only* s *modulates* ϕ. This result should be more carefully investigated with more variations of the experiment as it could be only by chance that the regimes R_3 and R_4 presented a mutual information lower than R_1 and R_2; however, it still remains interesting for opening the discussion on whether the uncertainty of neural oscillations about sensory stimuli decreases under modulation of motor activity.

Generally speaking, one contribution of the model studied in this chapter is the dynamical analysis of the HKB equation in a completely different context from that studied by Kelso. This is an important theoretical contribution to the Coordination Dynamics framework as it provides a proof of concept that helps to illustrate the notion of sensorimotor coordination coupling and multiple metastable regimes in the HKB model. The outcome of the dynamical analysis could not have been predicted in advance as there are a multiplicity of strategies to achieve the same behavioural and internal phase relation dynamics. The agent's correct behaviour could have been achieved by a monostable or multistable HKB equation (rather than metastable); and the agent's internal metastable dynamics could have been achieved by maintaining the control parameter over a threshold where the point attractors would never appear (differently from our model where the point attractors appear during short time-windows). In sum, our analysis has shown how an agent can perform functional behaviours under metastable regimes generated by a dynamic sensory input constantly reshaping the attractor landscape. This result has shed some light on how sensorimotor coordination can operate together with metastable

oscillatory dynamics; and it could not have been predicted before studying the model.

The metastable regimes that the HKB model can illustrate have been hypothesized to be the signature of brain functioning. Despite evidence of metastability in empirical experiment of animals performing perceptual motor coordination tasks (as described in the introduction), to our knowledge there was no previous model of a situated HKB system that operates in a metastable region, coupling internal metastable oscillations to sensorimotor coordination dynamics through a control parameter. The model we have developed and analyzed in this paper has contributed to fill this gap and has shown the tight dependency that can be established between an agent's neural oscillatory metastable regimes and the sensorimotor contingencies they make possible when coupled to the environment.

Conditional mutual information

Shannon's entropy (Shannon, 1948) is shown in Eq. (5.5), where $p(x_k)$ is probability mass function of the outcome x_k.

$$H(X) = -\sum_{k=1}^{b} p(x_k) log(x_k), \tag{5.5}$$

The *mutual information* (Shannon, 1948; Cover and Thomas, 2005) is shown in Eq. (5.6), where $H(X)$, $H(Y)$ are the entropies of the sets X and Y respectively, and $H(X,Y)$ is the joint entropy of both sets.

$$I(X;Y) = H(X) + H(Y) - H(X,Y), \tag{5.6}$$

The standard measure of *conditional mutual information* (Cover and Thomas, 2005) is shown in Eq. (5.7).

$$I(X;Y|Z) = \sum_{x\in X}\sum_{y\in Y}\sum_{z\in Z} p(x,y,z) log_2 \frac{p(x,y|z)}{p(x|z)p(y|z)} \tag{5.7}$$

where X, Y and Z are sets of discrete random variables; and p is the probability mass function for the given subscripts (x,y and z).

The temporal dynamics of the information-theoretic measures were captured by using a moving window of 10 seconds; i.e. the probability mass functions were calculated considering a moving window containing 10000 data points. The continuous value of $s \in [-3.92, 3.92]$, ϕ_c and $\phi_d \in [0, 2\pi)$ were discretized into 50 equally spaced bins.

5.6 Summary

In this chapter we have shown the that functional oscillatory regimes depend not only on the modulation of the network by the sensory activity, but also on a coordinated coupling between the agent's sensory and motor activities. In the next chapter we explore how functional oscillatory regimes are sustained by an agent's sensorimotor loop under the presence of plastic changes in the structure of the network and how a completely integrated network accommodates oscillatory regimes (adapts to new conditions) without affecting the functionality of pre-existing regimes.

Chapter 6

Accommodating functional oscillatory regimes within homeostatically stable boundaries

6.1 Introduction

The temporal structure of neural oscillations is affected not only by an agent's ongoing sensorimotor dynamics – as we have studied in previous chapters – but also by a mechanism of adaptation that changes the network connectivity in an ontogenetic timescale. A common problem that arises when the connectivity of a completely integrated network changes so that an agent adapts to a new situation is that the modification of the network structure (its connections) might interfere in the network dynamics under situations to which it had previously adapted – a problem known as "the neural interference" (Di Ferdinando et al., 2001). In this chapter we explore the problem of neural interference by developing a model where a simulated agent is performing phototaxis and is homeostatically stable – which, in this context, means that its internal oscillations are maintained within homeostatically stable boundaries. When the agent's visual field is inverted, its internal dynamics become homeostatically unstable and the agent does not perform phototaxis. The instability activates synaptic plasticity changing the connectivity of the network towards a configuration that accommodates functionally stable oscillations under normal and inverted vision (i.e. the agent adapts to perform phototaxis under both conditions).

Particularly, the problems we tackle with this model are the following. Firstly, we approach the problem of neural interference by studying how the oscillatory regime in which the agent engages when it is under normal vision changes after adaptation to inverted

vision. We will show how the process of adaptation moves and reshapes the attractor landscape of the network in a such a way that it accommodates a stable dynamical regime to deal with inverted vision without affecting the functionality and stability of the dynamical regime under normal vision. Secondly, we provide a dynamical explanation of the interplay between the network and the sensorimotor loop dynamics. This explanation works as a proof of concept to show how the network dynamics underlying coherent behaviours (e.g. phototatic behaviour under normal and inverted vision) are generated by and depend on the entire sensorimotor loop coordination. Thirdly, we explore the mechanism of transition between dynamical regimes (i.e. the transition from normal to inverted vision after adaptation) and show that homeostatic instability is not necessary for switching between dynamical regimes. Shortly, the first problem concerns the operation of the mechanism for adaptation, the second one concerns the interplay between the network and the sensorimotor loop dynamics, and the third one the mechanism for switching between dynamical regimes.

6.2 Preliminary considerations

6.2.1 Homeostasis and homeostatic adaptation

The concept of homeostasis coined by Cannon (1932) refers to a condition in which coordinated physiological processes maintain certain variables within limits. Although this concept was introduced by Cannon, an earlier work by Bernard (1927) had already identified regulatory systems in the organism's internal environment (*milieu interieur*). From these pioneering works, research in animal physiology found and studied homeostatic mechanisms controlling body temperature, heart rate, levels of blood sugar, breathing rate and others, see Cooper (2008) for a historical review. More recently, Turrigiano (1999) observed that neurons also have a mechanism of homeostatic regulation which increases or decreases the strength of their synaptic inputs ensuring the maintenance of their firing rates within boundaries. She has also reported the presence of homeostatic regulations of activity in cortical networks (Turrigiano, 1999; Turrigiano and Nelson, 2004).

Rather than working directly with physiology, Ashby (1947, 1960) focused on more abstract dynamical system models of homeostasis in the context of adaptive behaviour. According to him, an animal's behaviour is adaptive if it maintains essential variables within physiological limits. These variables are closely related to survival; they can be lethal (*e.g.* amount of oxygen in the blood), or only represent some approaching threat

(*e.g.* heat on the skin). When essential variables cross certain boundaries, a mechanism that changes the system configuration is activated until these variables return to homeostatically stable regions. The mechanism that pushes the variables back to their stable regions selects those configurations that not only recover stability at the current moment, but also leave the system stable in the presence of environmental conditions to which the system had previously adapted.

To illustrate the operation of this mechanism, consider an animal "A" interacting with its environment "E", see Fig. 6.1. When the environment changes (at $t2$) the animal's dynamic becomes homeostatically unstable (the homeostatic boundary is represented by the dashed line in "A"). Due to this instability, the mechanism that changes the animal's internal organisation is activated (see downstrokes in "M"). The new organisation found by "M" leaves the animal stable in the presence of both environmental conditions, as it is shown by the animal's dynamic at $t4$ and $t5$.

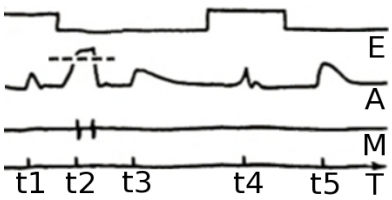

Figure 6.1: Schematic representation of homeostatic adaptation. Each line represents: (E)nvironment, (A)nimal, (M)echanism of homeostatic adaptation, and (T)ime. Adapted from Ashby (1960) p.116.

Ashby also postulated that different environmental conditions can move the state of the system to different regions in state space and that, within each region, the system can have different dynamical regimes – this is illustrated by different dynamical regimes presented by the animal at $t4$ and $t5$. Summing up Ashby's main points in the context of our work, we can say that: an adaptive system interacting with its environment switches and engages in different dynamical regimes and, when a regime becomes homeostatically unstable, the system reconfigures itself so that: 1) it accommodates a stable dynamical regime that deals with the condition that triggered instability; and 2) it maintains the stability of pre-existing dynamical regimes that deal with previously adapted conditions.

Notice that the homeostatic characteristic of a system does not impose any constraints on the dynamics inside the stable regions. As long as the state of the system is inside a homeostatic region, the system can be in an attractor or moving in a transient dynamics; it can also be monostable, bistable, multistable, or even without attractors inside the stable

regions.

6.2.2 The computational model

The computational model developed in this chapter is based on a related model implemented by Di Paolo (2000). In his model, Di Paolo minimally replicated a psychological experiment carried out by Taylor (1962) where a human being adapts his/her sensorimotor coordination under distortion of his/her visual field by continuously wearing a pair of spectacles. Di Paolo replicated this experiment by evolving a simulated agent to perform phototaxis. During the agent's lifetime, he inverted the agent's visual field (by switching the right and left sensors) and studied the process of behavioural adaptation. The agent's mechanism of adaptation was implemented by using homeostatic stability and synaptic plasticity[1].

Following Di Paolo, we implement an agent performing phototaxis using homeostatic stability and synaptic plasticity. However, our experimental setup differs from his in two points. Firstly, we replicate another experiment carried out by Taylor where a subject adapts his/her behaviour to intermittently (rather than continuously) wearing of spectacles. Secondly, in our model the inversion of the agent's visual field is done both during its lifetime and during evolution; that is, our agent is evolved to adapt during its lifetime to inverted vision, differing from Di Paolo's one which was evolved to perform phototaxis exclusively under normal vision.

The methodology to develop our computational model is based on four assumptions which are grounded on Ashby and Taylor's works. The assumptions are the following: 1) an agent's behaviour is adaptive if it maintains its internal dynamics homeostatically stable; 2) modifications on the network connectivity is a mechanism to recover homeostatic stability; 3) an agent is adaptive when its network connectivity is adjusted in such a way that the homeostatic stability of the networks is maintained in the presence of similar conditions that triggered instability in the past, and 4) a condition to which the agent is not adapted triggers homeostatic instability.

The dynamics of the agent's controller is governed by the Continuous-Time Recurrent Neural Network (CTRNN) (Beer, 1995). The CTRNN is an universal approximator of smooth dynamics (Funahashi and Nakamura, 1993; Kimura and Nakano, 1998) meaning that it can approximate the dynamics of a continuous neural oscillatory signal, such as non-spiking neural signals from the nematode worm *C. elegans* (Davis and Stretton, 1989;

[1]For a theoretical discussion of Di Paolo's model see Di Paolo (2003).

Goodman et al., 1998; Izquierdo and Lockery, 2010) and central pattern generators in the nervous system (Ijspeert, 2008; Santos and Campo, 2012). The CTRNN has been carefully studied by Beer (1995), is very well-known in the field of evolutionary robotics (Harvey et al., 2005; Floreano et al., 2008) and has been extensively analysed under learning conditions and plastic changes (Phattanasri et al., 2007; Iizuka and Paolo, 2008). The model developed in this chapter builds on this body of previous works related to the CTRNN by looking at its dynamics from a different angle; that is, by analysing it in terms of phase relations, by studying how it can learn a new dynamical regime without affecting the functionality of old ones, and by analysing the roles of homeostatic stability in the transition between dynamical regimes.

Whereas the models in previous chapters described either the phase (in the case of the Kuramto's equation) or the phase relation (in the case of the HKB equation), the CTRNN depicts the dynamics of a (oscillatory) signal itself. The dynamics of CTRNN nodes do not necessarily oscillate, they may saturate or converge to fixed points. Centre crossing (Mathayomchan and Beer, 2002) and homeostatic plasticity (Williams and Noble, 2007) are two techniques that have been used to increase the likelihood to obtain oscillations in CTRNN dynamics.

6.3 Theoretical model and methods

6.3.1 The task, the agent and its controller

The implementation of the agent and its controller follows, as much as possible, that one carried out by Di Paolo (2000). The main differences lie in the number of nodes used to implement the controller and in the evolutionary setup.

A genetic algorithm (GA) is used to evolve the parameters of our model. The range of each parameter, which defines the search space for the GA, is presented throughout the methodology together with the description of each variable.

The task involves an agent that moves in a simulated environment and has to perform phototaxis on a sequence of light presentations (one by one) for 15000 secs. During its lifetime, the agent's right and left sensors are switched at every 250 secs. The light is repositioned between 40 and 80 units away from the agent when either the sensors are switched or the agent spends 50 consecutive seconds at a distance smaller than 10 unit to the source of light.

The agent, shown in Fig. 6.2, has a circular body of 8 units diameter, two diametrically

opposed motors that receive a continuous signal in the range [-1,1] from the controller (nodes y_2 and y_3, respectively), and two light sensors separated by $120^\circ \pm 10^\circ$ whose output signal is given by $I_k = 1/\sqrt{d_k}$, where k represents each sensor, and d is the distance from the sensor k to the light source. $I_k = 0$ when the agent's body occludes the light and $I_k = 1$ when $d < 1$.

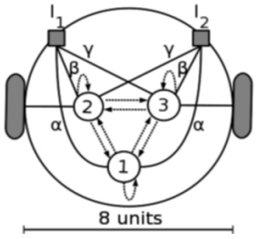

Figure 6.2: The agent and its controller.

The agent's behaviour is controlled by a fully-connected, 3 nodes, continuous-time recurrent neural network (Eq. 6.1) (Beer, 1995).

$$\begin{aligned} \tau_i \dot{y}_i &= -y_i + \sum_{j=1}^{N} w_{ji} z_j + \sum_{k=1}^{M} s_{ki} I_k, \\ z_i &= \frac{1}{1+e^{-(y_i+b_i)}} \end{aligned} \tag{6.1}$$

where y is the state of each node which is integrated with time step of 0.1 using the Euler method , τ is its time constant (range [0.4,4]), N is the number of CTRNN nodes (here 3); $w_{j,i}$ is the connection strength from the j^{th} to the i^{th} node (range [-8,8]), z_j is the node output signal defined by a sigmoid function, b_j is a bias (range [-3,3]), M is the number of inputs (here 2); I_k is the sensory signal, and s_{ki} is a constant that represents the sensory strength from the k^{ih} sensor to the i^{th} node. The values for s_{ki} are: $s_{11} = s_{21} = \alpha$; $s_{12} = s_{23} = \beta$; $s_{13} = s_{22} = \gamma$, where α, β and γ are in the range [0.01,10] (see representation of the sensory strengths in Fig. 6.2). Each connection between nodes ($w_{j,i}$) is adjusted by one out of four different homeostatic plastic rules, shown in (6.2). The rule used by each connection is defined by the genetic algorithm.

$$\begin{aligned} R0 &: \Delta w_{ji} = \delta\ \eta_{ji}\ p_i\ z_j\ z_i, \\ R1 &: \Delta w_{ji} = \delta\ \eta_{ji}\ p_i\ (z_j - z^o_{ji}) z_i, \\ R2 &: \Delta w_{ji} = \delta\ \eta_{ji}\ p_i\ (z_i - z^o_{ji}) z_j, \\ R3 &: \Delta w_{ji} = 0, \end{aligned} \tag{6.2}$$

where Δw_{ji} is the change in w_{ji}, δ is a linear damping function that constrains the weights between allowed values ([-8,8]), η_{ji} is the rate of change (range [-0.9,0.9]), and p_i

is the plastic facilitation defined by the function shown in the Fig. 6.3. Rule 0 is the Hebbian and anti-Hebbian rules (depending on p_i and n_{ji}); rules 1 and 2 potentiate or depress the connection depending on how the presynaptic or postsynaptic node activity relates to a threshold z^o_{ji}. This threshold linearly depends on w_{ji} ($z^o_{ji} = 0$ if w_{ji}=-8 and $z^o_{ji} = 1$ if w_{ji}=8).

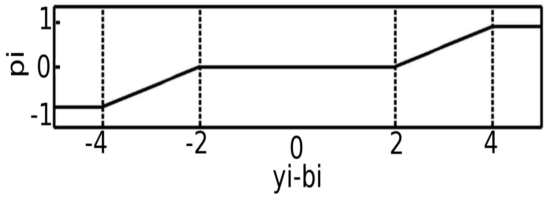

Figure 6.3: Local plasticity facilitation p_i. When the node activation minus its bias ($y_i - b_i$) is in the stable region ($[-2, 2]$), then plasticity is not activated as $p_i = 0$. Out of this region, p_i changes either positively or negatively according to the function.

The agent's right and left motors are controlled by $2z_2 - 1$ and $2z_3 - 1$, respectively. At each time step, a random noise from a normal distribution with mean 0 and standard deviation 0.02 is added to the motors and to the sensors.

6.3.2 Optimization with a genetic algorithm

A total of 36 network parameters encoded in a genotype as a vector of real numbers in the range [0,1] are evolved using the microbial genetic algorithm (Harvey, 2001) and linearly scaled, at each trial, to their corresponding range. The genetic algorithm setup is the following: population size (100); mutation rate (0.05); recombination (0.60); reflexive mutation; normal distribution for mutation $\left(\mu = 0, \sigma^2 = 0.1\right)$; and trials for each agent (8). At the end of the 8^{th} trial the worst fitness (out of 8) is used as the fitness of the agent.

The agent's lifetime is 15000 seconds and its sensors are inverted every 250 seconds. In total, the sensors are inverted 60 times, where 30 times the agent is under normal vision and 30 under inverted vision. At the end of each timeslot (at every 250 secs) a partial fitness of the agent is measured according to Eq. (6.3):

$$F_{ts} = \frac{F_b + F_s}{2} \tag{6.3}$$

where ts is the timeslot (out of 60), F_b is the behavioural-fitness, described in Eq. (6.4), and F_s is the stability-fitness, described in Eq. (6.5).

$$F_b = \left(P + \left(1 - \frac{d_f}{d_i}\right)\right)\frac{R}{T} \tag{6.4}$$

where d_i and d_f are initial and final distances to the light source, respectively, and d_f is clipped at 0 when $d_f > d_i$; P is the number of times the agent approaches the light in the current timeslot (the agent can approach the light more than once as the light moves when the agent completes 50 consecutive seconds near it); T is the timeslot length (250 secs) and R (250 secs) is the required time given to the agent to approach a light source. During evolution, as T=R the agent should approach the light at least once in order to obtain $F_b = 1$. When the agent approaches the light more than the number of times required, F_b is clipped at 1. The stability-fitness is measured according to Eq. (6.5).

$$F_s = \frac{1}{1 + e^{\left(\frac{u}{70} - 7\right)}} \tag{6.5}$$

where u is the number of times the nodes activate out of the stable region (at each Euler step, it can be incremented by 3 when the three nodes activate out of the stable region); the constants 70 and 7 define the shape of the function.

The final fitness of an agent is given by the weighted mean over the fitnesses at each timeslot.

$$F = \frac{1}{3K}\sum_{t=1}^{K} q_t;\; q_t = \begin{cases} F_{ts}; & if\ normal\ vision \quad and \quad \forall ts \\ 2(1 - F_{st}); & if\ inverted\ vision\ and\ ts \leq 30 \\ 2F_{ts}; & if\ inverted\ vision\ and\ ts > 30 \end{cases} \tag{6.6}$$

where K is the total number of timeslots (60 here); t the number of the time slot; and F_{ts} is defined in Eq. (6.3). Under normal vision the agent should get high fitness (F_{ts}) during its whole lifetime ($\forall ts$). Under inverted vision the agent should have low fitness (F_{ts}) during the first 30 inversions ($ts \leq 30$) and high fitness during the last 30. By using this fitness function we expect the genetic algorithm to optimise the parameters in a such a way that: 1) the agent should perform phototaxis maintaining homeostatic stability under normal vision during the whole trial (30 timeslots under normal vision); 2) the agent should be homeostatically unstable and not perform phototaxis when its visual field is inverted; and 3) over time, after a sequence of inversions (normal $\rightarrow$ inverted $\rightarrow$ normal $\rightarrow$ inverted, and so on), the agent should maintain stability and perform phototaxis under inverted vision (the last 30 timeslots). Notice that the model obtained by using this fitness function replicates the behavioural adaptation from the experiment carried out by Taylor

(1962) and the proposed assumptions about how the underlying mechanism of adaptation might operate (Ashby, 1960; Taylor, 1962).

Apart from using homeostatic boundaries – which increases the likelihood to obtain oscillations in the CTRNN network (Williams and Noble, 2007) – we have not implemented any other constraint to obtain a CTRNN that oscillates.

6.3.3 Methods of analysis

Empirical Mode Decomposition and the Hilbert transform

In order to obtain the phase dynamics of CTRNN nodes, we have used the Hilbert transform method, which is defined in (6.7) (Zygmund, 1988):

$$H[f(t)] = -\frac{1}{\pi} \lim_{\epsilon \to \infty} \int_{\epsilon}^{\infty} \frac{f(t+\tau) - f(t-\tau)}{\tau} d\tau \tag{6.7}$$

The Hilbert Transform is basically a $\pi/2$ phase-shift operator in the original signal $f(t)$. The analytical signal is then obtained by (6.8):

$$f_a(t) = f(t) + iH(f)(t) \tag{6.8}$$

When the centre of an oscillatory signal deviates from zero the Hilbert Transform gives an inaccurate result. In order to guarantee a well-behaved Hilbert Transform we have obtained the first Intrinsic Mode Function (IMF) using the Empirical Mode Decomposition (EMD) algorithm (Huang et al., 1998), as follows:

$I_1(t) \leftarrow s(t)$

$i \leftarrow 1$

while I_i *has non negligible local mean* **do**

$U(t) \leftarrow$ *spline through local maxima of* I_i

$L(t) \leftarrow$ *spline through local minima of* I_i

$Av(t) \leftarrow \frac{1}{2}(U(t) + L(t))$

$I_i(t) \leftarrow I_i(t) - Av(t)$

$i = i + 1$

end while

$IMF_1(t) \leftarrow I_i(t)$

A critical point of the EMD method is to find the points of local minima and maxima. By using the zero-crossing of the first derivative, noise in the time series might be wrongly detected as oscillations; and by using a filter to remove noise, real oscillations might be

destroyed. To deal with this problem, before obtaining the first IMF we have used an algorithm to detect "real" troughs and peaks. The trick of the algorithm is the use of a threshold variable delimiting the minimum distance from a peak to the troughs around it (Billauer, 2012). When the threshold is zero, the algorithm works as the zero-crossing of the first derivative; for thresholds greater than 0, only those points of zero-crossing preceded by troughs lower than the threshold are considered a peak. After running this algorithm, the noise left in the time series were removed by interpolating the troughs and peaks using a piecewise cubic interpolation (Fritsch and Carlson, 1980). The resulting time series – generated from the interpolation of the troughs and peaks – were used as inputs for the EMD algorithm. The EMD algorithm stopped when the standard deviation of the average between the maximum and minimum envelopes was 10^{-5}. The input for the Hilbert transform was the first IMF obtained from the EMD method because this IMF preserves the frequency components of the time series – allowing the analysis of phase over time.

Attractor landscape

In order to find the attractors of the network while the agent was interacting with its environment, we took a snapshot of the system at each Euler step of the agent's lifetime and numerically estimated the limit $\lim_{t\to\infty} \langle y_1(t), y_2(t), y_3(t)\rangle$. The snapshot consisted of states of the CTRNN nodes y_1,y_2,y_3, which are the initial conditions to find the limit; the connection weights w_{ji}; the inputs I_1 and I_2, which are maintained fixed during the numerical estimation; the sensor strengths s_{ki}, the biases b_i; and time constants τ_i. The limit was found using Euler integration with time step 0.1 and 900000 steps. When the system did not converge to a point attractor, the Euler integration ran for a further 100000 steps in order to capture at least some points of either the limit cycle or the strange attractor the system was assumed to be following.

6.4 Results

6.4.1 The agent's sensorimotor behaviour

The best agent obtained from the evolutionary process was selected for the dynamical analysis. The agent's lifetime was changed from 15000 s (which was the lifetime during evolution) to 30000 s. During this extra time, the agent's sensors were switched at different frequency, as shown in Fig. 6.4-C.

The mean fitness of the population evolved was 0.77 and the fitness of the best agent 0.86. We ran the best agent for 10000 trials to analyse how the behavioural-fitness and stability-fitness change over the agent's lifetime (see Fig. 6.4). Under normal vision the behavioural-fitness and the stability-fitness maintain near 1 over the whole trial. Under inverted vision the behavioural-fitness increases during the first 5000 s while the stability-fitness maintains near 0. The reason for that is that the stability-fitness only increases when the dynamics of the nodes cross the discrete boundaries of stability $|y_n - b_n| < 2$ – which starts after 5000 s – and the behavioural-fitness increases as the dynamics of the nodes is moving towards the stable region.

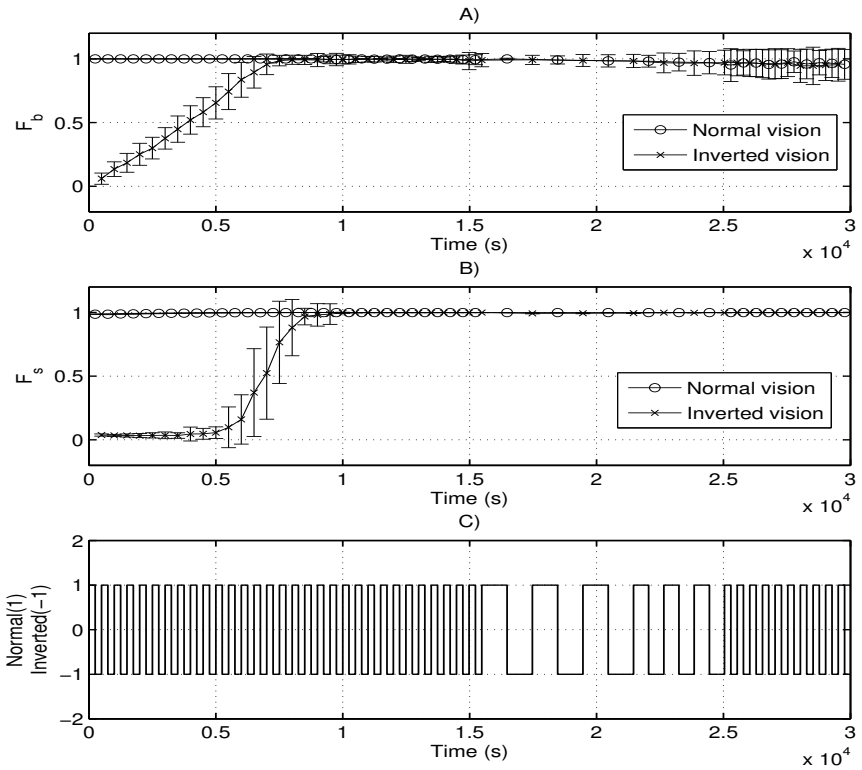

Figure 6.4: Fitnesses for the agent's behaviour (y-axis in graphic A) and internal stability (y-axis in graphic B) over time. Each point represents the mean fitness for a specific timeslot and the vertical bars the standard deviation over 10000 trials. Graphic **C** depicts the sensory configuration (1 for normal, and -1 for inverted). From t=0 to t=15500 the sensors are switched at every 250 s; from t=15500 to t=21500 at every 1000 s, from t=21500 to t=25100 at every 600 s, and the last 5000 s at every 250 s.

The distances from the agent to the light source before and after adaptation are presented in Fig. 6.5-A and B, respectively. After the first inversion, at $t = 250$ s, the agent keeps turning around itself without getting near the light within the timeslot given. After

adaptation the agent approaches the light under both conditions. Fig. 6.6 shows the agent's sensorimotor dynamics during the time-window highlighted by the black lines in graphic 6.5. In the case of the agent under inverted vision and before adaptation, the sensorimotor dynamics are shown for $t = [250, 350]$ s. From now on, the agent under Normal vision Before adaptation we will be referred to as NB; the agent under Inverted vision Before adaptation as IB; the agent under Normal vision After adaptation as NA; and the agent under Inverted vision After adaptation as IA.

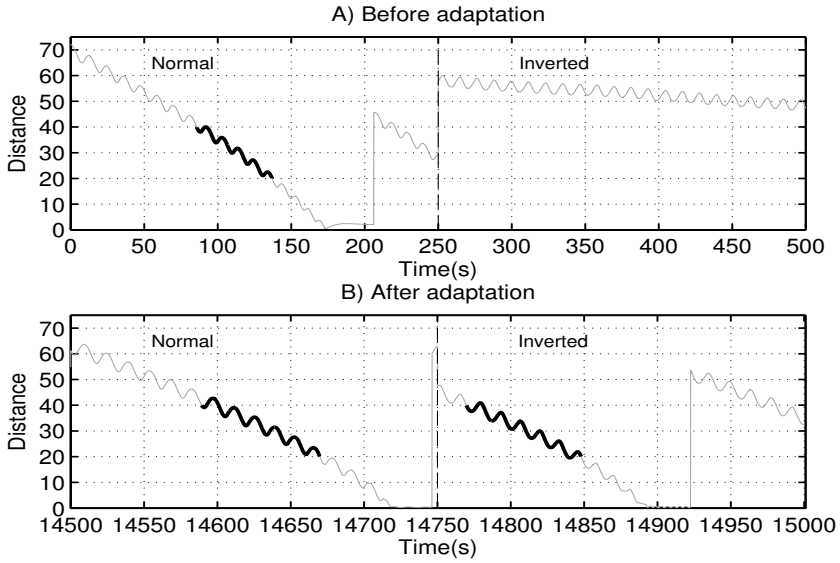

Figure 6.5: Distance from the agent to the light source before (graphic **A**) and after adaptation (graphic **B**). In graphic A, the agent is under normal vision during the first 250 s. Just after 200 s, the position of the light changes and agent starts moving towards it again. At t=250 s, the agent is under inverted vision and does not approach the light. After adaptation (graphic B) the agent approaches the light under both conditions. The black lines highlight how the distance is changing from the moment the agent crosses $d = 40$ until it gets to $d = 20$.

6.4.2 Oscillatory dynamics underlying sensorimotor behaviours

In this section we study the oscillations underlying the agent's sensorimotor dynamics. The main purpose here is investigate whether and how the oscillatory regime in which the agent engages under normal vision changes after adaptation to inverted vision. Firstly, we analyse the phase relation dynamics between the CTRNN nodes considering a single trial of the experiment and a specific time-window of the agent's lifetime. This analysis provides an overview of how the phase relations were obtained from the CTRNN oscillations. Next,

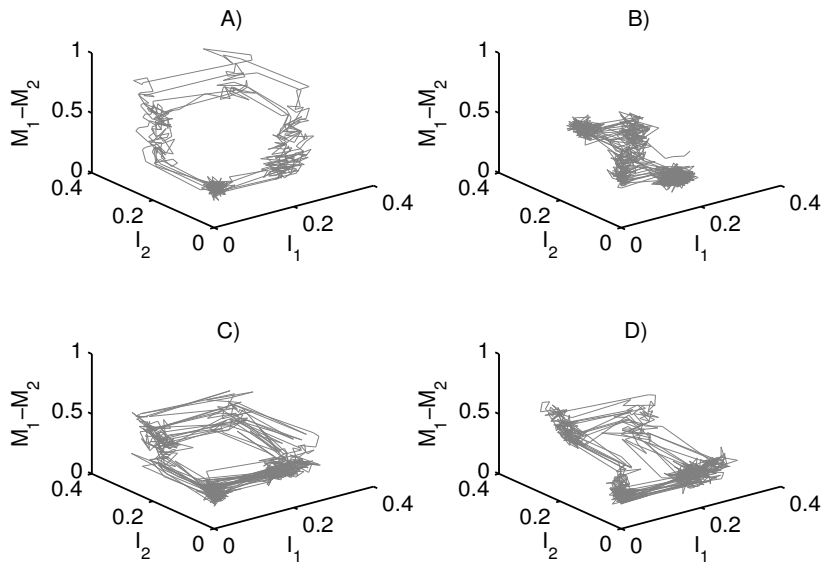

Figure 6.6: Agent's sensorimotor dynamics. The x and y-axes in the graphics show the agent's sensors (I_1 and I_2) and the z-axis the difference in the agent's motor activity ($M_1 - M_2$). Graphic **A**: agent under normal vision and before adaptation. Graphic **B**: agent under inverted vision and before adaptation. Graphic **C**: agent under normal vision and after adaptation. Graphic **D**: agent under inverted vision and after adaptation.

we analyse the phase relation dynamics underlying the agent's sensorimotor behaviour when it is moving towards the light from $d = 40$ to $d = 20$ (d is the distance to the light) and also considering many trials of the experiment.

Phase relations within a specific time-window of a single trial

Fig. 6.7 presents the (phase) dynamics of y_1 and y_2 for a specific time-window in a single trial where the agent is under normal vision before adaptation, namely $t = [85.8, 137]$ s (highlighted by the black line in Fig. 6.5-A). Graphic 6.7-A presents the dynamic of y_1 and its first imf. Notice that the imf captures the oscillations of the node, does not contain the noise from the real signal and is centred in 0. All peaks lower than 0.05 were considered as noise in the time series. Graphic 6.7-B is similar to 6.7-A apart from the fact that it shows the dynamics and the imf for the node y_2, rather than y_1. Graphic 6.7-C presents the phase dynamics of the nodes y_1 and y_2, which were obtained with the Hilbert Transform from the imfs shown in graphics 6.7-B and C. Graphic 6.7-D presents the phase relations $\phi_{1,2}$ between the nodes y_1 and y_2, which is given by $\phi_{1,2} = \theta_1 - \theta_2$. In order to keep the phase relations in the range $[0, 2\pi)$, the value of $\phi_{i,j}$ was incremented in 2π every time the phase difference was negative; i.e. $\phi_{i,j} = \phi_{i,j} + 2\pi \; \forall \; \phi_{i,j} < 0$.

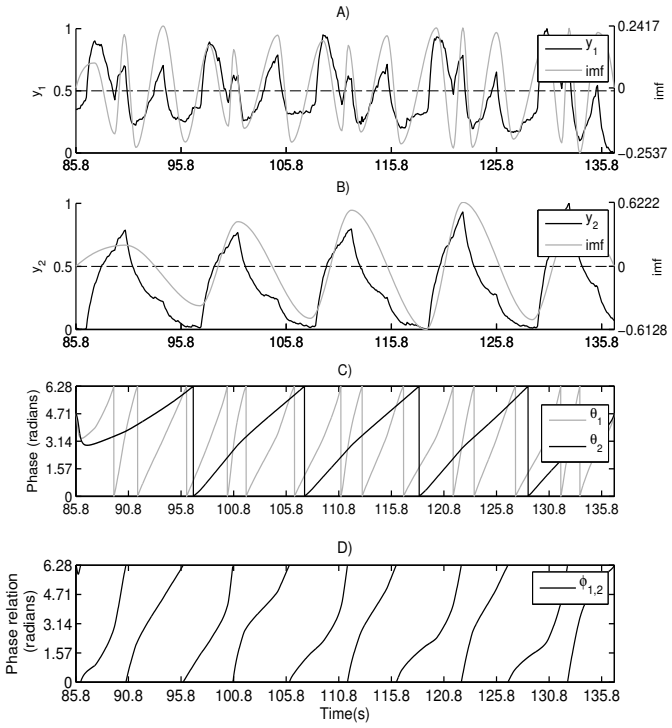

Figure 6.7: Phase relation dynamics between y_1 and y_2. In graphics **A**, the left y-axis shows the dynamics of y_1 in a scale from 0 to 1 and the right y-axis the first IMF of y_1, see legend. Graphic **B** is similar to graphic A, but for the node y_2. Graphic **C** shows the phase dynamics of the nodes y_1 (referred to as $\theta 1$) and y_2 (referred to as $\theta 2$), see legend. Graphic **D** shows the phase relation dynamics between y_1 and y_2 (referred to as $\phi_{1,2}$).

The other phase relations dynamics $\phi_{1,3}$ and $\phi_{2,3}$ for the same time window $t = [85.8, 137]$ s are presented in Figures 6.8 and 6.9, respectively. A preliminary analysis of the phase relations (graphics D of Figures 6.7, 6.8 and 6.9) suggests that $\phi_{1,3}$ is more synchronised than the other nodes – note how the dynamics of $\phi_{1,3}$ maintain around 0 radians, while the dynamics of $\phi_{1,2}$ and $\phi_{2,3}$ are constantly changing from 0 to 2π. It also suggests that y_1 and y_2 are the most desynchronised nodes – note how the rate of change of $\phi_{1,2}$ is higher than the rate of change of the other phase relations. A more precise analysis of the phase relations is presented in the following subsection.

Phase relations and the agent's behaviour when it is moving towards the light

We have shown the phase relations for a specific time-window in a single trial of the experiment. In this subsection, the phase relations are studied based on a 100 trials and on the dynamics of the nodes from the moment where the agent crosses $d = 40$ (where d is the distance to light) until it crosses d=20 for the last time before approaching the light. As

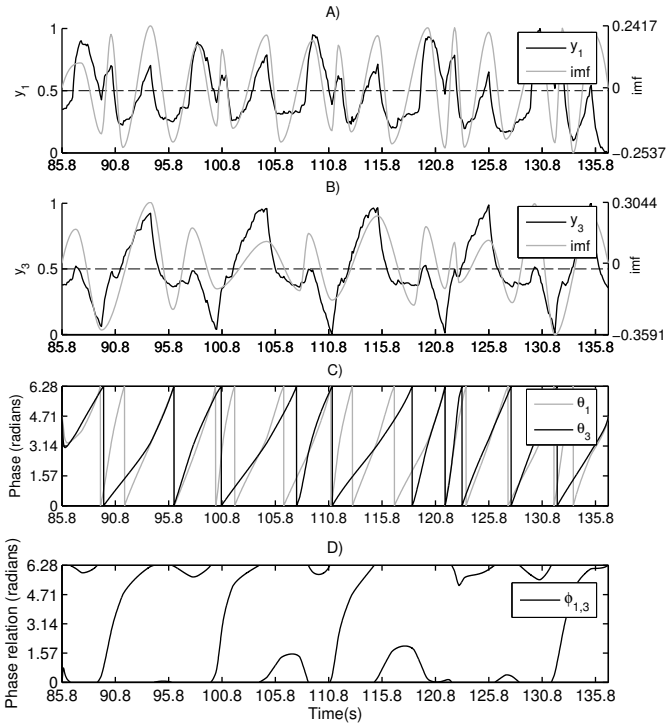

Figure 6.8: Phase relation dynamics between y_1 and y_3. See caption of Fig. 6.7.

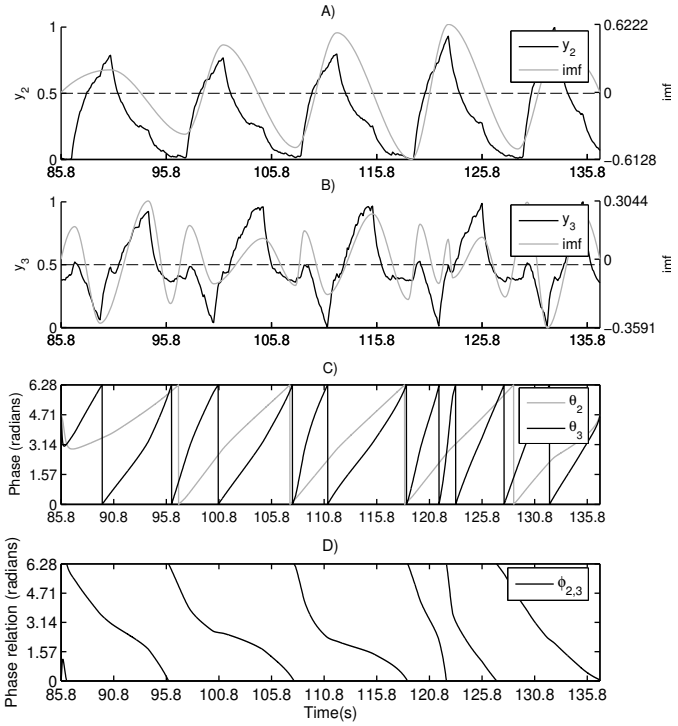

Figure 6.9: Phase relation dynamics between y_2 and y_3. See caption of Fig. 6.7.

after the first inversion the agent does not approach light, the phase relations are analysed during the first 100 seconds after the inversion (rather than when the agent is moving from

d=40 to d=20). Fig. 6.10 presents the density distributions of the phase relations $\phi_{1,2}$, $\phi_{1,3}$ and $\phi_{2,3}$. The distribution in graphic 6.10-A was generated based on the network dynamics underlying agent's behaviour before the first inversion, i.e. the 1^{st} timeslot of 250 s; the distribution in graphic 6.10-B was generated based on data from the first 100 seconds after the first inversion i.e. the 2^{nd} timeslot of 250 s; and the distributions in graphic 6.10-C and D were generated based on data from the 29^{th} and 30^{th} timeslots, respectively. The 29^{th} and 30^{th} timeslot correspond to the agent's behaviour after adaptation under normal and inverted vision, respectively. Note that the 1^{st}, 2^{nd}, 29^{th} and 30^{th} timeslots are the same as those presented in Fig. 6.5. The distributions are divided into 40 equally spaced bins in the range $[0, 2\pi)$. The entropies were calculated using the standard measure described in Equation (5.5) (Shannon, 1948; Cover and Thomas, 2005) and used in previous chapters.

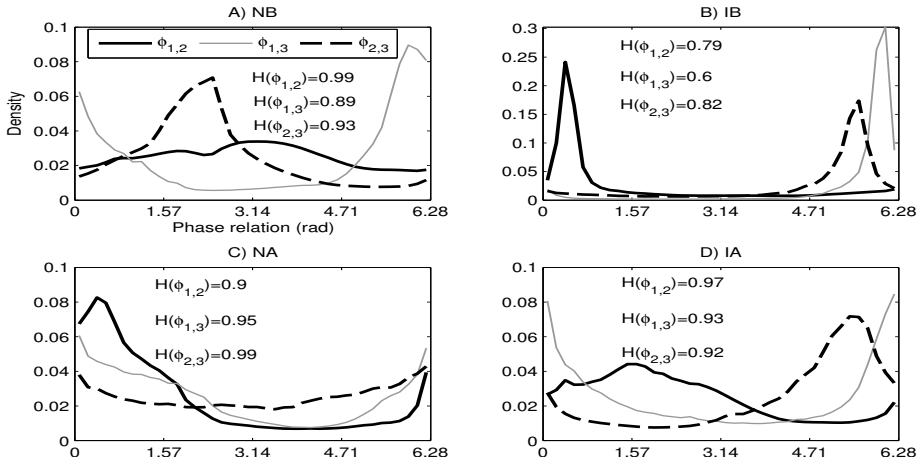

Figure 6.10: Density distributions of phase relations (see legend in graphic A) underlying agent's behaviour under normal vision before adaptation (**graphic A**), inverted vision before adaptation (**graphic B**), normal vision after adaptation (**graphic C**), and inverted vision after adaptation (**graphic D**). The Shannon's entropy of each distribution is indicated by $H(\phi_{i,j})$. The entropies are in a scaled from 0 (minimum entropy) to 1 (maximum entropy). Notice different y-axis in graphic B.

Under normal vision before adaptation (graphic 6.10-A), the entropy $H(\phi_{1,2}) = 0.99$ shows that y_1 and y_2 are highly desynchronised. The nodes y_1 and y_3 are the ones most synchronised with $H(\phi_{1,3}) = 0.89$. The synchronisation between y_1 and y_3 takes place around 0 radians, as shown by the peak in the density distribution of $\phi_{1,3}$ and by the phase relation dynamics for a single trial presented in graphic 6.8-D. The nodes y_2 and y_3 present a higher level of phase coherence in the phase range $[1.57, 3.14]$ than in the other ranges – this phase coherence is quantified by $H(\phi_{2,3}) = 0.93$.

The highest synchronisation level takes place during inverted vision before adaptation (graphic 6.10-B). See how the entropies of the phase relations are lower during IB than during the other conditions (i.e. NB, NA, IA). The highest level of synchrony takes place between y_1 and y_3 – quantified by $H(\phi_{1,3}) = 0.6$ – at a phase difference within $\approx [5.5, 6.28]$. After adaptation and under normal vision (graphic 6.10-C), y_1 and y_2 are the most synchronised nodes with $H(\phi_{1,2}) = 0.9$, and y_2 and y_3 are the most desynchronised ones with $H(\phi_{1,3}) = 0.99$. After adaptation and under inverted vision (graphic 6.10-D), y_2 and y_3 are the most synchronised nodes with $H(\phi_{2,3}) = 0.92$, and y_1 and y_2 are the most desynchronised ones with $H(\phi_{1,2}) = 0.97$.

Whereas under normal vision after adaptation y_1 and y_2 are the most synchronised nodes and y_2 and y_3 the most desynchronised; under inverted vision after adaptation y_1 and y_2 become the most desynchronised and y_2 and y_2 the most synchronised - as shown in graphics 6.10-C and D. The difference between these two conditions (i.e. normal and inverted vision after adaptation) can be better visualised by taking the difference of their density distributions, as shown in Fig. 6.11-A. Positive values in the y-axis indicate that the corresponding range of phase relations depicted in the x-axis is more synchronised during inverted vision than during normal vision. The phase relation $\phi_{2,3}$, for instance, is more synchronised in the range $\approx [4.71, 6.28]$ during inverted vision than during normal vision. On the other hand, $\phi_{1,2}$ is less synchronised in the range $\approx [0, 1.57]$ during inverted vision than during normal vision.

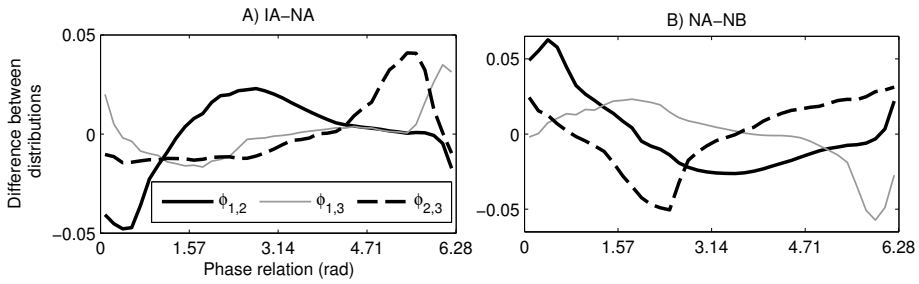

Figure 6.11: Difference between the density distributions of phase relations. Graphic **A** shows the difference between the density distributions of phase relations under inverted vision after adaptation (IA) and normal vision after adaptation (NA), see graphic title. Graphic **B** shows the difference NA-NB.

The process of adaptation to inverted vision changes the dynamics of the network under normal vision. The nodes y_1 and y_2 become more synchronised, as shown by $H(\phi_{1,2}) = 0.99$ before adaptation and $H(\phi_{1,2}) = 0.90$ after adaptation (see graphics 6.10-A and C).

On the other hand, the other pairs (y_1, y_3) and (y_2, y_3) become more desynchronized, as shown by their entropies in graphics 6.10-A and C. The difference between normal vision before and after adaptation can be better visualised by the difference of their density distributions, as shown in Fig. 6.11-B. The nodes y_1 and y_2 increase their synchrony in the range $\approx [0, 1.57]$ and lose synchrony in $\approx [1.57, 6.28]$. The nodes y_1 and y_3 gain synchrony in $\approx [0, 3.14]$ and lose synchrony in $\approx [3.14, 6.28]$. The nodes y_2 and y_3 become more desynchronised in $\approx [1.57, 3.14]$ and more synchronised in the other ranges of phase relations.

Effect of different thresholds on the phase relation dynamics

The dynamics of phase relations and the shape of the density distributions of phase relations are sensitive to the *threshold* used to detect oscillations in the time series. If the *threshold* is low, then noise in the time series will be detected as oscillations; on the other hand, if the threshold is high, real oscillations will be considered noise. The density distributions of phase relations presented in graphic 6.10 were generated using a threshold of 0.05. We now analyse how the density distributions of phase relations change as the *threshold* varies from 0.1 to 0.11. We took the density distributions for $threshold = 0.05$ as "references" (those distributions shown in graphic 6.10) and measured the correlation coefficient between these "reference distributions" and the distributions for different values of *threshold* (see Fig. 6.12).

The correlation coefficient is maximum (1) when $threshold = 0.05$ as the correlation is measured between the same distributions. Under normal vision before adaptation (graphic 6.12-A), the distributions for $\phi_{1,3}$ are highly correlated for all thresholds. For $\phi_{1,2}$ and $\phi_{2,3}$ the correlation is low when $threshold = 0.01$, meaning that the phase relations $\phi_{1,2}$ and $\phi_{2,3}$ obtained with $threshold = 0.05$ are different from the same phase relations obtained with $threshold = 0.01$. Under inverted vision before adaptation (graphic 6.12-B), all phase relations have high correlations ($r_{\phi_{i,j}} > 0.8$) for $threshold = [0.03, 0.11]$. Under normal vision after adaptation (graphic 6.12-C), the phase relation $\phi_{2,3}$ is highly sensitive to $threshold > 0.06$. Under inverted vision after adaptation (graphic 6.12-D), the correlation of $\phi_{1,2}$ is low for $threshold < 0.03$, but high for $threshold \geq 0.03$.

In essence, what these graphics tell us is that the phase relation dynamics analysed in this section hold for values of threshold within $[0.03, 0.06]$; i.e. the results do not change for any threshold within such range. The lower boundary of 0.03 is limited by the phase relation $\phi_{1,2}$ under inverted vision, see graphics 6.12-B and D; and the upper

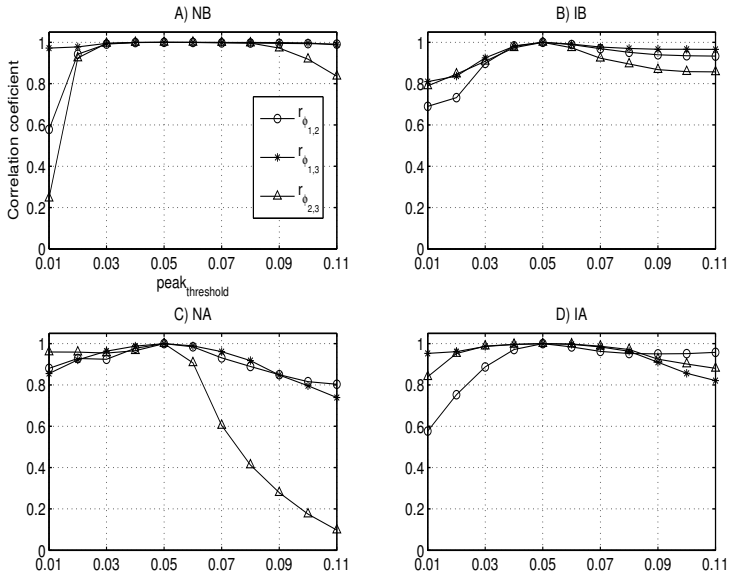

Figure 6.12: Correlation coefficient (y-axes) between the density distribution of phase relations (see legend) for $threshold = 0.05$ and the density distribution of phase relations for $threshold = [0.01, 0.11]$ (x-axes). Each graphic (**A**, **B**, **C** and **D**) shows the correlation coefficient under different conditions (see titles).

boundary of 0.06 is limited by $\phi_{1,3}$ under normal vision after adaptation, see graphics 6.12-C. Thresholds lower than 0.03 might wrongly detect noise as oscillations; and thresholds higher than 0.06 might miss real oscillations with low amplitude.

Some considerations

Briefly, so far we have presented the agent's sensorimotor behaviour under the conditions NB, IB, NA and IA and analysed the oscillatory dynamics underlying such behaviours. We have presented how the phase dynamics was obtained from the node's oscillations by using the threshold to detect oscillations, the Empirical Mode Decomposition to centre the time series in zero, and the Hilbert transform to obtain the phase dynamics from the first imf. We have shown the oscillatory regimes underlying the sensorimotor coordinations together with the synchronisation level between the oscillators (quantified by the Shannon's entropy of the density distributions of phase relations) and the range of phase in which synchronisation takes place.

The main point of the analyses we have done so far is that the process of adaptation to inverted vision has changed the previously adapted oscillatory dynamics under normal vision without affecting its functionality (i.e. the generation of phototatic behaviour). The modification of the oscillatory dynamics under normal vision was shown by the difference

in the density distributions of phase relations depicted in graphic 6.11-B.

This result helps answer the first problem we are tackling in this chapter, namely whether and how the network accommodates dynamical regimes without affecting the functionality of previously adapted regimes. In the next section we carry on with this analysis by showing how plasticity moves and reshapes the attractor landscape of the network. We will provide a dynamical explanation of how the CTRNN dynamics interacts with the sensorimotor loop dynamics (the second problem we are tackling in this chapter) and also analyse whether homeostatic instability play a role during the transition between dynamical regimes (third problem we are tackling in this chapter).

6.4.3 Generating oscillatory dynamics in the CTRNN

In this section we show that: i) oscillations in the CTRNN are generated by a transient dynamics towards an attractor that continuously moves in the state space; ii) adaptation to inverted vision reshapes the network attractor landscape; and iii) homeostatic instability is not necessary for the transition between dynamical regimes in the CTRNN.

Transient dynamics of the nodes in the state space

Fig. 6.13 shows the rhythmic dynamics of the CTRNN underlying the agent's sensorimotor behaviours under the conditions NB, IB, NA and IA. These regimes correspond to the network dynamics underlying the sensorimotor behaviours presented in Fig. 6.6; i.e. $regime_{NB}$, $regime_{NA}$, and $regime_{IA}$ underlie the agent's sensorimotor behaviours from $d = 40$ to $d = 20$; and $regime_{IB}$ underlies the sensorimotor behaviour during 100 s after the first inversion. Under normal vision and before the first inversion, the network engages in the homeostatically stable dynamical regime $regime_{NB}$. Just after the first inversion, the agent switches to the unstable regime $regime_{IB}$. After a sequence of visual field inversions, the instability of the dynamical regime under inverted vision decreases and changes from the unstable $regime_{IB}$ to the stable $regime_{IA}$. As the dynamics under inverted vision becomes stable, the stability of the dynamics under normal vision is not affected (as previously shown in Fig 6.4-B); however the shape of the dynamical regime under normal vision changes from $regime_{NB}$ to $regime_{NA}$ as a side effect of the adaptation to inverted vision.

The rhythmic dynamical regimes in which the CTRNN engages are generated by an attractor that continuously moves in the state space. The continuous movement of the attractor leaves the network in a transient state while the agent is behaving (see Fig. 6.14).

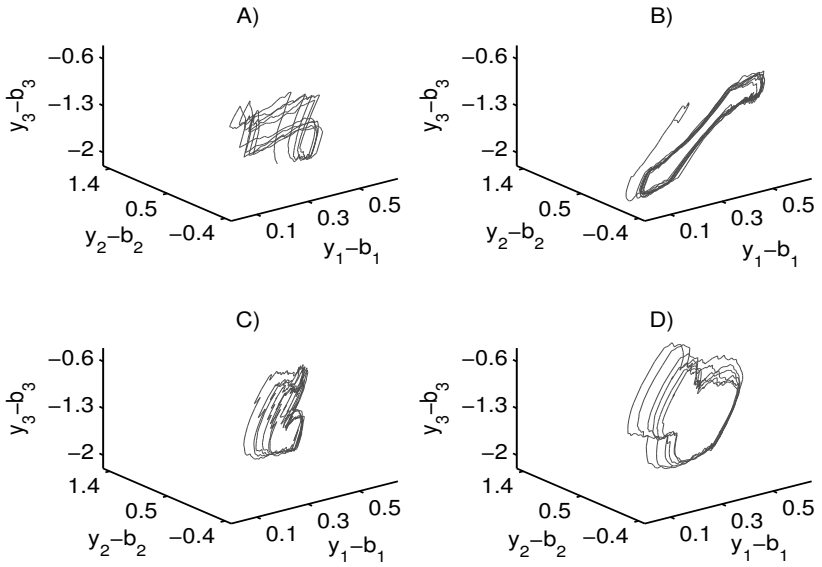

Figure 6.13: Rhythmic dynamics of the CTRNN underlying the agent's behaviour. The x, y and z-axes of each graphic represent the nodes y_1, y_2 and y_3 (minus their biases). Graphics **A**, **B**, **C** and **D** show the dynamical regimes under normal vision before adaptation (NB), inverted vision before adaptation (IB), normal vision after adaptation (NA) and inverted vision after adaptation (IA), respectively. For ease of description these regimes will be referred to as $regime_{NB}$, $regime_{IB}$, $regime_{NA}$ and $regime_{IA}$, respectively.

The system engages in a transient dynamics because different sensor values (generated by the agent's movement) define a different set of parameters for the CTRNN equations and, for each parameterisation the point attractor has a different position. In other words, the dynamics of the sensors continuously move the attractor leaving the state of the CTRNN in a transient dynamics moving towards the attractor.

We now analyse the surface on which the attractor is moving and also how the movement of the attractor on such surface generates the rhythmic regimes in the CTRNN.

The attractor surface

While the agent is engaged in a stable dynamical regime (e.g. $regime_{NA}$), the point attractor moves on a fixed 3D surface. At the beginning of the agent's lifetime, this surface resembles a rectangle with attractors lying on its corners, see the grey dots in Fig.6.15. The process of adaptation reshapes and moves this surface to a different position in the state space, see the black dots in Fig.6.15. The new position and shape of the attractor landscape accommodate the stable dynamical regimes under normal and inverted vision, meaning that both dynamical regimes $regime_{NA}$ and $regime_{IA}$ are generated by moving

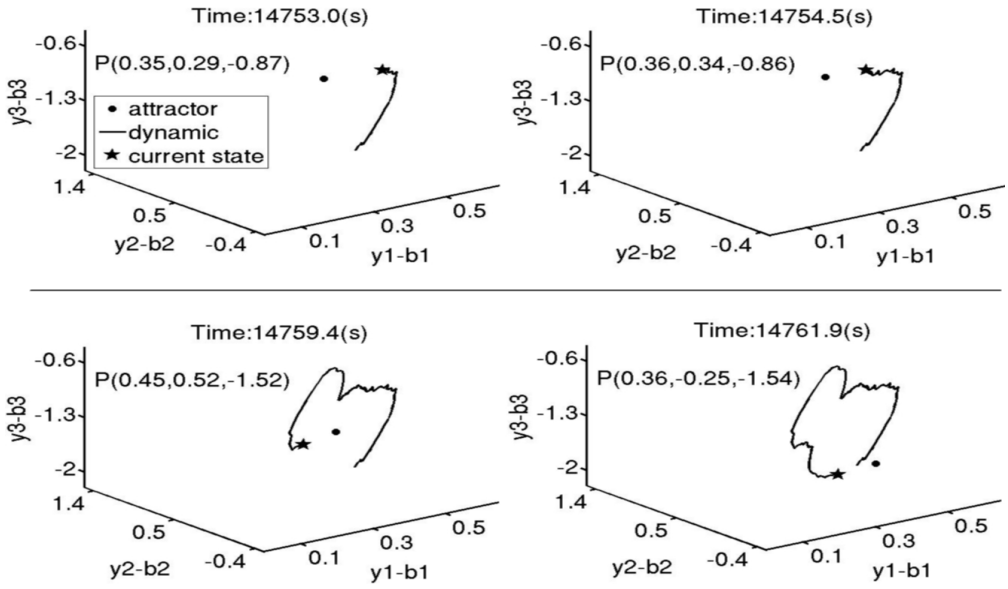

Figure 6.14: Transient dynamics that generate oscillations in the CTRNN. These graphics depict four snapshots of the trajectory in the state space of the CTRNN (see the black line) for the time interval $t = [14753.0, 14761.9]$ s (see graphic titles) corresponding to $regime_{IA}$. The star represents the state of the network at the time shown in the title of each graphic. The black point represents the point attractor towards which the state of the network is moving. The position of point attractors are represented by $\mathrm{P}(y_1 - b_1, y_2 - b_2, y_3 - b_3)$ in each graphic.

the attractor on the same surface.

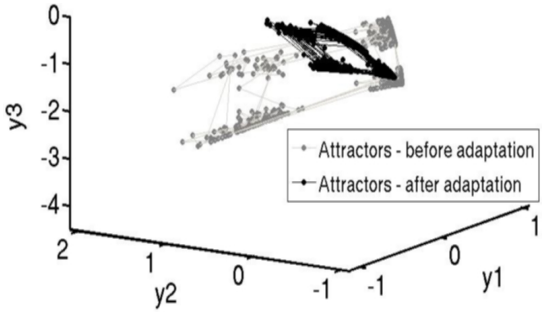

Figure 6.15: Attractor surfaces for the regimes $regime_{NB}$ and $regime_{NA}$ represented by the grey and black dots, respectively.

The points on the surfaces in Fig. 6.15 represent the position of the attractors during the regimes $regime_{NB}$ to $regime_{NA}$. In order to quantify the difference between the surfaces for all regimes $regime_{NB}$, $regime_{IB}$, $regime_{NA}$ and $regime_{IA}$ we identified clusters of attractors and their centroids on each surface by using the K-means method (Mac-

Queen, 1967), as presented in Fig. 6.16-A1, B1, C1, and D1, respectively. By comparing the centroids for $regime_{NB}$ and $regime_{NA}$ (graphics 6.16-A1, C1) we see how the surface under normal vision changes with the process of adaptation to inverted vision. By comparing the centroids for $regime_{NA}$ and $regime_{IA}$ (graphics 6.16-C1, D1) we see that the surfaces after adaptation are qualitatively the same under normal and inverted vision.

Although the attractor surfaces are qualitatively the same after adaptation (as shown in the graphics 6.16-C1 and D1), the way the attractors move on the surface is different under normal and inverted vision, see the movement of the attractor between the clusters in Fig. 6.16-C2, and D2. While $regime_{NA}$ is generated by moving the attractor in the clusters $4 \rightarrow 3 \rightarrow 2 \rightarrow 1$, $regime_{IA}$ is generated by the movement in the reverse order, i.e. $1 \rightarrow 2 \rightarrow 3 \rightarrow 4$. Notice that the rhythmic dynamic in the CTRNN is generated by a periodic movement of the attractor between the clusters.

We finish up the analysis of this model by showing that homeostatic instability is not necessary for the transition between the rhythmic regimes in the CTRNN. Fig. 6.17 shows the network dynamics, the movement of the attractor between clusters, and the number of homeostatically unstable activations in a time-window where there is a transition from normal to inverted vision. This single transition suffices to show that transition between the oscillatory regimes does not require homestatic instability.

In sum, in this section we have seen that the adaptation to inverted vision moves and reshapes the attractor landscape under normal vision (as shown in graphic 6.15). This result helps understand how a completely integrated network is able to accommodate a new dynamical regimes (e.g. the stable regime to deal with inverted vision) without affecting the functionality of previously adapted regimes (e.g. stable regime under normal vision). We have seen that the CTRNN dynamics moves in a transient towards a continuously moving attractor, and that the attractor moves due changes in the sensory values (variable I_k) caused by the agent's movement towards the light. This result contributes to show that a functional network dynamics depends on and is generated by a coordinated dynamics of the entire sensorimotor loop. Finally, we have also shown that homeostatic instability is not necessary for the transition between dynamical regimes.

6.5 Discussion

We minimally replicated the psychological experiment described by Taylor based on assumptions drawn from Ashby and Taylor's works (see assumptions in sec. 6.3). While Taylor's experiment shaped the desired behaviour, the assumptions constrained the dy-

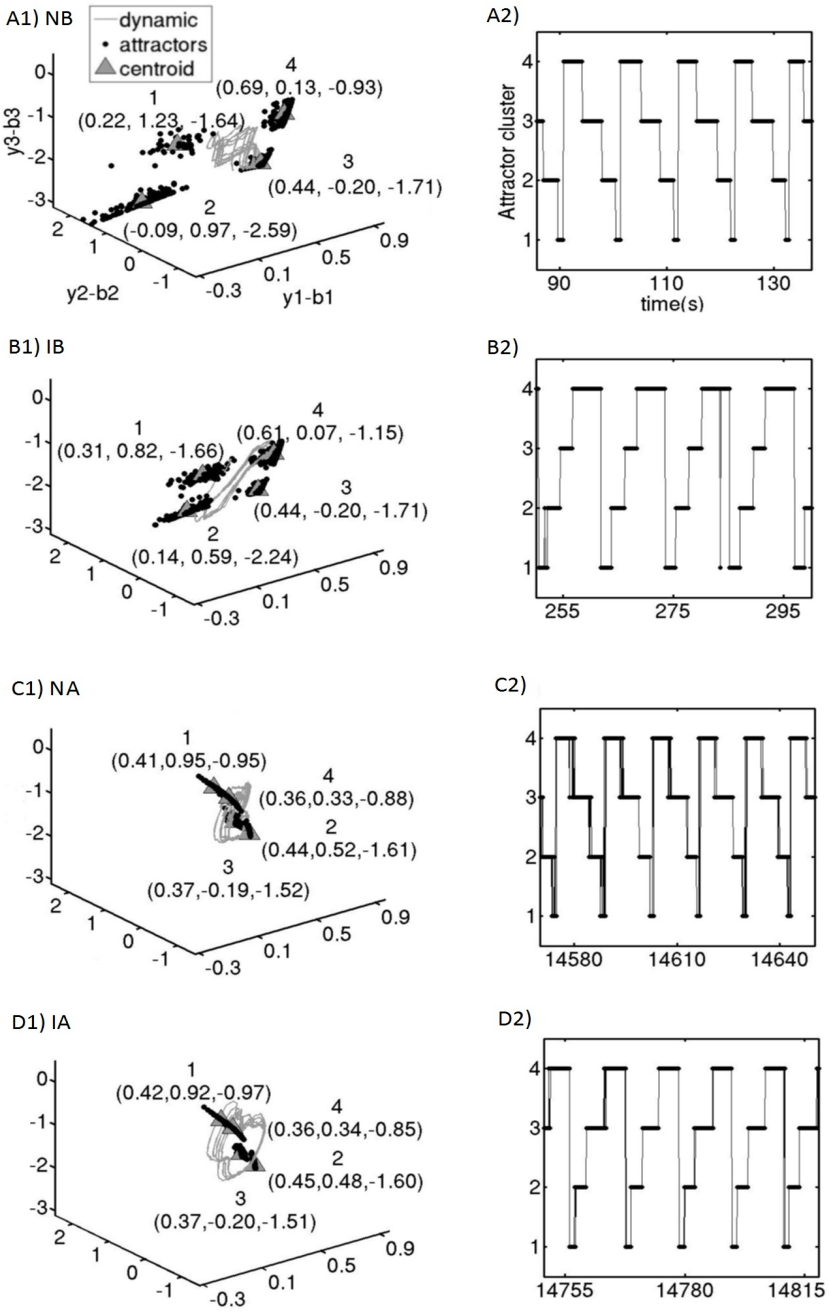

Figure 6.16: Centroids on the attractor surfaces and the rhythmic movement of the attractor on the surfaces. Graphics **A1**, **B1**, **C1**, and **D1** show the regimes $regime_{NB}$, $regime_{IB}$, $regime_{NA}$ and $regime_{IA}$ (the grey lines), the position of the attractors that have generated the transient regimes (the black dots) and the centroid of four clusters of attractors on the surface – indicated by the numbers from 1 to 4 in each graphic and by their position on the state space (numbers in parentheses). Graphics **A2**, **B2**, **C2**, and **D2** show the temporal sequence of how the attractor is moving between the clusters. The y-axis represent the number of the cluster (from 1 to 4).

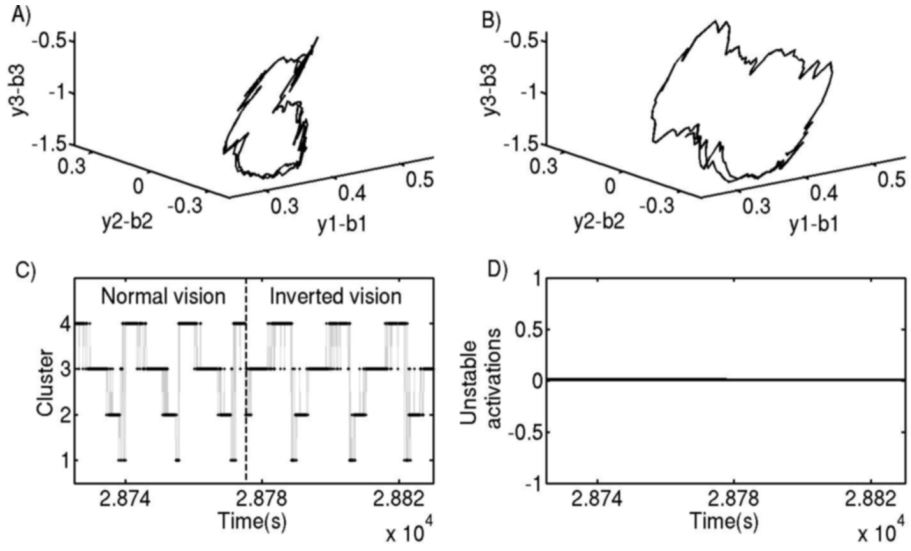

Figure 6.17: Transition between dynamical regimes without homeostatic instability. Graphic **A** and **B** show the dynamical regimes under normal and inverted vision, respectively. Graphic **C** depicts the movement of attractors between the clusters for each dynamical regimes shown in graphics A and B. Notice the transition between regimes in the middle of the time-window (represented by the vertical dashed line). Graphic **D** shows the number of homeostatically unstable activation of the CTRNN nodes (y-axis) over time (x-axis).

namics of the mechanism underlying behaviour. In this way, the methodology to obtain the model incorporated restrictions on the task and on the agent's internal dynamics. Once the model was obtained we studied its dynamic in order to help answer the problems we are tackling in this chapter, as explained in the following.

As the problem of neural interference is concerned, we have shown that the oscillatory regime in which a system engages when it is under normal vision changes after adaptation to inverted vision (as shown in graphic 6.11-B). Although the oscillatory regime under normal vision changed as a side-effect of the adaptation to inverted vision, its functionality was not affected by the adaptation process. While the difference in the density distributions of phase relations shown in graphic 6.11-B provides a dynamical description of the modifications on the oscillatory regimes under normal vision before and after adaptation, the difference on the attractor surfaces shown in graphic 6.15 sheds some light on the operation of the underlying mechanism that accommodates new stable dynamical regimes without losing the functionality and stability of the old ones. Notice that we are not proposing a solution for the problem of "neural interference", but only showing a proof

of concept that this problem can be solved by a completely integrated system without functional modularity, and giving some insights of how this problem could be solved (i.e. by moving and reshaping the attractor landscape and by different dynamical regimes on the same attractor surface).

Note that as the system is relatively simple (only 3 CTRNN nodes) and fully-connected, even a small reorganization to accommodate a new stable regime is expected to affect the pre-existing dynamics. For this reason, we can not generalize our results by saying that pre-existing stable regimes always change when the system adapts to a new condition. More complex system, such as the nervous system, probably engages in independent oscillatory regimes under different environmental conditions.

As the problem of how the network dynamics interact with the sensorimotor loop is concerned, we have provided a dynamical explanation of how homeostatically stable oscillations are generated by the CTRNN operating within a closed sensorimotor loop. Particularly, we have shown that i) oscillations in the CTRNN are generated by a transient dynamics towards an attractor that continuously moves in the state space, and ii) different periodic movement of this attractor in the manifold generates different oscillatory regimes, e.g. the regimes $regime_{NA}$ and $regime_{IA}$ are generated by the periodic movement of the attractor in the clusters $4 \rightarrow 3 \rightarrow 2 \rightarrow 1$ and $1 \rightarrow 2 \rightarrow 3 \rightarrow 4$, respectively (as show in graphic 6.16).

Notice that functional oscillatory regimes in the controller (e.g. $regime_{NA}$ and $regime_{IA}$) are generated and sustained by the dynamics of a closed sensorimotor loop, they depend on the coordinated coupling of the brain-body-environment system, and do not exist in the controller as a standalone functional entity. The sensors (variables I_k) change with the agent's movement in the environment; due to a different parametrisation of the CTRNN (different values of I_k), the attractor moves in the state space; the direction to which the attractor pulls the state of the system generates a coherent motor dynamics that move the agent towards the light and consequently modifies its sensors, which closes the sensorimotor loop dynamics. The dynamics of this closed loop is essential to sustain the transient dynamics that will eventually generate functional oscillations (e.g. $regime_{NA}$ and $regime_{IA}$). Without a well-coordinated coupling of controller-body-environment the agent's internal oscillations could settle down into the point attractor or move to a non-functional transient dynamics (i.e. a dynamics that does not generate phototatic behaviour).

Finally, we have shown that homeostatic instability is not necessary for switching between dynamical regimes. This result contributes to research on neural dynamics as it

complements a theoretical claim that instability (in the Lyapunov sense[2]) is a generic mechanism for flexible switching among multiple attractive states; that is, for entering and exiting patterns of behaviours (Kelso, 1995). Indeed Ashby has already demonstrated that a system can switch between dynamical regimes without homeostatic instability. The difference is that while Ashby uses the homeostat, we use a more complex model where the homeostatic mechanism is intertwined with the mechanism that coordinates the behaviour of an agent that is continuously interacting with its environment. Our investigation confirms Ashby's demonstration in a more complex environment and also complements Kelso's hypothesis about the importance of Lyapunov instability as a mechanism for transition between oscillatory regimes.

It is important to notice that the outcome of our analysis could not have been predicted in advance. Firstly, the optimization algorithm could have produced different solutions for the phototaxis task and for the agent's internal dynamics. Each functionality – phototaxis under normal and inverted vision – could correspond to different point attractors rather than different transient dynamics over the same attractor surface. Secondly, it was not possible to predict how the system would change in order to accommodate a new dynamical regimes to deal with inverted vision without losing the functionality of the old one under normal vision. We have seem that the attractor surface has moved and reshaped to accommodate a new dynamical regime, but alternatively a new point attractor in a different region of the state space could have been created without affecting the transient dynamics under normal vision. Thirdly, we have seem that the dynamical regimes $regime_{NA}$ and $regime_{IA}$ are characterized by different movements of the attractor on a fixed surface (i.e. by moving in the clusters $4 \rightarrow 3 \rightarrow 2 \rightarrow 1$ and $1 \rightarrow 2 \rightarrow 3 \rightarrow 4$). Alternatively, these regimes could have been characterized by different limit cycles in different regions of the state space. Lastly, we have seen that the oscillations in the CTRNN are tightly dependent on the agent's sensorimotor loop; outside the sensorimotor loop the CTRNN dynamics settles down in a point attractor. Alternatively, the CTRNN could operate as a central pattern generator oscillating even outside a sensorimotor loop. In this case, the sensorimotor loop could operate only as perturbations to the network's self-sustained oscillations. In sum, there are a multiplicity of possible dynamical strategies that the system could operate in and the conclusions we draw regarding i) how the system changes in order to accommodate different dynamical regimes maintaining the functionality of the old ones, ii) how the system can have different functionalities just by moving differently

[2]A fixed point x* is Lyapunov stable if all trajectories that start sufficiently close to x* remain close to it for all time. For a formal definition of Lyapunov stability see Strogatz (2000b) p.141

in a fixed attractor surface; and iii) how the agent's controller exploits the sensorimotor loop dynamics to engage in functional oscillations; all are far from obvious and could not have been predicted without a careful dynamical analysis of the system.

6.6 Summary

This chapter contributes to the overall story of the thesis by providing some dynamical explanations of how an agent's sensory and motor activities interacts with its internal oscillatory dynamics under the presence of plasticity in the connections of its controller. Whereas in the previous chapters we have used models describing the phase and phase relation dynamics (by using the Kuramoto and the HKB equations), in this chapter the phase dynamics had to be obtained from the oscillatory signal of the CTRNN equation by using EMD and Hilbert Transform. This equation allowed us to show, from a different perspective, a proof of concept that functional oscillatory dynamics depend on the coordinated coupling with the sensorimotor loop. We were also able to show how rhythmic dynamics can be sustained and generated within a closed sensorimotor loop – i.e. by a periodic movement of the attractor between the clusters maintained by a motor behaviour that constantly changes the sensory activity (variables I_k).

In sum, the model where the agent discriminates between the objects controlled by Kuramoto's equation (chapter 4), the models of the agents performing phototaxis controlled by the HKB equation and by the CTRNN, respectively (chapters 5 and 6), they all provide proof of concepts about the dependency of functional oscillatory neural dynamics on the sensorimotor loop. The overlapping take-home message obtained from all these models is explained in the conclusions.

Chapter 7

Conclusions

In section 7.1 we discuss some methodological issues about the models developed in this thesis. In the next sections we discuss the contributions of this thesis to each of the central issues approached in this thesis, namely the informational and causal relevance of oscillatory regimes to the sensorimotor dynamics (discussed in section 7.2), and the interplay between neural oscillatory dynamics and the sensorimotor loop (discussed in section 7.3).

7.1 Methodological issues

As far as methodological aspects of the models developed in this thesis are concerned, we have combined evolutionary robotics with oscillatory networks to study the roles played by synchronous and desynchronous oscillations in the context of a sensorimotor coordination task and also to provide dynamical explanations about the co-modulation involving the temporal structure of the oscillations and the sensorimotor dynamics. The combination of evolutionary robotics and oscillatory networks allowed us to explore current issues in neuroscience in the context of situated and embodied cognitive dynamics. As far as the analysis of the model is concerned, we have mainly used tools from Information Theory (e.g. entropy, mutual information) and Dynamical System Theory (e.g. vector fields, point attractors, limit cycles).

The goal of our models was not to target any specific biological mechanism nor to show the potential of oscillatory controllers for complex adaptive tasks, but rather to use the model as an exploratory tool to address theoretical questions by using an embodied oscillatory network within a continuous-time closed sensorimotor loop and without assuming any *a priori* functional decomposition of oscillatory components. Each oscillator of the

robot's controller can be interpreted in various ways: a) as chemical oscillatory dynamics controlling unicellular motility, b) as individual oscillatory neurons, c) as the activity of neuronal groups, tissues or brain regions d) as the macroscopic result of the activity of interactions between such regions, like EEG recordings. It is not necessary, however, to adhere to any of these levels of interpretation, we take the oscillators to be theoretical entities at an undetermined level of abstraction. What mattered to us was not the level of empirical accuracy of the model but its capacity to raise theoretical issues and its potential to open new insights into dynamical modelling and analysis of neural oscillatory dynamics and sensorimotor activity.

7.2 Informational content of causal relevance of oscillatory regimes

As the informational content and causal relevance of desynchronous oscillations are concerned, the analyses of the models – in chapters 3 and 4 – have indicated that the informational content about the sensorimotor activity is equally distributed throughout the entire range of phase relations; the more the dynamical description is reduced the less information it carries about the sensorimotor coordination. Neither synchronised nor desynchronised oscillations was found to carry a privileged status in terms of informational content in relation to the agent's sensorimotor activity. Besides, the results have also suggested that although the phase relations of oscillations with a narrow frequency difference carry a relatively higher causal relevance than the rest of the phase relations to sensorimotor coordinations, overall there is no privileged functional causal contribution to either synchronous or desynchronous oscillations.

Some contemporary cognitive neuroscience studies focus on synchronised activities between different brain areas after a given stimuli onset and assume that such activities are functional units representing the stimuli. The high level of synchronisation found by empirical experiments represent only part of the explanatory picture that involves the entire phase relation dynamics and, as our results have suggested, the reduction of phase relations to synchrony might be hindering relevant information about neural oscillatory activity underlying sensory and motor dynamics. Thus, an alternative procedure should consider the entire regime of phase relations between distinct brain areas as the functional unit correlated to the stimuli.

7.3 Sensorimotor and oscillatory dynamics

As the the interplay between sensorimotor and oscillatory dynamics is concerned, we have analysed how the spontaneous oscillations of a weakly coupled network are modulated by an agent's sensory dynamics generating stable limit cycles underlying the agent's behavioural response under the interaction with a circle and a triangle (chapter 4). This analysis was carried out by comparing the structure of the vector field under a constant sensory input equals *zero* with the same vector field under a continuous sensory input generated as a result of the agent's movement in the environment.

We have also analysed how the metastable regimes of the HKB equation are modulated by the agent' sensorimotor loop and showed how different metastable dynamical patterns in the HKB equation are generated and sustained by the continuous interaction between the agent and its environment (chapter 5). Apart from raising theoretical issues about neural oscillatory dynamics, this model has also contributed to Kelso's Coordination Dynamics framework. The metastable regimes that the HKB model can illustrate have been hypothesized to be the signature of brain functioning. Despite the evidence of metastability in empirical experiments of animals performing perceptual motor coordination tasks, to our knowledge there was no previous model of a situated HKB system that operates in a metastable region, coupling metastable oscillations to sensorimotor coordination dynamics. The model we have developed and analysed in this thesis has contributed to fill this gap and has shown the tight dependency that can be established between an agent's neural oscillatory metastable regimes and its sensorimotor dynamics; a dependency that has passed unnoticed along many studies of the HKB equation.

We have shown how the oscillatory regimes and the attractor landscape of a completely integrated network change over a process of homeostatic adaptation to the visual field inversion of an agent performing phototaxis. We have also shown how the sensorimotor loop is essential to sustain a network's rhythmic dynamics by keeping it in a transient towards a continuously moving attractor (chapter 6). Some important implications of these results are the following. Firstly, it has practical importance for the design of artificial neural network systems that can learn different behaviours. It is commonly believed that when a network system learns a new behaviour, the activation of neural plasticity will perturb the existing weight configuration of previously acquired behaviours and therefore will have a detrimental effect on the system's overall performance. One traditional way to address this so-called "problem of neural interference" is by taking inspiration from the modular computer architecture, namely by dividing the neural system

into non-overlapping neuronal groups. However, here we have demonstrated that this kind of structural modularity is not the only way for one system to realise different types of behaviour. Even a completely integrated system can achieve behavioural differentiation by different transient dynamical regimes on a fixed attractor surface.

Accordingly, this model also has important implications for our scientific understanding of the neural system. It is a widely held belief in neuroscience that different cognitive functions map onto distinct regions of the brain, a belief reinforced by the advent of various brain imaging methods. This appeal to structural localizability may be valid to some extent. However, the model presented in this paper is a proof of concept that this is not the only way of realising functional differentiation. Rather than focusing on anatomical divisions alone, it is also possible to take the nervous system as one integrated system which can realise a multiplicity of behaviours by transiting between different dynamical regimes.

Overlapping take-home message

The results obtained from the analyses of the models in chapters 4, 5 and 6 contribute to the ongoing philosophical debate about whether actions are either *causally relevant* or a *constituent* of cognitive functionalities such as perception and coherent sensorimotor coordination. Whereas proponents of the former (Clark, 2006; Prinz, 2006) claim that actions are causally relevant but not necessary for cognitive functionalities to occur, proponents of the latter (O'Regan and Noe, 2001b,a; Noe, 2004; Myin and O'Regan, 2008) concede that actions are constituents of a process involving the entire brain-body-environment system from which the functionality emerges. The models we have developed in this thesis contribute to this debate by illustrating the constitutive notion of action to cognitive functionalities in the context oscillatory neurodynamics, as explained below.

In all models, the oscillatory regimes underlying the agent's coherent behaviours (e.g. the limit cycles underlying the discrimination of circles and triangles, the metastable regimes underlying gradient climbing behaviour, and the transient oscillatory dynamics underlying the agent's phototatic behaviour with normal and inverted vision) were not generated as a network response to a specific sensory pattern, but from the ongoing coordinated coupling involving the entire sensorimotor loop (sensor $\rightarrow$ oscillatory network $\rightarrow$ motor $\rightarrow$ environment $\rightarrow$ sensor). Note, for instance, that as the agent controlled by the CTRNN (chapter 6) moves in the environment, its sensors change and, due to a different parametrisation of the CTRNN, the attractor moves in the state space. The direction to which the attractor pulls the state of the system generates a coherent motor dynam-

ics that move the agent towards the light and consequently modifies its sensory activity closing the sensorimotor loop. The dynamics of this closed loop is essential to sustain the transient dynamics that generate the oscillatory regimes underlying the agent's phototatic behaviour. Note that the CTRNN does not process the input in order to generate a "correct" output; instead the whole system is evolving together in an ongoing dynamics where the motors are constantly shaping the sensory activity, the sensory activity constantly shaping the network, and the network constantly generating the motor output.

Notice as well that it is essential to have a closed and coordinated sensorimotor loop to assure that the network will converge to a coherent oscillatory regime. This was illustrated by the HKB model where we have seen that it was not sufficient to present a sensory input pattern to the agent for its network to converge to functional oscillatory regimes, such pattern had to be generated by the motor dynamics. The motor-sensory coordination assured the convergence of the network to functional oscillatory dynamics. It is in this sense that our models illustrate that a *cognitive functionality is not a standalone entity in the neural system that is activated by a specific sensory stimulation, instead we have seen that it is tightly dependent on on the entire sensorimotor loop where the oscillatory network, the agent's body and the environment are the constituents of an interaction process from which a functionality emerges. As a result, if one is to interpret a particular oscillatory regime as a neural correlate of a cognitive functionality, she/he should be aware that the oscillations are only part of the explanatory picture and that they have been achieved with the right sensorimotor coordination being generated-by and, in turn, modulating the very oscillatory regime.* Whether these observations can be generalized to natural cognition is open to empirical investigation. In this thesis we have provided conceptual, mathematical and computational tools to help carry out this task.

We need richer methods to analyse oscillatory phenomena in order to systematically relate behavioural and neural oscillatory dynamics capable of producing a coherent picture of situated cognition. As we have seem in this thesis, artificial Life models, more specifically Evolutionary Robotics, can provide the means to explore such methods contributing with proofs of concept, testing empirical assumption and building minimal scenarios that can improve our conceptual and mathematical understanding of the complex interplay between brain, body and world that gives rise to cognitive functionalities.

Bibliography

Adrian, E. D. (1926). The impulses produced by sensory nerve endings. *The Journal of Physiology*, 61(1):49–72. 13

Aramaki, Y. (2005). Neural correlates of the spontaneous phase transition during bimanual coordination. *Cerebral Cortex*, 16(9):1338–1348. 6

Aramaki, Y., Honda, M., Okada, T., and Sadato, N. (2006). Neural correlates of the spontaneous phase transition during bimanual coordination. *Cerebral Cortex*, 16(9):1338–1348. 76

Ashby, W. R. (1947). Principles of the self-organizing dynamic system. *Journal of General Psychology*, 37:125–128. 7, 97

Ashby, W. R. (1960). *Design for a brain : the origin of adaptive behaviour*. Chapman: London, 2nd edition. 7, 97, 98, 104

Aviyente, S., Bernat, E. M., Evans, W. S., and Sponheim, S. R. (2010). A phase synchrony measure for quantifying dynamic functional integration in the brain. *Human Brain Mapping*. 4

Aviyente, S., Bernat, E. M., Evans, W. S., and Sponheim, S. R. (2011). A phase synchrony measure for quantifying dynamic functional integration in the brain. *Human Brain Mapping*, 32(1):80–93. 1

Bair, W. and Koch, C. (1996). Temporal precision of spike trains in extrastriate cortex of the behaving macaque monkey. *Neural Computation*, 8(6):1185–1202. 2, 15

Barandiaran, X. and Moreno, A. (2006). ALife models as epistemic artefacts. In *Proceeding of the 10th International Conference on Artificial Life*, pages 513–519. MIT Press, Cambridge: MA. 47

Bechtel, W. and Abrahamsen, A. (2010). Dynamic mechanistic explanation: computational modeling of circadian rhythms as an exemplar for cognitive science. *Studies In History and Philosophy of Science Part A*, 41(3):321–333. 6

Beer, R. D. (1995). On the dynamics of small continuous-time recurrent neural networks. *Adaptive Behavior*, 3:469–509. 9, 99, 100, 101

Bernard, C. (1927). *An introduction to the study of experimental medicine.* Macmillan, New York. 97

Billauer, E. (2012). Peakdet: detect peaks in a vector. http://www.billauer.co.il/peakdet.html. 105

Breakspear, M., Heitmann, S., and Daffertshofer, A. (2010). Generative models of cortical oscillations: neurobiological implications of the kuramoto model. *Frontiers in Human Neuroscience*, 4(190). 24

Bressler, S. L., Coppola, R., and Nakamura, R. (1993). Episodic multiregional cortical coherence at multiple frequencies during visual task performance. *Nature*, 366:153–156. 18

Bressler, S. L. and Kelso, J. A. S. (2001). Cortical coordination dynamics and cognition. *TRENDS in Cognitive Sciences*, 5(1):26–36. 6, 22, 23, 74, 76

Brown, T. G. (1914). On the nature of the fundamental activity of the nervous centres; together with an analysis of the conditioning of rhythmic activity in progression, and a theory of the evolution of function in the nervous system. *The Journal of Physiology*, 48(1):18–46. 51

Burns, S. P., Xing, D., and Shapley, R. M. (2010). Comparisons of the dynamics of local field potential and multiunit activity signals in macaque visual cortex. *The Journal of Neuroscience*, 30(41):13739 –13749. 17

Buzsaki, G. (2006). *Rhythms of the brain.* Oxford University Press. 1, 2, 5, 6, 13, 17, 47, 51, 74

Cannon, W. B. (1932). *The wisdom of the body.* New York, NY, US: W W Norton & Co. 97

Ceguerra, R. V., Lizier, J. T., and Zomaya, A. Y. (2011). Information storage and transfer in the synchronization process in locally-connected networks. In *Proc. IEEE Symposium*

Series in Computational Intelligence (SSCI 2011) - IEEE Symposium on Artificial Life, pages 54–61. IEEE. 4

Chemero, A. (2009). *Radical Embodied Cognitive Science*. The MIT Press. 6, 23

Clark, A. (2006). Vision as dance? three challenges for sensorimotor contingency theory. *Psyche*, 12(1):110. 127

Cohen, M. X. and van Gaal, S. (2012). Dynamic interactions between large-scale brain networks predict behavioral adaptation after perceptual errors. *Cerebral Cortex*. 2

Cooper, S. J. (2008). From claude bernard to walter cannon. emergence of the concept of homeostasis. *Appetite*, 51:419–427. 97

Cover, T. M. and Thomas, J. A. (2005). *Elements of Information Theory*. John Wiley & Sons, Inc., Hoboken, NJ, USA. 8, 31, 94, 111

Darian-Smith, I., Johnson, K. O., and Dykes, R. (1973). "Cold" fiber population innervating palmar and digital skin of the monkey: responses to cooling pulses. *Journal of Neurophysiology*, 36(2):325–346. 13

Davis, R. E. and Stretton, A. O. (1989). Signaling properties of ascaris motorneurons: graded active responses, graded synaptic transmission, and tonic transmitter release. *The Journal of Neuroscience*, 9(2):415–425. 99

de Ruyter van Steveninck, R. R., Lewen, G. D., Strong, S. P., Koberle, R., and Bialek, W. (1997). Reproducibility and variability in neural spike trains. *Science*, 275(5307):1805 –1808. 15

Denker, M., Roux, S., Marc, T., Riehle, A., and Grn, S. (2007). Phase synchronization between LFP and spiking activity in motor cortex during movement preparation. *Neurocomputing*, 70:20962101. 2, 16

Di Ferdinando, A., Calabretta, R., and Parisi, D. (2001). Evolving modular architectures for neural networks. In French, R. and Sough{\'e}, J., editors, *Connectionist models of learning, development, and evolution*. Springer Verlag. 7, 96

Di Paolo, E. (2000). Homeostatic adaptation to inversion of the visual field and other sensorimotor disruptions. In J-A. Meyer, A. B. and Wilson, S. W., editors, *From Animals to Animals, Proc. of the Sixth International Conference on the Simulation of Adaptive Behavior, SAB'2000*, pages 440–449. MIT Press. 7, 99, 100

Di Paolo, E. (2003). Dynamical systems approach to embodiment and sociality. In Murase, K. and T, A., editors, *Dynamical Systems Approach to Embodiment and Sociality*, pages 19–42. Advanced Knowledge International, Adelaide, Australia. 99

Dubovik, S., Pignat, J.-M., Ptak, R., Aboulafia, T., Allet, L., Gillabert, N., Magnin, C., Albert, F., Momjian-Mayor, I., Nahum, L., Lascano, A. M., Michel, C. M., Schnider, A., and Guggisberg, A. G. (2012). The behavioral significance of coherent resting-state oscillations after stroke. *NeuroImage*, 61(1):249–257. 1

Eckhorn, R., Bauer, R., Jordan, W., Brosch, M., Kruse, W., Munk, M., and Reitboeck, H. J. (1988). Coherent oscillations: A mechanism of feature linking in the visual cortex? *Biological Cybernetics*, 60(2):121–130. 17, 18

Engel, A., Konig, P., Kreiter, A., and Singer, W. (1991a). Interhemispheric synchronization of oscillatory neuronal responses in cat visual cortex. *Science*, 252(5009):1177–1179. 18

Engel, A. K., Konig, P., Gray, C. M., and Singer, W. (1990). Stimulus-dependent neuronal oscillations in cat visual cortex: Inter-columnar interaction as determined by cross-correlation analysis. *European Journal of Neuroscience*, 2(7):588–606. 3, 17, 18, 26

Engel, A. K., Knig, P., Kreiter, A. K., Schillen, T. B., and Singer, W. (1992). Temporal coding in the visual cortex: new vistas on integration in the nervous system. *Trends in Neurosciences*, 15(6):218–226. 17

Engel, A. K., Knig, P., and Singer, W. (1991b). Direct physiological evidence for scene segmentation by temporal coding. *Proceedings of the National Academy of Sciences*, 88(20):9136 –9140. 18

Fell, J. and Axmacher, N. (2011). The role of phase synchronization in memory processes. *Nat Rev Neurosci*, 12(2):105–118. 1

Floreano, D., Husbands, P., and Nolfi, S. (2008). Evolutionary robotics. In Siciliano, B. and Khatib, O., editors, *Springer Handbook of Robotics*, pages 1423–1451. Springer. 100

Forrester, L. and Whitall, J. (2000). Bimanual finger tapping: Effects of frequency and auditory information on timing consistency and coordination. *Journal of Motor Behavior*, 32(2):176–191. 76

Fries, P. (2005). A mechanism for cognitive dynamics: neuronal communication through neuronal coherence. *Trends in Cognitive Sciences*, 9(10):474–480. 3, 26, 49

Fries, P., Nikolic, D., and Singer, W. (2007). The gamma cycle. *Trends in Neurosciences*, 30(7):309–316. 2, 16

Fritsch, F. N. and Carlson, R. E. (1980). Monotone piecewise cubic interpolation. *SIAM Journal on Numerical Analysis*, 17(2):238–246. 105

Fuchs, A. and Jirsa, V. K., editors (2008). *Coordination: Neural, Behavioral and Social Dynamics*. Springer Berlin Heidelberg, Berlin, Heidelberg. 76

Funahashi, K.-i. and Nakamura, Y. (1993). Approximation of dynamical systems by continuous time recurrent neural networks. *Neural Networks*, 6(6):801–806. 99

Gerstner, W. (1999). Spiking neurons. In Maas, W. and Christopher, M. B., editors, *Pulsed Neural Networks*. MIT Press. 14

Getchell, T. V. (1986). Functional properties of vertebrate olfactory receptor neurons. *Physiological Reviews*, 66(3):772 –818. 13

Gollisch, T. and Meister, M. (2008). Rapid neural coding in the retina with relative spike latencies. *Science*, 319(5866):1108–1111. 2, 15

Goodman, M. B., Hall, D. H., Avery, L., and Lockery, S. R. (1998). Active currents regulate sensitivity and dynamic range in c. elegans neurons. *Neuron*, 20(4):763–772. PMID: 9581767. 100

Gray, C. M. (1999). The temporal correlation hypothesis of visual feature IntegrationStill alive and well. *Neuron*, 24(1):31–47. 18

Gray, C. M. and Singer, W. (1989). Stimulus-specific neuronal oscillations in orientation columns of cat visual cortex. *Proceedings of the National Academy of Sciences*, 86(5):1698 –1702. 3, 17, 18, 26

Haken, H. (1978). *Synergetics: An Introduction. Nonequilibrium Phase Transitions and Self- Organization in Physics Chemistry and Biology*. Springer Verlag, Berlin, Heidelberg, New York, 2nd enlarged edition edition. 1, 20

Haken, H., Kelso, J. A. S., and Bunz, H. (1985). A theoretical model of phase transitions in human hand movements. *Biological Cybernetics*, 51(5):347–356. 21, 75, 76

Harvey, I. (2001). Artificial evolution: A continuing SAGA. In Gomi, T., editor, *Evolutionary Robotics: From Intelligent Robots to Artificial Life - Proc. of 8th Intl. Symposium*

on Evolutionary Robotics, volume 2217, pages 94–109. Springer-Verlag Lecture Notes in Computer Science LNCS. 30, 54, 78, 102

Harvey, I., Paolo, E. D., Wood, R., and Quinn, M. (2005). Evolutionary robotics: A new scientific tool for studying cognition. *Artificial Life*, 11:79–98. 100

Hebb, D. O. (1949). *The organization of behavior: a neuropsychological theory*. Wiley. 14

Heil, P. (2004). First-spike latency of auditory neurons revisited. *Current Opinion in Neurobiology*, 14(4):461–467. 2, 15

Hipp, J. F., Engel, A. K., and Siegel, M. (2011). Oscillatory synchronization in large-scale cortical networks predicts perception. *Neuron*, 69(2):387–396. 2, 3, 6, 17, 19, 26, 49, 72, 74

Huang, N. E., Shen, Z., Long, S. R., Wu, M. C., Shih, H. H., Zheng, Q., Yen, N.-C., Tung, C. C., and Liu, H. H. (1998). The empirical mode decomposition and the hilbert spectrum for nonlinear and non-stationary time series analysis. *Proceedings of the Royal Society of London. Series A: Mathematical, Physical and Engineering Sciences*, 454(1971):903–995. 9, 104

Huyck, C. R. and Passmore, P. J. (2013). A review of cell assemblies. *Biological Cybernetics*, 107(3):263–288. 49

Iizuka, H. and Paolo, E. A. D. (2008). Extended homeostatic adaptation: Improving the link between internal and behavioural stability. In *From Animats to Animals 10, The Tenth International Conference on the Simulation of Adaptive Behavior*, Osaka, Japan. 100

Ijspeert, A. J. (2008). Central pattern generators for locomotion control in animals and robots: A review. *Neural Networks*, 21(4):642–653. 100

Izhikevich, E. M. (2006). Polychronization: computation with spikes. *Neural Computation*, 18(2):245–282. 2

Izhikevich, E. M. (2007). *Dynamical Systems in Neuroscience: The Geometry of Excitability and Bursting*. MIT Press. 2, 13, 47

Izhikevich, E. M., Gally, J. A., and Edelman, G. M. (2004). Spike-timing dynamics of neuronal groups. *Cerebral Cortex*, 14(8):933 –944. 4

Izhikevich, E. M. and Hoppensteadt, F. C. (2009). Polychronous wavefront computations. *International Journal of Bifurcation and Chaos*, 19(05):1733. 2

Izquierdo, E. J. and Lockery, S. R. (2010). Evolution and analysis of minimal neural circuits for klinotaxis in caenorhabditis elegans. *Journal of Neuroscience*, 30(39):12908–12917. 100

Jantzen, K. J. (2004). Brain networks underlying human timing behavior are influenced by prior context. *Proceedings of the National Academy of Sciences*, 101(17):6815–6820. 6

Jantzen, K. J., Steinberg, F. L., and Kelso, J. (2009). Coordination dynamics of large-scale neural circuitry underlying rhythmic sensorimotor behavior. *Journal of Cognitive Neuroscience*, 21(12):2420–2433. PMID: 19199411. 76

Jirsa, V. K., Fuchs, A., and Kelso, J. (1998). Connecting cortical and behavioral dynamics: bimanual coordination. *Neural Computation*, 10(8):2019–2045. 23, 76

Jirsa, V. K. and Kelso, J. (2004). *Coordination dynamics: issues and trends*. Springer. 20, 21

Johansson, R. S. and Birznieks, I. (2004). First spikes in ensembles of human tactile afferents code complex spatial fingertip events. *Nature Neuroscience*, 7(2):170–177. 15

Kaliukhovich, D. A. and Vogels, R. (2012). Stimulus repetition affects both strength and synchrony of macaque inferior temporal cortical activity. *Journal of Neurophysiology*, 107(12):3509–3527. 1

Kandel, E. R., Schwartz, J. H., and Jessell, T. M., editors (2000). *Principles of neural science*. McGraw-Hill, Health Professions Division, 4th edition. 14

Kaplan, D. M. and Bechtel, W. (2011). Dynamical models: An alternative or complement to mechanistic explanations? *Topics in Cognitive Science*, 3(2):438–444. 6

Kayser, C., Montemurro, M. A., Logothetis, N. K., and Panzeri, S. (2009). Spike-phase coding boosts and stabilizes information carried by spatial and temporal spike patterns. *Neuron*, 61(4):597–608. 2, 16

Kelso, J. (1995). *Dynamic patterns: the self-organization of brain and behavior*. MIT Press. iii, 5, 6, 20, 21, 74, 75, 76, 81, 122

Kelso, J. (2008). Haken-kelso-bunz model. *Scholarpedia*, 3(10):1612. 76

Kelso, J., DelColle, J., and Schoner, G. (1990). Action-perception as a pattern formation process. In Jeannerod, M., editor, *Attention and performance XIII*, pages 139–169. Hillsdale, NJ: Erlbaum. 74, 81

Kelso, J. and Engstrm, D. A. (2008). Coordination dynamics of the complementary nature. *Gestalt theory*, 30:121–134. PMID: 20634938 PMCID: 2903971. 21

Kelso, J., Guzman, G. C. d., Reveley, C., and Tognoli, E. (2009). Virtual partner interaction (VPI): exploring novel behaviors via coordination dynamics. *PLoS ONE*, 4(6):e5749. 23, 75

Kelso, J. and Tognoli, E. (2009). Toward a complementary neuroscience: Metastable coordination dynamics of the brain. In Murphy, N., Ellis, G. F., and O'Connor, T., editors, *Downward Causation and the Neurobiology of Free Will*, Understanding Complex Systems, pages 103–124. Springer Berlin / Heidelberg. 6, 74, 91

Kelso, J. A. S. (2002). The complementary nature of coordination dynamics: Self-organization and agency. *Nonlinear Phenomena in Complex Systems*, 5(4):364–371. 23

Kelso, J. A. S. (2012). Multistability and metastability: understanding dynamic coordination in the brain. *Philosophical Transactions of the Royal Society B: Biological Sciences*, 367(1591):906–918. 76

Kimura, M. and Nakano, R. (1998). Learning dynamical systems by recurrent neural networks from orbits. *Neural Networks*, 11(9):1589–1599. 99

Kitzbichler, M. G., Smith, M. L., Christensen, S. R., and Bullmore, E. (2009). Broadband criticality of human brain network synchronization. *PLoS Computational Biology*, 5(3). 24

Kohler, I. (1963). The formation and transformation of the perceptual world. *Psychological Issues*, 3(4, Monogr. No. 12):1–173. 7

Kuramoto, Y. (1984). *Chemical oscillations, waves, and turbulence*. Springer, New York. 5, 8, 24, 30, 53

Lagarde, J. and Kelso, J. A. S. (2006). Binding of movement, sound and touch: multimodal coordination dynamics. *Experimental Brain Research*, 173(4):673–688. 6

Lutz, A. (2002). Toward a neurophenomenology as an account of generative passages: a first empirical case study. *Phenomenology and the Cognitive Sciences*, 1:133–167. 17

MacQueen, J. B. (1967). Some methods for classification and analysis of multivariate observations. In *Proceedings of the Fifth Symposium on Math, Statistics and Probability*, pages 281–297. Berkeley, CA: University of California Press. 117

Mainen, Z. and Sejnowski, T. (1995). Reliability of spike timing in neocortical neurons. *Science*, 268(5216):1503 –1506. 2, 15

Mathayomchan, B. and Beer, R. D. (2002). Center-crossing recurrent neural networks for the evolution of rhythmic behavior. *Neural Computation*, 14(9):2043–2051. 100

Meyer-Lindenberg, A. (2002). Transitions between dynamical states of differing stability in the human brain. *Proceedings of the National Academy of Sciences*, 99(17):10948–10953. 6

Moioli, R., Vargas, P., and Husbands, P. (2012). Synchronisation effects on the behavioural performance and information dynamics of a simulated minimally cognitive robotic agent. *Biological Cybernetics*, pages 1–21. 24

Moioli, R. C., Vargas, P. A., and Husbands, P. (2010). Exploring the kuramoto model of coupled oscillators in minimally cognitive evolutionary robotics tasks. In *IEEE World Congress on Computational Intelligence*, pages 1–8. IEEE. 24

Montemurro, M. A., Rasch, M. J., Murayama, Y., Logothetis, N. K., and Panzeri, S. (2008). Phase-of-firing coding of natural visual stimuli in primary visual cortex. *Current Biology*, 18(5):375–380. 2, 16

Moreno, Y. and Pacheco, A. F. (2004). Synchronization of kuramoto oscillators in scale-free networks. *Europhysics Letters (EPL)*, 68(4):603–609. 24

Mountcastle, V. B., Talbot, W. H., and Kornhuber, H. H. (1966). The neural transformation of mechanical stimuli delivered to the monkey's hand. In de Reuck, A. and Knight, J., editors, *Touch, heat and pain*, Ciba Foundation, pages 325–351. Churchill, London. 13

Myin, E. and O'Regan, J. K. (2008). Situated perception and sensation in vision and other modalities: from an active to a sensorimotor account. In Robbins, P. and Aydede, A., editors, *Cambridge Handbook of Situated Cognition*, page 185200. Oxford University Press. 127

Neymotin, S. A., Jacobs, K. M., Fenton, A. A., and Lytton, W. W. (2010). Synaptic information transfer in computer models of neocortical columns. *Journal of Computational Neuroscience*, 30(1):69–84. 4

Noe, A. (2004). *Action in perception*. MIT Press. 127

O'Keefe, J. and Recce, M. L. (1993). Phase relationship between hippocampal place units and the EEG theta rhythm. *Hippocampus*, 3(3):317–330. 16

O'Regan, J. K. and Noe, A. (2001a). A sensorimotor account of vision and visual consciousness. *The Behavioral and Brain Sciences*, 24(5):939–973; discussion 973–1031. PMID: 12239892. 127

O'Regan, J. K. and Noe, A. (2001b). What it is like to see: A sensorimotor theory of perceptual experience. *Synthese*, 129(1):79103. 127

Parameshwaran, D., Crone, N. E., and Thiagarajan, T. C. (2012). Coherence potentials encode simple human sensorimotor behavior. *PLoS ONE*, 7(2):e30514. 2

Perfetti, B., Moisello, C., Landsness, E. C., Kvint, S., Lanzafame, S., Onofrj, M., Di Rocco, A., Tononi, G., and Ghilardi, M. F. (2011). Modulation of gamma and theta spectral amplitude and phase synchronization is associated with the development of visuo-motor learning. *The Journal of Neuroscience*, 31(41):14810 –14819. 2, 19

Phattanasri, P., Chiel, H. J., and Beer, R. D. (2007). The dynamics of associative learning in evolved model circuits. *Adaptive Behavior*, 15(4):377–396. 100

Pikovsky, A., Rosenblum, M., and Kurths, J. (2003). *Synchronization: a universal concept in nonlinear sciences*. Cambridge University Press. 28

Pockett, S., Bold, G. E., and Freeman, W. J. (2009). EEG synchrony during a perceptual-cognitive task: Widespread phase synchrony at all frequencies. *Clinical Neurophysiology*, 120(4):695–708. 3, 6, 17, 26, 49, 74

Prinz, J. (2006). Putting the brakes on enactive perception. *Psyche*, 12(1):119. 127

Raichle, M. E. (2010). Two views of brain function. *Trends in Cognitive Sciences*, 14(4):180–190. 51

Reich, D. S., Victor, J. D., Knight, B. W., Ozaki, T., and Kaplan, E. (1997). Response variability and timing precision of neuronal spike trains in vivo. *Journal of Neurophysiology*, 77(5):2836 –2841. 2, 15

Reinagel, P. and Reid, R. C. (2002). Precise firing events are conserved across neurons. *The Journal of Neuroscience*, 22(16):6837 –6841. 2, 15

Rieke, F. (1999). *Spikes: Exploring the Neural Code*. MIT Press, new edition edition. 14

Rilk, A. J., Soekadar, S. R., Sauseng, P., and Plewnia, C. (2011). Alpha coherence predicts accuracy during a visuomotor tracking task. *Neuropsychologia*, 49(13):3704–3709. 19

Robertson, S. D. (2001). Development of bimanual skill: The search for stable patterns of coordination. *Journal of Motor Behavior*, 33(2):114–126. 76

Rodriguez, E., George, N., Lachaux, J., Martinerie, J., Renault, B., and Varela, F. (1999). Perception's shadow: long-distance synchronization of human brain activity. *Nature*, 397(6718):430–433. 6, 17, 18, 19, 27, 74

Roelfsema, P. R., Engel, A. K., Konig, P., and Singer, W. (1997). Visuomotor integration is associated with zero time-lag synchronization among cortical areas. *Nature*, 385:157–161. 18

Roskies, A. L. (1999). The binding problem. *Neuron*, 24(1):7–9. 17

Rubino, D., Robbins, K. A., and Hatsopoulos, N. G. (2006). Propagating waves mediate information transfer in the motor cortex. *Nature Neuroscience*, 9(12):1549–1557. 4

Russell, D. M., Kalbach, C. R., Massimini, C. M., and Martinez-Garza, C. (2010). Leg asymmetries and coordination dynamics in walking. *Journal of Motor Behavior*, 42(3):157–168. 76

Sakurai, Y., Nakazono, T., Ishino, S., Terada, S., Yamaguchi, K., and Takahashi, S. (2013). Diverse synchrony of firing reflects diverse cell-assembly coding in the prefrontal cortex. *Journal of Physiology-Paris*. 49, 72

Santos, J. and Campo, A. (2012). Biped locomotion control with evolved adaptive center-crossing continuous time recurrent neural networks. *Neurocomputing*, 86:86–96. 100

Sauseng, P., Klimesch, W., Gruber, W., Doppelmayr, M., Stadler, W., and Schabus, M. (2002). The interplay between theta and alpha oscillations in the human electroencephalogram reflects the transfer of information between memory systems. *Neuroscience Letters*, 324(2):121–124. 4

Shadlen, M. N. and Newsome, W. T. (1994). Noise, neural codes and cortical organization. *Current Opinion in Neurobiology*, 4(4):569–579. 14

Shannon, C. E. (1948). A mathematical theory of communication. *The Bell System Technical Journal*, 27:379 — 423 and 623 – 656. 8, 31, 58, 94, 111

Sharafi, N., Benda, J., and Lindner, B. (2012). Information filtering by synchronous spikes in a neural population. *Journal of Computational Neuroscience*, 34(2):285–301. 49, 72

Sherrington, C. S. (1906). *The integrative action of the nervous system*, volume xvi of *Yale University Mrs. Hepsa Ely Silliman memorial lectures.* Yale University Press, New Haven, CT, US. 51

Sinclair, B. R., Seto, M. G., and Bland, B. H. (1982). Theta-cells in CA1 and dentate layers of hippocampal formation: relations to slow-wave activity and motor behavior in the freely moving rabbit. *Journal of Neurophysiology*, 48(5):1214–1225. 2, 16

Singer, W. (2011). Dynamic formation of functional networks by synchronization. *Neuron*, 69(2):191–193. 2, 3, 6, 17, 26, 49, 72, 74

Skardal, P. S. and Restrepo, J. G. (2012). Hierarchical synchrony of phase oscillators in modular networks. *Physical Review E*, 85(1):016208. 4

Sporns, O. (2010). *Networks of the Brain.* The MIT Press, 1 edition. 5, 51

Stanley, G. B. (2013). Reading and writing the neural code. *Nature Neuroscience*, 16(3):259–263. 50

Steels, L. and Brooks, R. A. (1995). *The artificial life route to artificial intelligence: building embodied, situated agents.* Routledge. 1

Stepp, N., Chemero, A., and Turvey, M. T. (2011). Philosophy for the rest of cognitive science. *Topics in Cognitive Science*, 3(2):425–437. 6

Strogatz, S. H. (2000a). From kuramoto to crawford: exploring the onset of synchronization in populations of coupled oscillators. *Physica D: Nonlinear Phenomena*, 143(1-4):1–20. 24

Strogatz, S. H. (2000b). *Nonlinear Dynamics and Chaos: With Applications to Physics, Biology, Chemistry and Engineering.* Perseus Books. 28, 122

Swinnen, S. P. (2002). Intermanual coordination: from behavioural principles to neural-network interactions. *Nature Reviews. Neuroscience*, 3(5):348–359. 6

Taylor, J. G. (1962). *The Behavioral Basis of Perception.* New Haven: Yale University Press. 7, 99, 103, 104

Thorpe, S., Fize, D., and Marlot, C. (1996). Speed of processing in the human visual system. *Nature*, 381(6582):520–522. 15

Thorpe, S. J. (1990). Spike arrival times: A highly efficient coding scheme for neural networks. In Eckmiller, R., Hartmann, G., and Hauske, G., editors, *Parallel processing in neural systems and computers*, pages 91–94. Elsevier. 15

Tognoli, E. and Kelso, J. A. S. (2009). Brain coordination dynamics: True and false faces of phase synchrony and metastability. *Progress in Neurobiology*, 87:31–40. 6, 74, 76

Tononi, G. and Edelman, G. M. (1998). Consciousness and complexity. *Science*, 282:1846–1851. 3, 17, 23, 26

Traub, R. and Whittington, M. (2010). *Cortical Oscillations in Health and Disease*. Oxford University Press. 1, 13

Triplett, B. I., Klein, D. J., and Morgansen, K. A. (2006). Discrete time kuramoto models with delay. In Antsaklis, P. J. and Tabuada, P., editors, *Networked Embedded Sensing and Control*, volume 331, pages 9–23. Springer-Verlag, Berlin/Heidelberg. 24

Turrigiano, G. G. (1999). Homeostatic plasticity in neuronal networks: the more things change, the more they stay the same. *Trends in Neurosciences*, 22(5):221–227. 97

Turrigiano, G. G. and Nelson, S. B. (2004). Homeostatic plasticity in the developing nervous system. *Nature Reviews Neuroscience*, 5:97–107. 97

Uhlhaas, P. J., Pipa, G., Lima, B., Melloni, L., Neuenschwander, S., Nikolic, D., and Singer, W. (2009). Neural synchrony in cortical networks: history, concept and current status. *Front. Integr. Neurosci*, 3(17). 3, 26, 49, 72

Vanrullen, R. (2003). Visual saliency and spike timing in the ventral visual pathway. *Journal of Physiology-Paris*, 97(2-3):365–377. 15

VanRullen, R., Guyonneau, R., and Thorpe, S. J. (2005). Spike times make sense. *Trends in Neurosciences*, 28(1):1–4. 2, 15

Varela, F., Lachaux, J.-P., Rodriguez, E., and Martinerie, J. (2001). The brain web: phase synchronization and large-scale integration. *Nature Reviews Neuroscience*, 2:229–239. 3, 6, 17, 26, 28, 47, 74

Vertes, R. P. and Stackman, R. W., editors (2011). *Electrophysiological Recording Techniques*. Humana Press, 1st edition. edition. 2

Vogels, T. P., Rajan, K., and Abbott, L. (2005). Neural network dynamics. *Annual Review of Neuroscience*, 28(1):357–376. 5, 51, 72

von der Malsburg, C. (1981). The correlation theory of brain function. Departmental technical report, Max-Planck-Institute for Biophysical Chemistry. 3, 17, 26

von der Malsburg, C. (1987). Synaptic plasticity as basis of brain organization. In Changeux, J. and Konishi, M., editors, *The Neural and Molecular Bases of Learning*, pages 411–431. Wiley & Sons Ltd., Chichester. 14

Williams, H. and Noble, J. (2007). Homeostatic plasticity improves signal propagation in continuous-time recurrent neural networks. *Biosystems*, 87(23):252–259. 100, 104

Winfree, A. T. (1967). Biological rhythms and the behavior of populations of coupled oscillators. *Journal of Theoretical Biology*, 16(1):15–42. 24

Winfree, A. T. (1980). *The geometry of biological time*, volume 12. Springer-Verlag. 24

Yeung, M. K. S. and Strogatz, S. H. (1999). Time delay in the kuramoto model of coupled oscillators. *Physical Review Letters*, 82(3):648–651. 24

Zhang, W., Qiao, Q., Zheng, X., and Tian, X. (2008). The synchronization and associative memory of izhikevich neural network. In Wang, R., Shen, E., and Gu, F., editors, *Advances in Cognitive Neurodynamics ICCN 2007*, pages 237–242. Springer Netherlands. 10.1007/978-1-4020-8387-7_42. 4

Zygmund, A. (1988). *Trigonometric Series*. Cambridge University Press, 2 edition. 104